Relaxation for an Open System of Interacting Spins

A Thesis
Presented to
The Division of Mathematical and Natural Sciences
Reed College

In Partial Fulfillment
of the Requirements for the Degree
Bachelor of Arts

Alex Striff

May 2021

Approved for the Division
(Physics)

Darrell Schroeter

Acknowledgements

To Darrell — for being a great thesis advisor and guiding me throughout this process.

To Lucas, Alison, Mark, John, Andrew, Joel, Johnny, and Darrell — for being amazing and caring professors, and for all your insights into life, the universe and everything.

To the Physics seniors — for being great people to go on a wild ride with.

To Reilly, Usman Evan, Isadora, and Théo, — for all we've done and the sights we've seen these four years together. You have shown me the life of being bougie, trying not to become a corporate slave, and studying for hours on end. I wish all of you well wherever you travel in life.

ABSTRACT

This thesis studies open quantum systems and their relaxation to thermal equilibrium. Candidate systems for use in quantum sensing or computing often require long coherence times, but models of the environment-induced decoherence these systems face are often simplistic. We consider a more complete model for the relaxation of two to five spins in the transverse-field Ising model as they interact with an electromagnetic bath at some temperature. As the field strength is tuned for an appropriately renormalized Hamiltonian, a single spin is found to vary its relaxation time by approximately a factor of ten for all temperatures.

Table of Contents

Introduction 5

Note on Notation 7

Chapter 1: Open quantum systems 9

1.1 The mathematical formalism 11
1.2 Composite systems 13
1.3 Closed dynamics 15
1.4 Canonical quantization 17
1.5 Open dynamics 19
1.6 The weak-coupling limit 21
1.7 Relaxation to thermal equilibrium 25

Chapter 2: Application to interacting spins 27

2.1 The closed two-dimensional system 27
2.2 Relaxation of the two-dimensional system 28
2.3 The transverse-field Ising chain 30
2.4 The weak-coupling limit for the Ising chain 32

Chapter 3: Computing jump operators 43

3.1 Interpolating Hamiltonians 45
3.2 Computation of jump operators 46
3.3 Numerical solution of the Lindblad equation 48
3.4 Obtaining relaxation from spaghetti (diagrams) 49
3.5 Results 53

Conclusion 67

Appendix A: The generator of a quantum dynamical semigroup 71

Appendix B: The transverse-field Ising model 75

Appendix C: Computer details 83
- C.1 Julia version information 83
- C.2 Notebook Preamble 85

Index 95

LIST OF FIGURES

1 Interacting spins. 5

1.1 The original Stern-Gerlach experiment [2]. 10
1.2 Early detection plates from a postcard Gerlach sent to Niels Bohr (Courtesy of the Niels Bohr Archive in Copenhagen). 10

2.1 Elementary excitation spectra of the transverse-field Ising model across g. 31
2.2 $M_z = \left\langle \sigma_i^z \right\rangle /2$ as a function of $g/2 = \Gamma/J$ [25]. The dotted line is the result from mean-field theory. *Reprinted under STM guidelines [30].* 32

3.1 A spaghetti diagram [33]. 44
3.2 Example time evolution for $N = 2$ spins. 54
3.3 Exponential fit for $N = 2$ spins. 54
3.4 Energy levels of eq. (2.34) for $N = 2$ spins. 55
3.5 Dissipation rate spaghetti diagram for $N = 2$ spins. 55
3.6 Example time evolution for $N = 3$ spins. 56
3.7 Exponential fit for $N = 3$ spins. 56
3.8 Energy levels of eq. (2.34) for $N = 3$ spins. 57
3.9 Dissipation rate spaghetti diagram for $N = 3$ spins. 57
3.10 Example time evolution for $N = 4$ spins. 58
3.11 Exponential fit for $N = 4$ spins. 58
3.12 Energy levels of eq. (2.34) for $N = 4$ spins. 59
3.13 Dissipation rate spaghetti diagram for $N = 4$ spins. 59
3.14 Example time evolution for $N = 5$ spins. 60
3.15 Exponential fit for $N = 5$ spins. 60
3.16 Energy levels of eq. (2.34) for $N = 5$ spins. 61
3.17 Dissipation rate spaghetti diagram for $N = 5$ spins. 61
3.18 Single-spin relaxation rates in different temperature regimes for $N = 2$ spins. 62

3.19 Single-spin relaxation rates in different temperature regimes for $N = 3$ spins. 63
3.20 Single-spin relaxation rates in different temperature regimes for $N = 4$ spins. 64
3.21 Single-spin relaxation rates in different temperature regimes for $N = 5$ spins. 65

INTRODUCTION

Applications of quantum mechanics include exciting topics like the many-body physics of materials like high-temperature superconductors, or new technologies for quantum sensing and computation. One barrier towards making progress in these areas is that quantum systems are notoriously difficult to simulate. Consider simulating eight interacting spins (fig. 1), which can be thought of as similar to bar magnets. The analog in classical computing is to manipulate memory on the scale of a few bytes (8 bits), which is trivial to do. However, the way that we will simulate the spins requires diagonalizing a matrix with dimension $4^8 = 65\,536$, which is significantly more difficult.

Figure 1: Interacting spins.

Nonetheless, this thesis must take the classical simulation approach to address another barrier to these technologies: decoherence. Any novel quantum system that we create is not isolated from the rest of the world. On one hand, it is difficult to perfectly isolate a system, and on the other hand, if the system were perfectly isolated, we could not communicate with it. Due to the inevitable interaction of a system with its environment, the quantum states that an experimenter so carefully sets up threaten to be destroyed with time. If the quantum state of the spins is like a house of cards, then environment-induced decoherence is a bit like leaving the cards out in the rain. Depending on how hard it rains, the cards may fall sooner or later. The cards might even buckle with no rain due to the humidity of being outside. An important aspect of the different approaches to making quantum computers is the coherence time: how long the quantum state goes without being destroyed.

In the context of quantum computing, this decoherence is often modeled as a kind of random error, like a bit flipping unexpectedly. However, this is not the full story for decoherence. We generally expect the interaction with an environment at some temperature to result in the system relaxing towards that temperature, like an ice cube melting in the sun. The rate at which this happens depends on the details of the interaction with the environment and the system itself. A bit flip type model for decoherence may be too reductive. The situation is like timing how long it takes an ice cube to melt in the sun, and then trying to use that to predict how long it takes an ice sculpture to melt. If the sculpture is a bigger ice cube, you might predict well, but if the sculpture is a snowman under an ice umbrella, your calculations might be off by quite a bit. This thesis will investigate a particular model of interacting spins to assess the effect of system composition on the relaxation time.

In particular, chapter 1 will review quantum mechanics and develop the relevant theory of open quantum systems needed to study the relaxation of a system due to environment-induced decoherence. Chapter 2 will give a simple application of the theory to a two-level atom, and then discuss a more involved application to our main system of study, the transverse-field Ising model. These results will then enable numerical computations for the relaxation rates of the transverse-field Ising model in chapter 3, which we will use to assess the effect of the spin interactions on relaxation.

NOTE ON NOTATION

The mathematical formalism for quantum mechanics requires three levels of linear algebra: vectors, operators (maps between vectors), and superoperators (maps between operators). We will write each object with slightly differerent notation so that the type of an expression may be inferred if the reader is confused.

Vector	$\lvert v\rangle$	Real numbers	$\mathbb{R}$
$\lvert v\rangle$ in coordinates	$\boldsymbol{v}$	Complex numbers	$\mathbb{C}$
Tuple	$\boldsymbol{n}$	Integers modulo n	$\mathbb{Z}_n$
Operator	A	Hilbert space	$\mathcal{H}$
Vector operator	$\boldsymbol{B}$	Bounded operators	$\mathcal{B}(\mathcal{H})$
A in coordinates	$\boldsymbol{A}$	Liouville space	$\mathcal{L}(\mathcal{H})$
Superoperator	$\mathcal{A}$	Hamiltonian operator	H
One	1	Density operator	ρ
Identity operator	1	Pauli operators	σ_i
Identity superoperator	$\mathbb{1}$	Spin operators	$S_i = \hbar\sigma_i/2$
Zero	0	Inner product on $\mathcal{L}$	$\langle A\vert B\rangle$
Zero operator	0	Transpose of $\boldsymbol{A}$	$\boldsymbol{A}^\top$
Zero superoperator	$\mathbb{0}$	Adjoint of A	$A^\dagger$
		Trace of A	$\operatorname{tr} A$
Sign of x	$\operatorname{sgn} x$	Partial trace over S	tr_S
Sinc function	$\operatorname{sinc} x = \dfrac{\sin x}{x}$	Expected value of A	$\langle A\rangle = \operatorname{tr}(\rho A)$
		Hermitian part of A	$\operatorname{He} A = \dfrac{A + A^\dagger}{2}$

The text uses **natural units** where $\hbar = c = m_e = 1$ and $\mu_0 = 4\pi$.

This is the color version of the document. Plots, code, and links are colored. Example: continue to chapter 1.

CHAPTER 1

OPEN QUANTUM SYSTEMS

SOMEBODY flips a coin. Which side will it land on? Physics should be able to provide an answer to this question. All that we need to answer this question is the initial state of the coin and the mechanics of the flipping process. However, we do not know which side the coin starts on, so the best we can do is assign probabilities to each side. Starting from heads, flipping the coin will produce either heads or tails with some probabilities, and similar if the coin starts as tails, though perhaps the probabilities are different. We may then assign probabilities to the outcomes of the flipping operation (heads or tails), given the initial belief for the probabilities of each starting side. In doing this analysis, we have neglected all details about the atomic composition of the coin and the details of how the coin is flipped. This situation suggests a new way of looking at the coin. If we are only interested in determining the side the coin lands on, then we may model the system with only the probabilities of the different flip outcomes, and we do not need to consider the positions and momenta of the atoms that make up the coin. Just as Newtonian mechanics abstracts away the atomic details of the coin and only considers an effective Newtonian system with an ideal rigid body, we may consider "coin mechanics" where we abstract away details and consider an ideal "coin system." A coin system would specify an initial "coin state" and the probabilities needed to analyze the flipping operation. Such a probabilistic theory is more general than classical mechanics, which requires deterministic operations.

In 1924, a similar situation was discovered in a beam of silver atoms by Otto Stern and Walther Gerlach [1]. With the apparatus in fig. 1.1, silver atoms were vaporized in a furnace, passed through collimators, subjected to a non-uniform magnetic field, and then detected on a plate. The initial state of a silver atom is thought to be random (isotropic) because of

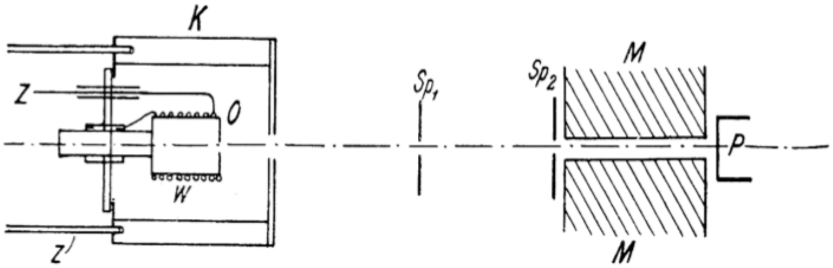

Figure 1.1: The original Stern-Gerlach experiment [2].

the furnace and the lack of a reason to think otherwise, and the operation being performed is simply that of waiting until the atom hits the plate. Surprisingly, the plate looked like fig. 1.2. With no magnet (left), the atoms are not deflected, yet with the magnet (right), the atoms are separated cleanly into two beams. This happens for all orientations of the magnet around the beam. As experiments of this type improved, it became clear that the classical probability theory used in a coin system was insufficient to describe which side a silver atom would be deflected towards. Rather than coin mechanics, a new theory known as **quantum mechanics** emerged. This theory uses a different mathematical formalism to calculate the probabilities of outcomes, and provides some guidance on how to represent physical systems within that formalism.

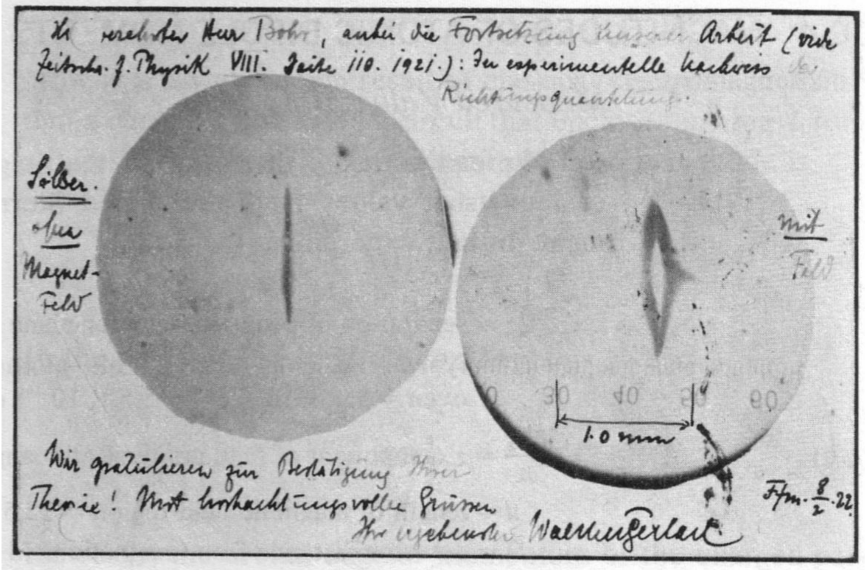

Hochverehrter Herr Bohr, anbei die Fortsetzung unserer Arbeit (vide Zeitschr. f. Physik VIII. Seite 110. 1921.): Der experimentelle Nachweis der Richtungsquantelung.

Silber. ohne Magnet-Feld

mit Feld

Wir gratulieren zur Bestätigung Ihrer Theorie! Mit hochachtungsvollen Grüssen
Ihr ergebenster Walther Gerlach

Ffm. $\frac{8}{2}$.22

30
40
50
60
1.0 mm

Figure 1.2: Early detection plates from a postcard Gerlach sent to Niels Bohr (Courtesy of the Niels Bohr Archive in Copenhagen).

We will develop this quantum theory from the ground up. Sections 1.1 to 1.4 have some overlap with the standard undergraduate curriculum. However, because we use a fully general notion of the quantum state without any reference to a physical system, the development is initially different from the usual approach that considers the wavefunctions of particles. In particular, section 1.2 on composite systems is not usually covered. After these preliminaries, we start to develop the theory of open quantum systems in section 1.5.

1.1 THE MATHEMATICAL FORMALISM

Different mathematical formalisms for quantum theory differ in how they represent states and operations, but they agree on the assignment of probabilities to outcomes. We will now give postulates for the widely used Hilbert space description of the quantum probability theory.

Postulate 1. A quantum system is described by a separable complex Hilbert space $\mathcal{H}$.[1]

Postulate 2. An outcome corresponds to an **effect** E, which is a Hermitian operator on $\mathcal{H}$ such that $0 \leqslant E \leqslant 1$.[2]

Postulate 3. A state corresponds to a **probability measure** P on effects. That is:

1. $0 \leqslant P(E) \leqslant 1$ for all effects E,
2. $P(1) = 1$,
3. $P(E_1 + E_2 + \cdots) = P(E_1) + P(E_2) + \cdots$ for any sequence of events with $E_1 + E_2 + \cdots \leqslant 1$.

Postulate 4. States form a convex set. If $\sum_i p_i = 1$, the convex sum of states $\{P_i\}$ is defined by

$$\left(\sum_i p_i P_i\right)(E) = \sum_i p_i P_i(E). \tag{1.1}$$

Such a combination is known as an **ensemble**.

Note that the convex structure of the set of quantum states is necessary for consistency. One must obtain the same results when one makes two state assignments, predicts outcomes for each, and averages the results, as when one assigns the average state first and then predicts outcomes.

---

[1] Since a quantum system is identified only by its dimension d, we may wonder which d-dimensional Hilbert space to assign. However, all finite d-dimensional (separable) complex Hilbert spaces are isometrically isomorphic to $\mathbb{C}^d$, and all infinite-dimensional separable Hilbert spaces are isometrically isomorphic to ℓ^2 (square-summable sequences) and to L^2 (square-integrable functions).

[2] The notation $A \leqslant B$ means that $\langle v|A|v\rangle \leqslant \langle v|B|v\rangle$ for all $v \in \mathcal{H}$.

It is simple to prove that any probability measure P on an effect E may be represented by the **Born rule**

$$P(E) = \operatorname{tr}(\rho E), \tag{1.2}$$

where $\rho \geqslant 0$ is a Hermitian operator known as a **density operator** [3, 4].[3] Equation (1.2) implies that $\operatorname{tr}\rho = 1$ and that a convex sum of states is represented by the same sum of density operators. The Born rule uniquely identifies density operators with states, so we will use the term state to refer to density operators from now on.

An **observable** result of an operation is described by an assignment of each outcome m to an effect E_m, where $\sum_m E_m = 1$. Since effects are positive operators that determine the probabilities of each outcome, such an observable is called a **positive operator valued measure** (POVM). The special case where the effects are projectors is called a **projection valued measure** (PVM). A PVM with the maximum number of outcomes may be conveniently represented by the Hermitian operator

$$M = \sum_m m \left|v_m\middle\rangle\!\middle\langle v_m\right|. \tag{1.3}$$

By virtue of this definition, the expected value of the PVM is

$$\begin{aligned}
\langle M\rangle &= \sum_m mP(m) && (1.4)\\
&= \sum_m m \operatorname{tr}(\rho \left|v_m\middle\rangle\!\middle\langle v_m\right|) && (1.5)\\
&= \operatorname{tr}\left(\rho\left(\sum_m m \left|v_m\middle\rangle\!\middle\langle v_m\right|\right)\right) && (1.6)\\
&= \operatorname{tr}(\rho M). && (1.7)
\end{aligned}$$

From here on, most observables will be PVMs represented by Hermitian operators.

We now describe how operations change states.

Postulate 5. An **operation** with outcome m is described by a map $\mathcal{O}_m$. The state ρ after the operation becomes

$$\rho'_m = P(m)^{-1}\mathcal{O}_m(\rho). \tag{1.8}$$

---

[3] The more specific case where effects are restricted to be projections $|v\rangle\langle v|$ for $v \in \mathcal{H}$ is significantly harder, and is known as Gleason's theorem [5].

Since ρ'_m must be a density operator, postulate 5 implies that $\mathcal{O}_m\rho \geqslant 0$ and

$$\operatorname{tr}\mathcal{O}_m(\rho) = P(m) = \operatorname{tr}(\rho E_m). \tag{1.9}$$

If an operation is performed but the outcome is unknown, we may assign the state

$$\rho' = \sum_m P(m)\rho'_m = \sum_m \mathcal{O}_m(\rho), \tag{1.10}$$

so that the next outcome with effect E has the expected probability

$$\begin{aligned} P(E) &= \operatorname{tr}(\rho' E) && (1.11)\\ &= \sum_m P(m)\operatorname{tr}(\rho'_m E) && (1.12)\\ &= \sum_m P(m)P(E\,|\,m). && (1.13) \end{aligned}$$

The state of the ensemble $\rho = \sum_i p_i\rho_i$ after an operation with outcome m is

$$\frac{\mathcal{O}_m(\rho)}{\operatorname{tr}\mathcal{O}_m(\rho)} = \sum_i P(i\,|\,m)\frac{\mathcal{O}_m(\rho_i)}{\operatorname{tr}\mathcal{O}_m(\rho_i)} \tag{1.14}$$

By Bayes' theorem,

$$P(i\,|\,m) = \frac{P(i)P(m\,|\,i)}{P(m)} = \frac{p_i\operatorname{tr}\mathcal{O}_m(\rho_i)}{\operatorname{tr}\mathcal{O}_m(\rho)}. \tag{1.15}$$

Now eq. (1.14) becomes

$$\mathcal{O}_m\left(\sum_i p_i\rho_i\right) = \sum_i p_i\mathcal{O}_m(\rho_i). \tag{1.16}$$

Thus operations are convex linear.

1.2 COMPOSITE SYSTEMS

The success of physics lies in the apparent lack of causal connections between phenomena separated in space and time. Different things are different, and the actions of someone on the other side of the world have no immediate effect on an experiment performed now. We then expect that some physical systems are composed of a number of subsystems. The whole system may be affected as different parts that each respond the same way as if nothing else was there.[4]

---

[4] For example, we will later consider each spin in a spin chain to be a subsystem, since each spin may be separately affected. However, each of two electrons would not be a subsystem, since removal of one electron changes where the other electron is likely to be found.

Given a quantum system with Hilbert space $\mathcal{H}$, a decomposition into **subsystems** is described by Hilbert spaces $\mathcal{H}_i$ with $\prod_i \dim \mathcal{H}_i = \dim \mathcal{H}$ and maps f_i, g_i such that

$$\operatorname{tr}(\rho f_i(E_i)) = \operatorname{tr}(g_i(\rho) E_i) \tag{1.17}$$

for any state ρ on $\mathcal{H}$ and effect E_i on $\mathcal{H}_i$. The maps f_i lift an effect from the subsystem to the composite system, while the g_i reduce a composite state to a subsystem state.

What are f_i and g_i? We will first consider their action on states of definite composition. Consider states ρ_A and ρ_B on $\mathcal{H}_A$ and $\mathcal{H}_B$ where $\dim \mathcal{H}_A \dim \mathcal{H}_B = \dim \mathcal{H}$. How do we represent the **product state** ρ, which satisfies $g_A(\rho) = \rho_A$ and $g_B(\rho) = \rho_B$? Perhaps ρ is just the pair (ρ_A, ρ_B). By postulate 4, a convex combination of such pairs is also a composite state. However, suppose that $\rho_A = \sum_i \alpha_i \rho_i^A$ and $\rho_B = \sum_j \beta_j \rho_j^B$. We mean the same state when we consider either an ensemble of composites or a composite of ensembles, which is the equivalence

$$\left(\sum_i \alpha_i \rho_i^A, \sum_j \beta_j \rho_j^B \right) \sim \sum_{ij} \alpha_i \beta_j \big(\rho_i^A, \rho_j^B \big) \tag{1.18}$$

on the composite states. Thus the product state is not a pair, but an equivalence class $[(\rho_A, \rho_B)]$ of $(\mathcal{B}(\mathcal{H}_A) \times \mathcal{B}(\mathcal{H}_B))/{\sim}$. These classes are called **tensors**. The product state equivalence class is written with the **tensor product** as $\rho_A \otimes \rho_B$, and the whole space is called $\mathcal{B}(\mathcal{H}_A) \otimes \mathcal{B}(\mathcal{H}_B) \cong \mathcal{B}(\mathcal{H})$.[5] The same argument gives the **product effect** $E_A \otimes E_B$. Yet the same could be said for the operator $\rho_A E_A$, which leads us to define $(\rho_A \otimes \rho_B)(E_A \otimes E_B) = \rho_A E_A \otimes \rho_B E_B$.

What is $\operatorname{tr}(A \otimes B)$? Product effects represent independent events. For the probabilities to multiply, we must have

$$\operatorname{tr}(A \otimes B) = \operatorname{tr} A \operatorname{tr} B. \tag{1.19}$$

Thus an effect E_A is lifted as $f_A(E_A) = E_A \otimes 1$.

We now extend to non-product states, which are called **entangled** states. Consider a map

---

[5] Is this Hilbert space separable as required by postulate 1? Yes, but later we will consider a bath described by an infinite tensor product of harmonic oscillators. Such a Hilbert space is not separable, but the subspace that is physically relevant is separable. Since we will neglect high-frequency modes anyway, it also suffices to truncate the product once the energies are sufficiently high. For more discussion, see [6, pp. 84–87].

f of the f_i and the countable sum of events $E = \sum_a E_a$. By eq. (1.17),

$$\operatorname{tr}\left(\rho \sum_a f(E_a)\right) = \sum_a \operatorname{tr}\left(\rho f(E_a)\right) \tag{1.20}$$

$$= \sum_a \operatorname{tr}\left(g(\rho) E_a\right) \tag{1.21}$$

$$= \operatorname{tr}\left(g(\rho) \sum_a E_a\right) \tag{1.22}$$

$$= \operatorname{tr}\left(\rho f\left(\sum_a E_a\right)\right) \tag{1.23}$$

for all ρ. Thus f is countably additive. If $E_1 \leqslant E_2$, then

$$0 \leqslant \operatorname{tr}(g(\rho)(E_2 - E_1)) \tag{1.24}$$

$$= \operatorname{tr}(\rho f(E_2 - E_1)), \tag{1.25}$$

so $f(E_1) \leqslant f(E_2)$. It then follows that the f_i are convex.[6] By symmetry, the same argument shows that the g_i are convex.

The map g_A is known as a **partial trace**. The partial trace over B of $\rho_A \otimes \rho_B$ is

$$g_A(\rho) = \operatorname{tr}_B(\rho_A \otimes \rho_B) \equiv \rho_A \operatorname{tr} \rho_B = \rho_A, \tag{1.26}$$

and is extended linearly to combinations of product states.

1.3 CLOSED DYNAMICS

Now that we have described the composition of quantum systems, how do they change in time? We are often interested in the case where the information held by the quantum state does not change. This is called a **closed** quantum system. While all isolated physical systems are thought to correspond to closed quantum systems, the converse is not true. For example, atomic spins subject to external control from lasers are still closed systems.

The change in a closed system is the result of an operation $\mathcal{O}$ with a single, definite outcome. The operation $\mathcal{O}$ is convex by eq. (1.16). Since the information in the state ρ cannot change, $\mathcal{O}$ must be invertible. Kadison's theorem[7] states that all such operations have the form

$$\mathcal{O}(\rho) = U \rho U^\dagger, \tag{1.27}$$

---

[6] The argument is the same as that for the real linearity of a probability measure on effects given in [4].

[7] Wigner's theorem on symmetries of pure states is a special case [7, p. 77]. Many similar results hold, such as that only unitary transformations preserve the entropy (relative or not) [8, 9].

where the operator U is either **unitary** ($U^\dagger U = 1$) or **antiunitary** ($U^\dagger U = -1$) [7, 10].

In contexts like quantum computation or control, all that matters is the state before and after the operation. To consider the notion of an isolated physical system, we must relate the quantum state to the physical time. We then have an operator $U(t)$ which gives the state

$$\rho(t) = U(t)\rho(0)U^\dagger(t) \tag{1.28}$$

as a function of time. We expect that $U(t)$ changes continuously[8] and satisfies

$$U(t + t') = U(t)U(t') \tag{1.29}$$

for real t, t'. Then since $U(0) = 1$ is unitary, $U(t)$ is unitary. We would like a description of $U(t)$ that does not depend on time. This is provided by Stone's theorem [12], which states that there is a Hermitian operator H such that

$$U(t) = e^{-\mathrm{i}Ht}. \tag{1.30}$$

This allows us to differentiate eq. (1.28) to find

$$\begin{aligned}\dot\rho &= \dot U(t)\rho(0)U^\dagger(t) + U(t)\rho(0)\dot U^\dagger(t) && (1.31)\\ &= -\mathrm{i}H\big(U(t)\rho(0)U^\dagger(t)\big) + \big(U(t)\rho(0)U^\dagger(t)\big)\mathrm{i}H && (1.32)\\ &= -\mathrm{i}[H, \rho], && (1.33)\end{aligned}$$

which is known as the **Liouville** or **von Neumann equation**.[9]

Given an observable A, its expected value over time is

$$\begin{aligned}\langle A\rangle &= \mathrm{tr}(\rho(t)A) && (1.34)\\ &= \mathrm{tr}\big(U(t)\rho(0)U^\dagger(t)A\big) && (1.35)\\ &= \mathrm{tr}\big(\rho(0)U^\dagger(t)AU(t)\big). && (1.36)\end{aligned}$$

This suggests that the state may be regarded as constant, while an observable changes in time as

$$A_H(t) = U^\dagger(t)AU(t). \tag{1.37}$$

---

[8] More precisely, $U(t)$ is **strongly continuous** if $\lim_{t\to t_0} U(t)\,|v\rangle = U(t_0)\,|v\rangle$ for all real t_0 and $|v\rangle \in \mathcal{H}$. Stone's theorem is novel since it allows us to consider the time derivative of $U(t)$, even though we only assume that the map $t \mapsto U(t)$ is strongly continuous. Von Neumann showed that the strong continuity requirement may be relaxed to only being weakly measurable [11].

[9] Equation (1.33) is given in **natural units** where $\hbar = c = m_e = 1$ and $\mu_0 = 4\pi$. Otherwise $\dot\rho = -\mathrm{i}[H, \rho]/\hbar$.

This perspective is known as the **Heisenberg picture**, and leads to the analogous **Heisenberg equation of motion**

$$\dot{A}_H = -\mathrm{i}[A_H, H] \tag{1.38}$$

for observables. For reference, the usual perspective where the state changes in time is known as the **Schrödinger picture**.

1.4 CANONICAL QUANTIZATION

The discussion of quantum theory thus far has been fully general. The Liouville equation (eq. (1.33)) specifies how a state ρ changes in time, given the Hilbert space for the system, the operator H, and the initial state $\rho(0)$. How does one determine these quantities for a particular physical system? We will only consider physical systems that can be modeled by nonrelativistic classical mechanics. Consider a classical system with generalized coordinates q_i and momenta p_i. If the system has classical Hamiltonian $H(\boldsymbol{q}, \boldsymbol{p})$, then Hamilton's equations of motion are

$$\dot{q}_i = \frac{\partial H}{\partial p_i} = \{q_i, H\} \tag{1.39}$$

$$\dot{p}_i = -\frac{\partial H}{\partial q_i} = \{p_i, H\}, \tag{1.40}$$

in terms of the **Poisson bracket**

$$\{f, g\} = \sum_i \left(\frac{\partial f}{\partial q_i}\frac{\partial g}{\partial p_i} - \frac{\partial g}{\partial q_i}\frac{\partial f}{\partial p_i} \right). \tag{1.41}$$

We notice that Hamilton's equations are similar to the Heisenberg equations of motion

$$\dot{q}_i = -\mathrm{i}[q_i, H] \tag{1.42}$$

$$\dot{p}_i = -\mathrm{i}[p_i, H], \tag{1.43}$$

where the time-evolution operator H takes the place of the Hamiltonian. This suggests the idea of a quantization map Q that maps functions f and g on phase space to operators. We expect that $Q(1) = 1$, $Q(q_i) = q_i$ and $Q(p_i) = p_i$. Then to obtain the Heisenberg equations of motion we must require that

$$Q(\{f, g\}) = -\mathrm{i}[Q(f), Q(g)]. \tag{1.44}$$

In particular, since $\left\{q_i, p_j\right\} = \delta_{ij}$, Q must yield the **canonical commutation relations** (CCRs)

$$\left[q_i, p_j\right] = \mathrm{i}\delta_{ij}. \tag{1.45}$$

For the moment, consider a classical system with only one degree of freedom.[10] One can show that the only possible quantization for polynomials in q and p with degree less than four is the **Weyl quantization**. This simply averages over all possible operator orders.[11] For example,

$$Q(3qp^2) = qp^2 + pqp + p^2q. \tag{1.47}$$

What about a degree four polynomial like q^2p^2? One may compute that

$$q^2p^2 = \frac{1}{9}\{q^3, p^3\} = \frac{1}{3}\{q^2p, qp^2\}, \tag{1.48}$$

yet

$$\frac{1}{9}\big[Q(q^3), Q(p^3)\big] \neq \frac{1}{3}\big[Q(q^2p), Q(qp^2)\big], \tag{1.49}$$

so there is no quantization of q^2p^2. This result on the nonexistence of a general quantization map is known as Groenewold's theorem [14, p. 272]. Luckily, we will only consider systems where the Weyl quantization satisfies eq. (1.44), and we may put the issue of quantization aside.

Now we know that q and p must satisfy the CCR. But what are they? Weyl showed that q and p must be operators on an infinite-dimensional Hilbert space [15]. The usual assignment for square-integrable functions f is $qf(q) = qf(q)$ and $pf(q) = -\mathrm{i}f'(q)$, which satisfies the CCR. How do we know that this is the right assignment? What if one should assign a different Hilbert space $\mathcal{H}$ with other position and momentum operators q' and p'? By Stone's theorem, there are unitary operators $U(t) = e^{\mathrm{i}tq'}$ and $V(s) = e^{\mathrm{i}sp'}$. Then a formal application of the Baker-Campbell-Hausdorff (BCH) formula[12] gives that

$$U(t)V(s) = e^{-\mathrm{i}st}V(s)U(t), \tag{1.51}$$

---

[10] All the considerations to follow generalize naturally to many degrees of freedom.

[11] In general, the Weyl quantization of f is

$$Q(f) = \exp\left(\frac{1}{2\mathrm{i}}\sum_i \frac{\partial^2}{\partial q_i \partial p_i}\right)\hat{f}(\boldsymbol{q}, \boldsymbol{p}), \tag{1.46}$$

where $\hat{f}$ is f in the normal form where q_i always precedes p_i [13].

[12] Namely that if $[A, [A, B]] = [B, [A, B]] = 0$, then

$$e^A e^B = e^{A+B+[A,B]/2}. \tag{1.50}$$

which is known as the Weyl relation [14, p. 281].[13] The Stone-von Neumann theorem[14] is that there is a unitary operator $T : L^2(\mathbb{R}) \to \mathcal{H}$ such that

$$T^\dagger U(t) T = e^{itq} \tag{1.52}$$

$$T^\dagger V(s) T = e^{isp}. \tag{1.53}$$

Differentiating and setting $t = s = 0$ then gives that

$$T^\dagger q' T = q \tag{1.54}$$

$$T^\dagger p' T = p. \tag{1.55}$$

Given a density operator ρ on $L^2(\mathbb{R})$, we may assign a density operator on $\mathcal{H}$ by $\rho' = T\rho T^\dagger$, which satisfies that

$$\operatorname{tr}(\rho' q') = \operatorname{tr}(\rho q) \tag{1.56}$$

$$\operatorname{tr}(\rho' p') = \operatorname{tr}(\rho p), \tag{1.57}$$

and similar for polynomials in p and q. Thus the predictions of quantum theory do not depend on the representation of a system's canonical coordinates, and we are justified in making the usual assignment for q and p.

1.5 OPEN DYNAMICS

An **open system** is a quantum system where the information held by the quantum state may change. We will consider only open quantum systems that model interacting physical systems. First, a larger closed system $\mathcal{H}$ is identified and separated into two subsystems: the open system $\mathcal{H}_S$ of interest and the environment or bath $\mathcal{H}_B$ that the open system interacts with. We know that the initial state of the open system is ρ_0. The system is said to follow **open dynamics** if the state at time t is determined by the following procedure.

1. The state ρ_0 is promoted to a state of the composite system according to an **assignment map** $\mathcal{A}(\rho_0)$. A consistent assignment map should have the following intuitive properties: [16]

   (a) $\mathcal{A}$ is convex,

---

[13] Since the Weyl relation was derived through a merely formal procedure, not all operators satisfying the CCR satisfy the Weyl relation. The usual q and p do satisfy the Weyl relation, so we may as well stipulate that any putative operators q' and p' must satisfy it as well.

[14] The Stone-von Neumann theorem was also used to prove the equivalence between the Schrödinger equation and Heisenberg's matrix mechanics.

   (b) $\mathrm{tr}_B\,\mathcal{A}(\rho_0) = \rho_0$,

   (c) $\mathcal{A}(\rho_0)$ is a density operator.

2. The assigned composite state becomes $\rho(t) = U(t)\mathcal{A}(\rho_0)U^\dagger(t)$ as usual for a closed system.

3. The state $\rho(t)$ is reduced to give the open system state $\rho_S(t) = \mathrm{tr}_B\,\rho(t)$.

In summary, the state at time t is

$$\rho_S(t) = \mathrm{tr}_B(U(t)\mathcal{A}(\rho_0)U^\dagger(t)), \tag{1.58}$$

which we may express as the **dynamical map** $\mathcal{V}(t)\rho_S(0) = \rho_S(t)$. Note that property (b) of $\mathcal{A}$ ensures that $\rho_S(0) = \rho_0$, which is consistent.

One can show that the only consistent assignment maps for a two-dimensional system are of the form $\mathcal{A}(\rho_0) = \rho_0 \otimes \rho_B$, where ρ_B is a constant density operator on $\mathcal{H}_B$ [17]. We will consider ρ_B to be a stationary state of the bath, such as a thermal state at some temperature. Why do we not require that the composite state $\rho(t)$ is always assignable, remaining within the image of $\mathcal{A}$? This would make $\mathcal{V}$ satisfy that

$$\mathcal{V}(t+s) = \mathcal{V}(t)\mathcal{V}(s). \tag{1.59}$$

Since ρ_B does not change in time, this requires that the system does not interact with the bath. The only allowed open systems would be closed systems! What is wrong with requiring the composite state to be assignable? The issue is that interactions will inevitably entangle the system with the bath, causing one to be unable to consider the composite as the two subsystems in the product assignment.

However, we are interested in the reduced dynamics of the system, and what happens on the timescale τ_R where the system changes appreciably. If the timescale of the correlations in the bath is τ_C, then from the perspective of a system with $\tau_C \ll \tau_R$, the bath is effectively stationary. Thus $\rho(t)$ is approximately assignable if we only aim to consider the coarse-grained system dynamics. The notion of reduced dynamics only makes sense on system timescales, and requires several conditions on eq. (1.58) for the coarse-graining to be possible. Since the system must be weakly coupled to the bath for the bath to remain approximately stationary, these simplifications are collectively called the **weak-coupling limit**.

This process will lead to a differential equation (eq. (1.100)) for ρ_S. It is worth mentioning that this equation, known as the Lindblad equation, is in the general form for any map

$\mathcal{V}(t)$ on density matrices that satisfies eq. (1.59), with the technical condition that it is also completely positive.[15] This is shown in appendix A. On these grounds, it is often asserted that all reduced dynamics must be completely positive. This is not the case if the initial condition of the composite system is not a product state, and we have argued that the notion of reduced dynamics does not make sense outside of the weak-coupling limit. The debate concerning complete positivity remains a contentious issue [17, 19, 20].

1.6 THE WEAK-COUPLING LIMIT

We will now determine the conditions on the Hamiltonian of the composite system that give rise to reduced dynamics when the bath is in an equilibrium state ρ_B. We decompose the Hamiltonian as

$$\begin{aligned} H &= H_0 + H_I && (1.60) \\ &= H_S \otimes 1 + 1 \otimes H_B + H_I, && (1.61) \end{aligned}$$

where H_S is the Hamiltonian of the system, H_B is the Hamiltonian of the bath, and H_I is the interaction Hamiltonian between the system and the bath. First, we will recast the dynamics of the composite system into a convenient form. Recall the Heisenberg picture from section 1.3. Given eq. (1.60), we may similarly decompose the expected value of an observable A for the composite system. If we let

$$\begin{aligned} U_0(t) &= e^{-\mathrm{i}H_0 t} && (1.62) \\ U_I(t) &= U_0^\dagger(t)U(t), && (1.63) \end{aligned}$$

then we may decompose the expected value as

$$\begin{aligned} \langle A \rangle &= \operatorname{tr}\Big(AU(t)\rho(0)U^\dagger(t)\Big) && (1.64) \\ &= \operatorname{tr}\Big(U_0^\dagger(t)AU_0(t)\,U_I(t)\rho(0)U_I^\dagger(t)\Big). && (1.65) \end{aligned}$$

This suggests that we define the time-dependent operators

$$\begin{aligned} A_I(t) &= U_0^\dagger(t)AU_0(t) && (1.66) \\ \rho_I(t) &= U_I(t)\rho(0)U_I^\dagger(t). && (1.67) \end{aligned}$$

---

[15] For any Hilbert space $\mathcal{H}'$, define the combined operation $\mathcal{V}(t) \otimes \mathbb{1}$ by $(\mathcal{V}(t) \otimes \mathbb{1})(A \otimes B) = \mathcal{V}(t)A \otimes B$ and extending linearly. We say that $\mathcal{V}(t)$ is **completely positive** if $(\mathcal{V}(t) \otimes \mathbb{1})(C)$ is positive for every positive operator C on $\mathcal{H}_S \otimes \mathcal{H}'$ [18, p. 89].

This perspective is known as the **interaction picture**, and the associated equation of motion is

$$\dot{\rho}_I = -\mathrm{i}[H_I, \rho_I]. \tag{1.68}$$

We will use eq. (1.68) in its integral form

$$\rho_I(t) = \rho_I(0) - \mathrm{i}\int_0^t \mathrm{d}s\,[H_I(s), \rho_I(s)]. \tag{1.69}$$

It will also be helpful to relate the interaction Hamiltonian to transition frequencies of the system as follows.[16] First, we write a general interaction Hamiltonian as

$$H_I = \sum_\alpha A_\alpha \otimes B_\alpha, \tag{1.70}$$

where A_α and B_α are Hermitian. If E is an eigenvalue of H_S, let $\Pi(E)$ denote the projector onto the eigenspace for E. Now we let

$$A_\alpha(\omega) = \sum_{E'-E=\omega} \Pi(E) A_\alpha \Pi(E'), \tag{1.71}$$

which satisfy that

$$A_\alpha^\dagger(\omega) = A_\alpha(-\omega). \tag{1.72}$$

By the completeness of the energy projectors,

$$\begin{aligned} \sum_\omega A_\alpha(\omega) &= \sum_\omega \sum_{E'-E=\omega} \Pi(E) A_\alpha \Pi(E') &(1.73)\\ &= \sum_{E_1, E_2} \Pi(E_1) A_\alpha \Pi(E_2) &(1.74)\\ &= A_\alpha. &(1.75) \end{aligned}$$

The $A_\alpha(\omega)$ also satisfy

$$[H_S, A_\alpha(\omega)] = -\omega A_\alpha(\omega). \tag{1.76}$$

Using eq. (1.76) to commute past the exponential in eq. (1.66) establishes that the corresponding interaction picture operators are

$$A_\alpha^I(\omega) = e^{-\mathrm{i}\omega t} A_\alpha(\omega). \tag{1.77}$$

---

[16] This decomposition requires that the spectrum of H_S is discrete.

Thus the interaction Hamiltonian in the interaction picture is

$$H_I(t) = \sum_{\alpha\omega} e^{-\mathrm{i}\omega t} A_\alpha(\omega) \otimes B_\alpha^I(t), \tag{1.78}$$

where by eq. (1.66)

$$B_\alpha^I(t) = e^{\mathrm{i}H_B t} B_\alpha e^{-\mathrm{i}H_B t}. \tag{1.79}$$

From here on we will drop the superscript I and consider all time-dependent operators to be in the interaction picture. For example, $\rho_S(t)$ is the reduced state of the system in the interaction picture.

Since we are interested in how fluctuations in different environment modes are related, we will consider the **reservoir correlation functions**

$$\left\langle B_\alpha^\dagger(t) B_\beta(t-s) \right\rangle. \tag{1.80}$$

Because ρ_B is a stationary state of the bath, the correlation functions do not depend on time.[17] We may then express the correlation functions as

$$\left\langle B_\alpha^\dagger(s) B_\beta(0) \right\rangle \tag{1.85}$$

and consider their one-sided Fourier transforms

$$\Gamma_{\alpha\beta}(\omega) := \int_0^\infty \mathrm{d}s\, e^{\mathrm{i}\omega s} \left\langle B_\alpha^\dagger(s) B_\beta(0) \right\rangle \tag{1.86}$$

$$=: \frac{1}{2}\gamma_{\alpha\beta}(\omega) + \mathrm{i}S_{\alpha\beta}(\omega), \tag{1.87}$$

where the corresponding matrix $\boldsymbol{S} = (\boldsymbol{\Gamma} - \boldsymbol{\Gamma}^\dagger)/2\mathrm{i}$ is Hermitian and the matrix corresponding to the full Fourier transforms

$$\gamma_{\alpha\beta}(\omega) = \int_{-\infty}^\infty \mathrm{d}s\, e^{\mathrm{i}\omega s} \left\langle B_\alpha^\dagger(s) B_\beta(0) \right\rangle \tag{1.88}$$

is positive.

---

[17] To see this, we use the product rule, eq. (1.38), and the fact that $[\rho_B, H_B] = 0$ to find that

$$\frac{\mathrm{d}}{\mathrm{d}t}\left\langle B_\alpha^\dagger(t) B_\beta(t-s) \right\rangle = \mathrm{i}\left\langle \left[H_B, B_\alpha^\dagger(t)\right] B_\beta(t-s) + B_\alpha^\dagger(t)\left[H_B, B_\beta(t-s)\right] \right\rangle \tag{1.81}$$

$$= \mathrm{i}\left\langle H_B B_\alpha^\dagger(t) B_\beta(t-s) - B_\alpha^\dagger(t) B_\beta(t-s) H_B \right\rangle \tag{1.82}$$

$$= \mathrm{i}\,\mathrm{tr}\Big([\rho_B, H_B] B_\alpha^\dagger(t) B_\beta(t-s)\Big) \tag{1.83}$$

$$= 0. \tag{1.84}$$

With this setup, we may now move to the main derivation of the Lindblad equation in the interaction picture. Applying eq. (1.68) to eq. (1.69) and tracing out the environment gives the closed equation

$$\dot{\rho}_S(t) = -\int_0^t \mathrm{d}s \, \mathrm{tr}_B \, [H_I(t), [H_I(s), \rho_S(s) \otimes \rho_B]] \tag{1.89}$$

for the system density operator. In doing so we have made two assumptions. The first is the **Born approximation**, which states that ρ_B is stationary (in the coarse-grained sense mentioned previously):

$$\rho(t) = \rho_S(t) \otimes \rho_B. \tag{1.90}$$

The second is the **weak-coupling approximation**, which states that

$$\mathrm{tr}_B \, [H_I(t), \rho(0)] = 0. \tag{1.91}$$

Because

$$\begin{aligned}
\mathrm{tr}_B \, [H_I(t), \rho(0)] &= \sum_\alpha \left(A_\alpha(t)\rho_S(t) \, \mathrm{tr}(B_\alpha(t)\rho_B) - \rho_S(t) A_\alpha(t) \, \mathrm{tr}(\rho_B B_\alpha(t)) \right) && (1.92) \\
&= \sum_\alpha [A_\alpha(t), \rho_S(t)] \, \langle B_\alpha(t) \rangle \, , && (1.93)
\end{aligned}$$

this is equivalent to the statement that the reservoir averages of the interactions vanish:

$$\langle B_\alpha(t) \rangle = 0. \tag{1.94}$$

We would now like to perform a set of approximations that makes eq. (1.89) depend only on $\rho_S(t)$, called the **Markov approximation**. First, we suppose that $\rho_S(s) = \rho_S(t)$, so that the time-evolution only depends on the present time. Then eq. (1.89) becomes the **Redfield equation**

$$\dot{\rho}_S(t) = -\int_0^t \mathrm{d}s \, \mathrm{tr}_B \, [H_I(t), [H_I(s), \rho_S(t) \otimes \rho_B]]. \tag{1.95}$$

To simplify further, we make the substitution $s \mapsto t - s$ and set the upper limit of the integral to infinity:

$$\dot{\rho}_S = -\int_0^\infty \mathrm{d}s \, \mathrm{tr}_B \, [H_I(t), [H_I(t-s), \rho_S(t) \otimes \rho_B]]. \tag{1.96}$$

The Markov approximation is justified when the reservoir correlation functions (eq. (1.80)) vanish quickly over a time τ_C that is smaller than the relaxation time τ_R. Substituting eq. (1.78) into eq. (1.96) and using eq. (1.86) gives

$$\dot{\rho}_S = 2 \, \mathrm{He} \sum_{\alpha\beta\omega\omega'} e^{\mathrm{i}(\omega'-\omega)t} \Gamma_{\alpha\beta}(\omega) \Big(A_\beta(\omega)\rho_S A_\alpha^\dagger(\omega') - A_\alpha^\dagger(\omega') A_\beta(\omega) \rho_S \Big), \tag{1.97}$$

where $\operatorname{He} C := (C + C^\dagger)/2$. We would like eq. (1.97) to have the simple form $\dot{\rho}_S = \mathcal{L}(\rho_S)$, where $\mathcal{L}$ is a time-independent **superoperator** called the **Liouvillian**. If the typical times

$$\tau_S = |\omega' - \omega|^{-1} \quad \text{for} \quad \omega' \neq \omega \tag{1.98}$$

for system evolution are small compared to the relaxation time τ_R, then the contribution from the fast-oscillating terms of eq. (1.97) where $\omega' \neq \omega$ may be neglected. This **rotating wave** or **secular approximation** is analogous to how we consider the high-energy position distribution in the infinite square well to be uniform, even though it is actually a fast-oscillating function. We then obtain

$$\dot{\rho}_S = 2 \operatorname{He} \sum_{\alpha\beta\omega} \Gamma_{\alpha\beta}(\omega)\Big(A_\beta(\omega)\rho_S A_\alpha^\dagger(\omega) - A_\alpha^\dagger(\omega)A_\beta(\omega)\rho_S\Big). \tag{1.99}$$

Now applying the decomposition of $\Gamma_{\alpha\beta}$ (eq. (1.87)) gives the interaction picture **Lindblad equation**

$$\dot{\rho}_S = -\mathrm{i}[H_{LS}, \rho_S] + \mathcal{D}(\rho_S) := \mathcal{L}(\rho_S), \tag{1.100}$$

where the **Lamb shift Hamiltonian** is

$$H_{LS} = \sum_{\alpha\beta\omega} S_{\alpha\beta}(\omega)A_\alpha^\dagger(\omega)A_\beta(\omega) \tag{1.101}$$

and the **dissipator** is

$$\mathcal{D}(\rho_S) = \sum_{\alpha\beta\omega} \gamma_{\alpha\beta}(\omega)\Big(A_\beta(\omega)\rho_S A_\alpha^\dagger(\omega) - \frac{1}{2}\Big\{A_\alpha^\dagger(\omega)A_\beta(\omega), \rho_S\Big\}\Big). \tag{1.102}$$

To transform back to the Schrödinger picture, one only needs to add the system Hamiltonian H_S to H_{LS}. One may then diagonalize $\gamma_{\alpha\beta}$ to put eq. (1.100) into the standard form of eq. (A.17). In our examples $\gamma_{\alpha\beta}$ will already be diagonal. In this case, we call the operators $A_\alpha(\omega)$ (eq. (1.71)) in the dissipator the **jump operators** of the open system.

1.7 RELAXATION TO THERMAL EQUILIBRIUM

If the bath is in the **thermal state**

$$\rho_B = \frac{e^{-\beta H_B}}{\operatorname{tr} e^{-\beta H_B}}, \tag{1.103}$$

then we expect that the system will generally relax from any initial configuration to the thermal state

$$\rho_{\text{th}} = \frac{e^{-\beta H_S}}{\operatorname{tr} e^{-\beta H_S}}. \tag{1.104}$$

We will now prove that ρ_{th} is a stationary state. First, we see that the Lamb shift Hamiltonian commutes with the system Hamiltonian, since eq. (1.76) implies that

$$[H_S, A_\alpha^\dagger(\omega)A_\beta(\omega)] = 0. \tag{1.105}$$

Thus ρ_{th} is unchanged by the unitary part of $\mathcal{L}$, and may turn our attention towards showing that $\mathcal{D}(\rho_{\text{th}}) = 0$. We may also use eq. (1.76) to find that

$$\rho_{\text{th}} A_\alpha(\omega) = e^{\beta\omega} A_\alpha(\omega)\rho_{\text{th}} \tag{1.106}$$

$$\rho_{\text{th}} A_\alpha^\dagger(\omega) = e^{-\beta\omega} A_\alpha^\dagger(\omega)\rho_{\text{th}}. \tag{1.107}$$

We may rearrange the reservoir correlation functions to find that

$$\begin{aligned}
\left\langle B_\alpha^\dagger(t)B_\beta(0)\right\rangle &= \left(\operatorname{tr} e^{-\beta H_B}\right)^{-1} \operatorname{tr}\left(e^{-\beta H_B} B_\alpha^\dagger(t) B_\beta(0)\right) && (1.108)\\
&= \left(\operatorname{tr} e^{-\beta H_B}\right)^{-1} \operatorname{tr}\left(e^{-\beta H_B} e^{\mathrm{i}H_B t} B_\alpha e^{-\mathrm{i}H_B t} B_\beta\right) && (1.109)\\
&= \left(\operatorname{tr} e^{-\beta H_B}\right)^{-1} \operatorname{tr}\left(e^{-\beta H_B} B_\beta e^{\mathrm{i}H_B(t+\mathrm{i}\beta)} B_\alpha e^{-\mathrm{i}H_B(t+\mathrm{i}\beta)}\right) && (1.110)\\
&= \left\langle B_\beta(0) B_\alpha^\dagger(t+\mathrm{i}\beta)\right\rangle, && (1.111)
\end{aligned}$$

which is known as the the **KMS boundary condition** [21, 22].[18] Fourier-transforming eq. (1.111) gives a relation for $\gamma_{\alpha\beta}$ (eq. (1.88)):

$$\gamma_{\alpha\beta}(-\omega) = e^{-\beta\omega}\gamma_{\beta\alpha}(\omega). \tag{1.112}$$

We may then use eqs. (1.106), (1.107) and (1.112) to compute that the dissipator is

$$\begin{aligned}
\mathcal{D}(\rho_{\text{th}}) &= \sum_{\alpha\beta\omega} \gamma_{\alpha\beta}(\omega)\left(A_\beta(\omega)\rho_{\text{th}}A_\alpha^\dagger(\omega) - \frac{1}{2}\left\{A_\alpha^\dagger(\omega)A_\beta(\omega), \rho_{\text{th}}\right\}\right) && (1.113)\\
&= \sum_{\alpha\beta\omega} \gamma_{\alpha\beta}(\omega)\left(e^{-\beta\omega}A_\beta(\omega)A_\alpha^\dagger(\omega) - \frac{1}{2}A_\alpha^\dagger(\omega)A_\beta(\omega) - \frac{1}{2}A_\alpha^\dagger(\omega)A_\beta(\omega)\right)\rho_{\text{th}} && (1.114)\\
&= \left(\sum_{\alpha\beta\omega} \gamma_{\alpha\beta}(\omega)e^{-\beta\omega}A_\beta(\omega)A_\alpha^\dagger(\omega) - \sum_{\alpha\beta\omega}\gamma_{\alpha\beta}(\omega)A_\alpha^\dagger(\omega)A_\beta(\omega)\right)\rho_{\text{th}} && (1.115)\\
&= 0. && (1.116)
\end{aligned}$$

Thus $\dot{\rho}_{\text{th}} = 0$.

---

[18] The similarity between the thermal state $\rho_B \propto e^{-\beta H_B}$ and the time evolution operator $U(t) = e^{-\mathrm{i}tH_B}$ invites the study of the correlation functions in complex time. It is called a boundary condition because of its relevance for the theory of thermodynamic Green functions [23].

CHAPTER 2

APPLICATION TO INTERACTING SPINS

With the preceeding theory of open quantum systems in place, we are now in a position to consider the central problem of this thesis: How do interacting spins relax to thermal equilibrium? We will approach this question in stages, starting with a single spin.

2.1 THE CLOSED TWO-DIMENSIONAL SYSTEM

Our first task is to characterize the closed dynamics of the two-dimensional quantum system. An arbitrary two-dimensional density operator may be expressed in terms of the identity operator $1 \equiv \sigma^0$ and **Pauli operators** σ^a that satisfy the commutation relations

$$\left[\sigma^a, \sigma^b\right] = 2\mathrm{i}\varepsilon_{abc}\sigma^c, \tag{2.1}$$

where ε_{abc} is the Levi-Civita symbol. These will be abbreviated as a single vector $\boldsymbol{\sigma}$. Then a **Bloch vector** $\boldsymbol{v}$ with $|\boldsymbol{v}| \leqslant 1$ determines the density operator

$$\rho = \frac{1}{2}(1 + \boldsymbol{v} \cdot \boldsymbol{\sigma}). \tag{2.2}$$

The expectation values of the Pauli operators are $\langle \boldsymbol{\sigma} \rangle = \boldsymbol{v}$, so it suffices to determine the time evolution of $\boldsymbol{v}$. A similar vector $\boldsymbol{\omega}$ determines the general Hamiltonian[1]

$$H = \frac{1}{2}\boldsymbol{\omega} \cdot \boldsymbol{\sigma}. \tag{2.3}$$

---

[1] If the Hamiltonian $H = E1 + H_0$ includes an energy shift E, the corresponding unitary operator is $U(t) = e^{-\mathrm{i}tE}U_0(t)$. Then $U(t)\rho U^\dagger(t) = U_0(t)\rho U_0^\dagger(t)$, so there is no difference.

The Liouville equation (eq. (1.33)) is then

$$\dot{\rho} = -\frac{\mathrm{i}}{4}[\boldsymbol{\omega} \cdot \boldsymbol{\sigma}, \boldsymbol{v} \cdot \boldsymbol{\sigma}] \tag{2.4}$$

$$\frac{1}{2}\dot{\boldsymbol{v}} \cdot \boldsymbol{\sigma} = \frac{1}{2}(\boldsymbol{\omega} \times \boldsymbol{v}) \cdot \boldsymbol{\sigma}, \tag{2.5}$$

so the Bloch vector follows the differential equation

$$\dot{\boldsymbol{v}} = \boldsymbol{\omega} \times \boldsymbol{v}. \tag{2.6}$$

The solution of this equation is

$$\boldsymbol{v}(t) = e^{-t\boldsymbol{\omega}\cdot\boldsymbol{L}}\boldsymbol{v}(0), \tag{2.7}$$

where the components of $\boldsymbol{L}$ are generators of three-dimensional rotations which satisfy the commutation relations[2]

$$\left[L^a, L^b\right] = \varepsilon_{abc}L^c. \tag{2.8}$$

Thus the most general time evolution for the two-dimensional system is precession of the Bloch vector around $\hat{\boldsymbol{\omega}}$ with angular frequency ω.

2.2 RELAXATION OF THE TWO-DIMENSIONAL SYSTEM

Now what happens when a two-dimensional system is coupled to a thermal bath? The most relevant application is the electronic states of an atom coupled to the electromagnetic field. We will approximate the atom as just two energy levels: a ground and first excited state. For simplicity we will consider the system Hamiltonian

$$H_S = \frac{\omega}{2}\sigma^z, \tag{2.9}$$

where ω is the frequency of light emitted from the transition. The weak-coupling limit for the electric dipole interaction with the bath is similar to that for the magnetic dipole interaction considered later in section 2.4, so will simply state the results here and focus on investigating the dynamics.[3] To focus on the relaxation of the system, we ignore the Lamb shift and consider only the effect of the dissipator. The jump operators are

$$\sigma^{\pm} = \frac{\sigma^x \pm \mathrm{i}\sigma^y}{2} \tag{2.10}$$

---

[2] That is, $L^x\boldsymbol{r} = \boldsymbol{x} \times \boldsymbol{r}$, etc. Contrary to the norm in quantum mechanics, this representation of $\mathfrak{so}(3)$ does not use the imaginary unit i.

[3] A full derivation is given in [18, pp. 141–149].

and the simplified Lindblad equation $\dot{\rho} = \mathcal{D}\rho$ is

$$\dot{\rho} = \gamma_0(N+1)\Big(\sigma^-\rho\sigma^+ - \frac{1}{2}\{\sigma^+\sigma^-, \rho\}\Big) + \gamma_0 N\Big(\sigma^+\rho\sigma^- - \frac{1}{2}\{\sigma^-\sigma^+, \rho\}\Big), \tag{2.11}$$

where[4]

$$\gamma_0 = \frac{4}{3}|\boldsymbol{d}|^2\omega^3, \quad N = \frac{1}{e^{\beta\omega} - 1}, \tag{2.12}$$

and $\boldsymbol{d}$ is the transition matrix element of the dipole operator from the excited to ground state. Equation (2.11) describes stimulated emission with rate $\gamma_0 N$, spontaneous emission with rate γ_0, and absorption with rate $\gamma_0 N$. Substituting the density operator in the form of eq. (2.2) into the Lindblad equation gives the differential equations

$$\dot{v}_x = -\frac{\gamma}{2}v_x, \tag{2.13}$$

$$\dot{v}_y = -\frac{\gamma}{2}v_y, \tag{2.14}$$

$$\dot{v}_z = -\gamma v_z - \gamma_0, \tag{2.15}$$

where the total transition rate is

$$\gamma = \gamma_0(2N+1). \tag{2.16}$$

The equilibrium solution is seen to be

$$v_x^{\text{eq}} = v_y^{\text{eq}} = 0 \quad \text{and} \quad v_z^{\text{eq}} = -\frac{1}{2N+1}, \tag{2.17}$$

so the stationary population of the excited state is

$$n_e^{\text{eq}} = \frac{1}{2}(1 + v_z) = \frac{N}{2N+1} \tag{2.18}$$

and that of the ground state is

$$n_g^{\text{eq}} = \frac{1}{2}(1 - v_z) = \frac{N+1}{2N+1}. \tag{2.19}$$

Thus

$$\frac{n_e^{\text{eq}}}{n_g^{\text{eq}}} = \frac{N}{N+1} = e^{-\beta\omega}, \tag{2.20}$$

which is the expected Boltzmann factor from statistical mechanics. We explicitly see that v_z decays to its equilibrium value with rate γ because

$$v_z(t) = v_z^{\text{eq}} - e^{-\gamma t}\big(v_z^{\text{eq}} - v_z(0)\big). \tag{2.21}$$

---

[4] The rate γ_0 is also known as the **Einstein** A **coefficient** [24, p. 417]

2.3 THE TRANSVERSE-FIELD ISING CHAIN

We now move to studying interacting spins. Of the many interacting spin models to study, the **transverse-field Ising model**[5]

$$H = -J \sum_{i \in \mathbb{Z}_N} \left(S_i^x S_{i+1}^x + \frac{g}{2} S_i^z \right) \tag{2.22}$$

is an interesting candidate because it undergoes a so-called quantum phase transition. The model is that N spins with an anisotropic nearest-neighbor interaction in the x-direction are subject to an external magnetic field in the z-direction. We impose periodic boundary conditions so that $\sigma_N^a = \sigma_0^a$. The parameter g characterizes the strength of the magnetic field relative to the interaction energy J. To get a sense for the scale of J, take iron for reference.[6] The interaction energy for two electron spins $a = 1\,\text{Å}$ apart is [26, p. 292]

$$J_e = \frac{\mu_B^2 \mu_0}{4\pi a^3} \approx 0.05\,\text{meV}, \tag{2.23}$$

while the corresponding exchange energy is around [27, p. 325]

$$J \approx \frac{1}{2} k_B T_c \approx 45\,\text{meV}. \tag{2.24}$$

We will keep the larger value in mind. This model has also been simulated experimentally with trapped ions [28, 29].

The solution of the model by diagonalizing the Hamiltonian is straightforward but somewhat involved, so it is given in appendix B. The idea is to formally transform the interacting spins into free fermions. Each of the N free fermion modes may be occupied or not, and is indexed by numbers k that are evenly spaced across the interval the first Brillouin zone $[-\pi, \pi]$ (according to eq. (B.30)). Each mode has energy

$$E_k = \sqrt{g^2 + 2g\cos k + 1} \tag{2.25}$$

relative to $J/2$, so the total energy in a given occupation state $|\boldsymbol{n}\rangle\langle\boldsymbol{n}|$ is

$$E = \sum_k n_k E_k, \tag{2.26}$$

where each $n_k \in \{0, 1\}$. Since setting only one $n_k = 1$ excites a single mode from the ground state, eq. (2.25) also gives the energies of elementary excitations from the ground state. It is plotted for different values of g in fig. 2.1.

---

[5] The translation to Pfeuty's constants is $g = \lambda^{-1} = J/2\Gamma$ [25].

[6] α-Fe has $T_c = 1044\,\text{K}$.

```
isings = [1.5, 1.0, 0.5]'
plot([k -> √(1 + g^2 + 2g*cos(π - k)) for g in isings], xlim=(-1.0π, 1.0π),
    legendtitle=L”g”, label=[L”%$g” for g in isings], legend=:bottomright,
    xlabel=L”\pi - k”, ylabel=L”E_k”)
```

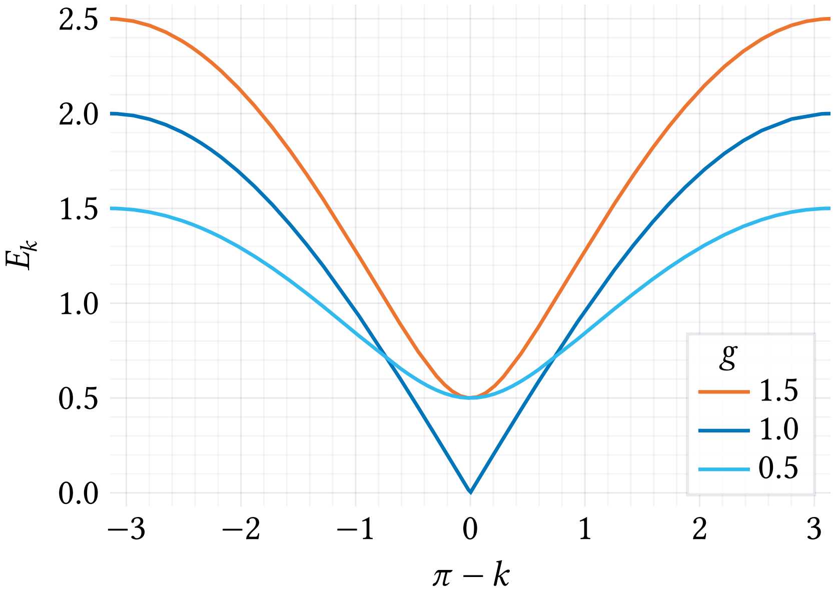

Figure 2.1: Elementary excitation spectra of the transverse-field Ising model across g.

From this, Pfeuty [25] has shown that the ground state in the continuum limit $N \to \infty$ has

$$\left\langle \sigma_i^z \right\rangle = G(0) \tag{2.27}$$

$$\left\langle \sigma_i^z \sigma_{i+n}^z \right\rangle = -G(n)G(-n), \tag{2.28}$$

where

$$G(n) = L(n) + \frac{1}{g} L(n+1) \tag{2.29}$$

$$L(n) = \frac{1}{\pi} \int_0^\pi \mathrm{d}k \, \frac{\cos(kn)}{E_k}. \tag{2.30}$$

Pfeuty's $\left\langle \sigma_i^z \right\rangle$ is shown in fig. 2.2. Similar investigation of eq. (2.28) shows evidence of a quantum phase transition at zero temperature.

- For $0 \leqslant g < 1$, the system is in a ferromagnetic ordered phase. The exchange interaction dominates and in the extreme case when $g = 0$, all spins align along the x-axis, giving the ground state twofold degeneracy.

- For $g = 1$, the system is said to undergo a quantum phase transition. The energy gap for excitations in fig. 2.1 vanishes.

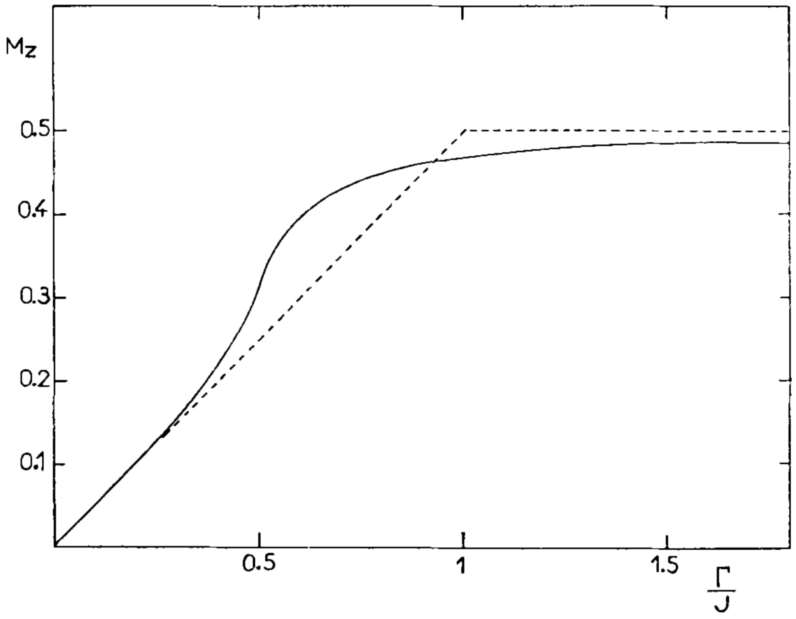

Figure 2.2: $M_z = \left\langle \sigma_i^z \right\rangle / 2$ as a function of $g/2 = \Gamma / J$ [25]. The dotted line is the result from mean-field theory. *Reprinted under STM guidelines [30].*

- For $g > 1$, the system is in a disordered phase. The transverse field dominates and in the extreme case where $g \to \infty$, all spins are aligned with the field along the z-axis.

2.4 THE WEAK-COUPLING LIMIT FOR THE ISING CHAIN

Does the presence of a quantum critical point influence the relaxation of the Ising spin chain at finite temperature, where the phase transition vanishes? What about at zero temperature, where the system may still relax due to interactions with the electromagnetic vacuum? To approach these questions, we carry out the weak-coupling limit for magnetic dipole interactions with the electromagnetic field as the bath.

Before we begin, the system Hamiltonian eq. (2.22) requires modification. We would like to study the effect of varying the parameter g on the relaxation rate of the open system. This means that we must be able to compare the rates for two system Hamiltonians H_1 and H_2. However, we are not interested in the absolute rate, but rather the rate relative to the time scale of the system. For example, if $H_2 = 2H_1$, then a system with H_2 will relax at a different rate than one with H_1. Both Hamiltonians describe the same dynamics at different time scales. Therefore, we first need to normalize the Hamiltonians with a map

$\mathcal{N}$ such that

$$\mathcal{N}(H_S) = \mathcal{N}(\alpha H_S) \tag{2.31}$$

for $\alpha > 0$. A related problem with eq. (2.22) is that we must consider $g \to \infty$ which causes the system energy to diverge. To enable comparison between different values of g, it would be convenient to consider a parameter in the interval $[0, 1]$. Both of these problems are solved by an appropriate interpolation between the extremal Hamiltonians

$$H_x = -\sum_{i\in\mathbb{Z}_N} \sigma_i^x \sigma_{i+1}^x \quad \text{and} \quad H_z = -\sum_{i\in\mathbb{Z}_N} \sigma_i^z \tag{2.32}$$

of the form

$$H_S = -J(g) \sum_{i\in\mathbb{Z}_N} \big(f(1-g)\sigma_i^x \sigma_{i+1}^x + f(g)\sigma_i^z\big). \tag{2.33}$$

The map $\mathcal{N}$ is implemented by the normalization $J(g)$ and the compactification is implemented by the function $f(g)$. A natural choice is to redefine g and use spherical linear interpolation to rotate between H_x and H_z with

$$H_S(g) = \sqrt{|H_x| \cdot |H_z|}\hat{H}_{\text{int}}(g), \quad 0 \leqslant g \leqslant 1, \tag{2.34}$$

where

$$H_{\text{int}}(g) = -\left(\frac{\sin((1-g)\theta)}{\sin\theta}\hat{H}_x + \frac{\sin(g\theta)}{\sin\theta}\hat{H}_z\right), \tag{2.35}$$

a normalized operator $\hat{A} = A/|A|$, and the angle θ between H_x and H_z are defined with respect to the inner product

$$\langle A|B\rangle = \text{tr}\big(A^\dagger B\big). \tag{2.36}$$

An overall magnitude $\sqrt{|H_x| \cdot |H_z|}$ is reintroduced so that systems with diffent numbers of spins may be more easily compared below. Because the energies are symmetric about zero ($\sum_i \tilde{E}_i = 0$), this normalization of the Hamiltonians ensures that the energy variance $\sum_i \tilde{E}_i^2$ is the same for all g. Thus the heat capacities

$$C = \frac{1}{k_B T^2}\big(\langle H_S^2\rangle - \langle H_S\rangle^2\big) \tag{2.37}$$

of any two systems for different g become the same as $\beta \to 0$ [31, p. 112]. It is in this sense that the normalization in eq. (2.34) makes different systems behave similarly.

Now we may add in the interaction with the bath. The field Hamiltonian is

$$H_B = \sum_{\boldsymbol{k},\lambda} \omega_{\boldsymbol{k}} a^{\dagger}_{\boldsymbol{k},\lambda} a_{\boldsymbol{k},\lambda}, \tag{2.38}$$

which is a collection of harmonic oscillators: one for each wavenumber $\boldsymbol{k}$ and polarization λ of photons that make up the electromagnetic field.[7] The vacuum energy $\sum_{\boldsymbol{k},\lambda} \omega_{\boldsymbol{k}}/2$ is dropped, since it diverges in the continuum limit.

The interaction Hamiltonian for electron spins in a magnetic field is[8]

$$\begin{aligned} H_I &= -\int \mathrm{d}\boldsymbol{r}\, \boldsymbol{\mu} \cdot \boldsymbol{B} && (2.39) \\ &= -\int \mathrm{d}\boldsymbol{r} \sum_i \mu_B \delta(\boldsymbol{r}_i) \boldsymbol{\sigma}_i && \\ &\quad \cdot \mathrm{i} \sum_{\boldsymbol{k},\lambda} \sqrt{\frac{1}{2V\omega_{\boldsymbol{k}}}} \Big((\boldsymbol{k} \times \boldsymbol{e}_{\boldsymbol{k},\lambda}) e^{\mathrm{i}\boldsymbol{k}\cdot\boldsymbol{r}} a_{\boldsymbol{k},\lambda} - (\boldsymbol{k} \times \boldsymbol{e}^{*}_{\boldsymbol{k},\lambda}) e^{-\mathrm{i}\boldsymbol{k}\cdot\boldsymbol{r}} a^{\dagger}_{\boldsymbol{k},\lambda} \Big) && (2.40) \\ &= -\sum_{i,\mu} \sigma_i^{\mu} B_i^{\mu}, && (2.41) \end{aligned}$$

where the components of the **magnetic field operator** evaluated at $\boldsymbol{r}_i$ are[9]

$$B_i^{\mu} = \mathrm{i}\mu_B \sum_{\boldsymbol{k},\lambda} \sqrt{\frac{2\pi}{V\omega_{\boldsymbol{k}}}} \Big((\boldsymbol{k} \times \boldsymbol{e}_{\boldsymbol{k},\lambda})_{\mu} e^{\mathrm{i}\boldsymbol{k}\cdot\boldsymbol{r}_i} a_{\boldsymbol{k},\lambda} - (\boldsymbol{k} \times \boldsymbol{e}^{*}_{\boldsymbol{k},\lambda})_{\mu} e^{-\mathrm{i}\boldsymbol{k}\cdot\boldsymbol{r}_i} a^{\dagger}_{\boldsymbol{k},\lambda} \Big). \tag{2.42}$$

This magnetic field operator includes the electron's magnetic moment so that the final rate γ (eq. (2.73)) carries the dimensions of frequency in the dissipator (eq. (1.102)).

To summarize, the composite Hamiltonian that we will study is

$$\begin{aligned} H &= H_S \otimes 1 + 1 \otimes H_B + H_I && (2.43) \\ &= -J(g) \sum_{i \in \mathbb{Z}_N} \big(f(1-g) \sigma_i^x \sigma_{i+1}^x + f(g) \sigma_i^z \big) \otimes 1 + 1 \otimes \sum_{\boldsymbol{k},\lambda} \omega_{\boldsymbol{k}} a^{\dagger}_{\boldsymbol{k},\lambda} a_{\boldsymbol{k},\lambda} - \sum_{i,\mu} \sigma_i^{\mu} \otimes B_i^{\mu}, && (2.44) \end{aligned}$$

where

---

[7] The polarization $\lambda = \pm 1$ marks either right or left circular polarization.

[8] An electron has spin $s = 1/2$ and g-factor $g_e \approx 2$, so its magnetic moment $\mu_e = sg\mu_B$ is approximately the Bohr magneton μ_B. The time dependence of the field is absorbed into the operators $a_{\boldsymbol{k},\lambda}$, and the prefactor is chosen so that these operators are dimensionless, but $\boldsymbol{B}$ is not.

[9] This operator arises from quantizing the electromagnetic field. The vector $\boldsymbol{e}_{\boldsymbol{k},\lambda}$ is $\boldsymbol{e}_{\boldsymbol{k},\pm 1} = \mp(\hat{\boldsymbol{e}}_{\boldsymbol{k},x} \pm \mathrm{i}\hat{\boldsymbol{e}}_{\boldsymbol{k},y})/\sqrt{2}$, with $\hat{\boldsymbol{e}}_{\boldsymbol{k},x}$ and $\hat{\boldsymbol{e}}_{\boldsymbol{k},y}$ perpendicular to $\boldsymbol{k}$. See the discussion of field quantization in [32, p. 506] for more details.

- $J(g) > 0$ for $0 \leqslant g \leqslant 1$,
- $f(g)$ is monotonic for $0 \leqslant g \leqslant 1$, $f(0) = 0$, and $f(1) = 1$, like for $f(g) = g$,
- The bath is a 3D continuum of modes according to eq. (2.59),
- The spin positions in eq. (2.42) are $\boldsymbol{r}_i = ai\hat{z}$ for some spacing a,
- The dipole approximation is valid. This requires that $a \ll c/\omega_{\boldsymbol{k}}$ for $\omega_{\boldsymbol{k}}$ up to the largest transition energy possible for H_S.

We will later nondimensionalize energy and time with respect to the system energy scale $J(g)$ so that the rates γ and S in the Lindblad equation (eq. (1.100)) are relative to the system timescale $\tau_S = 1/J(g)$.

In the interaction picture:

$$B_i^\mu(t) = e^{\mathrm{i}H_B t} B_i^\mu e^{-\mathrm{i}H_B t} \tag{2.45}$$

$$= \mathrm{i}\mu_B \sum_{\boldsymbol{k},\lambda} \sqrt{\frac{2\pi}{V\omega_{\boldsymbol{k}}}} \Big(\big(\boldsymbol{k} \times \boldsymbol{e}_{\boldsymbol{k},\lambda}\big)_\mu e^{\mathrm{i}(\boldsymbol{k}\cdot\boldsymbol{r}_i - \omega_{\boldsymbol{k}} t)} a_{\boldsymbol{k},\lambda} - \big(\boldsymbol{k} \times \boldsymbol{e}^*_{\boldsymbol{k},\lambda}\big)_\mu e^{-\mathrm{i}(\boldsymbol{k}\cdot\boldsymbol{r}_i - \omega_{\boldsymbol{k}} t)} a^\dagger_{\boldsymbol{k},\lambda} \Big). \tag{2.46}$$

The spectral correlation tensor is then

$$\Gamma_{i\mu,j\nu}(\omega) = \int_0^\infty \mathrm{d}s\, e^{\mathrm{i}\omega s} \left\langle B_i^\mu(t)^\dagger B_j^\nu(t-s) \right\rangle \tag{2.47}$$

$$\begin{aligned} &= -\frac{2\pi\mu_B^2}{V} \int_0^\infty \mathrm{d}s \sum_{\boldsymbol{k},\boldsymbol{k}',\lambda,\lambda'} \sqrt{\frac{1}{\omega_{\boldsymbol{k}}\omega_{\boldsymbol{k}'}}} \; : \\ &\big(\boldsymbol{k} \times \boldsymbol{e}_{\boldsymbol{k},\lambda}\big)_\mu \big(\boldsymbol{k}' \times \boldsymbol{e}_{\boldsymbol{k}',\lambda'}\big)_\nu e^{\mathrm{i}(\boldsymbol{k}\cdot\boldsymbol{r}_i - \omega_{\boldsymbol{k}} t + \boldsymbol{k}'\cdot\boldsymbol{r}_j - \omega_{\boldsymbol{k}'}(t-s) + \omega s)} \left\langle a_{\boldsymbol{k},\lambda} a_{\boldsymbol{k}',\lambda'} \right\rangle \\ &- \big(\boldsymbol{k} \times \boldsymbol{e}_{\boldsymbol{k},\lambda}\big)_\mu \Big(\boldsymbol{k}' \times \boldsymbol{e}^*_{\boldsymbol{k}',\lambda'}\Big)_\nu e^{\mathrm{i}(\boldsymbol{k}\cdot\boldsymbol{r}_i - \omega_{\boldsymbol{k}} t - \boldsymbol{k}'\cdot\boldsymbol{r}_j + \omega_{\boldsymbol{k}'}(t-s) + \omega s)} \left\langle a_{\boldsymbol{k},\lambda} a^\dagger_{\boldsymbol{k}',\lambda'} \right\rangle \\ &- \Big(\boldsymbol{k} \times \boldsymbol{e}^*_{\boldsymbol{k},\lambda}\Big)_\mu \big(\boldsymbol{k}' \times \boldsymbol{e}_{\boldsymbol{k}',\lambda'}\big)_\nu e^{-\mathrm{i}(\boldsymbol{k}\cdot\boldsymbol{r}_i - \omega_{\boldsymbol{k}} t - \boldsymbol{k}'\cdot\boldsymbol{r}_j + \omega_{\boldsymbol{k}'}(t-s) - \omega s)} \left\langle a^\dagger_{\boldsymbol{k},\lambda} a_{\boldsymbol{k}',\lambda'} \right\rangle \\ &+ \Big(\boldsymbol{k} \times \boldsymbol{e}^*_{\boldsymbol{k},\lambda}\Big)_\mu \Big(\boldsymbol{k} \times \boldsymbol{e}^*_{\boldsymbol{k}',\lambda'}\Big)_\nu e^{-\mathrm{i}(\boldsymbol{k}\cdot\boldsymbol{r}_i - \omega_{\boldsymbol{k}} t + \boldsymbol{k}'\cdot\boldsymbol{r}_j - \omega_{\boldsymbol{k}'}(t-s) - \omega s)} \left\langle a^\dagger_{\boldsymbol{k},\lambda} a^\dagger_{\boldsymbol{k}',\lambda'} \right\rangle. \end{aligned} \tag{2.48}$$

The thermal state is

$$\rho_B = \frac{e^{-\beta H_B}}{\operatorname{tr} e^{-\beta H_B}} = \prod_{\boldsymbol{k},\lambda} \Big(1 - e^{-\beta\omega_{\boldsymbol{k}}}\Big) e^{-\beta\omega_{\boldsymbol{k}} a^\dagger_{\boldsymbol{k},\lambda} a_{\boldsymbol{k},\lambda}}. \tag{2.49}$$

Since $\left[a_{\boldsymbol{k},\lambda}, a^\dagger_{\boldsymbol{k}',\lambda'}\right] = \delta_{\boldsymbol{k}\boldsymbol{k}'}\delta_{\lambda\lambda'}1$,

$$\left\langle a^\dagger_{\boldsymbol{k},\lambda} a_{\boldsymbol{k}',\lambda'}\right\rangle = \operatorname{tr}\!\left(e^{-\beta H_B}\right)^{-1} \operatorname{tr}\!\left(e^{-\beta H_B} a^\dagger_{\boldsymbol{k},\lambda} a_{\boldsymbol{k}',\lambda'}\right) \tag{2.50}$$

$$= \operatorname{tr}\!\left(e^{-\beta H_B}\right)^{-1} \operatorname{tr}\!\left(e^{-\beta H_B} a_{\boldsymbol{k}',\lambda'} a^\dagger_{\boldsymbol{k},\lambda}\right) - \delta_{\boldsymbol{k}\boldsymbol{k}'}\delta_{\lambda\lambda'} \tag{2.51}$$

$$= \operatorname{tr}\!\left(e^{-\beta H_B}\right)^{-1} \operatorname{tr}\!\left(e^{\beta\omega_{\boldsymbol{k}}} a_{\boldsymbol{k}',\lambda'} e^{-\beta H_B} a^\dagger_{\boldsymbol{k},\lambda}\right) - \delta_{\boldsymbol{k}\boldsymbol{k}'}\delta_{\lambda\lambda'} \tag{2.52}$$

$$= e^{\beta\omega_{\boldsymbol{k}}} \left\langle a^\dagger_{\boldsymbol{k},\lambda} a_{\boldsymbol{k}',\lambda'}\right\rangle - \delta_{\boldsymbol{k}\boldsymbol{k}'}\delta_{\lambda\lambda'}, \tag{2.53}$$

so we find that

$$\left\langle a^\dagger_{\boldsymbol{k},\lambda} a_{\boldsymbol{k}',\lambda'}\right\rangle = \delta_{\boldsymbol{k}\boldsymbol{k}'}\delta_{\lambda\lambda'} n_B(\omega_{\boldsymbol{k}}), \tag{2.54}$$

where

$$n_B(\omega) = \frac{1}{e^{\beta\omega} - 1}. \tag{2.55}$$

Similarly,

$$\left\langle a_{\boldsymbol{k},\lambda} a_{\boldsymbol{k}',\lambda'}\right\rangle = \left\langle a^\dagger_{\boldsymbol{k},\lambda} a^\dagger_{\boldsymbol{k}',\lambda'}\right\rangle = 0 \tag{2.56}$$

$$\left\langle a_{\boldsymbol{k},\lambda} a^\dagger_{\boldsymbol{k}',\lambda'}\right\rangle = \delta_{\boldsymbol{k}\boldsymbol{k}'}\delta_{\lambda\lambda'}(1 + n_B(\omega_{\boldsymbol{k}})). \tag{2.57}$$

Then for a thermal bath, the spectral correlation tensor becomes

$$\begin{aligned}\Gamma_{i\mu,j\nu}(\omega) = \frac{2\pi\mu_B^2}{V}\int_0^\infty \mathrm{d}s \sum_{\boldsymbol{k},\lambda} \frac{1}{\omega_{\boldsymbol{k}}} &: \\ &\left(\boldsymbol{k}\times\boldsymbol{e}_{\boldsymbol{k},\lambda}\right)_\mu \left(\boldsymbol{k}\times\boldsymbol{e}^*_{\boldsymbol{k},\lambda}\right)_\nu e^{\mathrm{i}(\boldsymbol{k}\cdot(\boldsymbol{r}_i-\boldsymbol{r}_j)+s(\omega-\omega_{\boldsymbol{k}}))}(1+n_B(\omega_{\boldsymbol{k}})) \\ &+ \left(\boldsymbol{k}\times\boldsymbol{e}^*_{\boldsymbol{k},\lambda}\right)_\mu \left(\boldsymbol{k}\times\boldsymbol{e}_{\boldsymbol{k},\lambda}\right)_\nu e^{-\mathrm{i}(\boldsymbol{k}\cdot(\boldsymbol{r}_i-\boldsymbol{r}_j)-s(\omega+\omega_{\boldsymbol{k}}))} n_B(\omega_{\boldsymbol{k}}).\end{aligned} \tag{2.58}$$

To evaluate eq. (2.58), we now consider a chain of N spins along the z-axis, so that $\boldsymbol{r}_i = r_i\hat{\boldsymbol{z}}$.[10] Then $\boldsymbol{k}\cdot(\boldsymbol{r}_i - \boldsymbol{r}_j) = k_z \Delta r_{ij}$.

In the continuum limit,

$$\frac{1}{V}\sum_{\boldsymbol{k}} \mapsto \int \frac{\mathrm{d}\boldsymbol{k}}{(2\pi)^3} = \frac{1}{(2\pi)^3}\int_0^\infty \mathrm{d}\omega_k\, \omega_k^2 \int \mathrm{d}\Omega\,, \tag{2.59}$$

where the integral over solid angle is

$$\int \mathrm{d}\Omega = \int \mathrm{d}\phi \int \mathrm{d}\theta \sin\theta. \tag{2.60}$$

---

[10] We could consider any axis given the spherical symmetry, but the z-axis is the simplest to evaluate.

To apply this limit to eq. (2.58), we first note that

$$\sum_{\lambda}\left(\boldsymbol{k}\times\boldsymbol{e}_{\boldsymbol{k},\lambda}\right)_{\mu}\left(\boldsymbol{k}\times\boldsymbol{e}^{*}_{\boldsymbol{k},\lambda}\right)_{\nu} = \sum_{abcd}\varepsilon_{\mu ab}\varepsilon_{\nu cd}k^a k^c\sum_{\lambda}e^{b}_{\boldsymbol{k},\lambda}\left(e^{d}_{\boldsymbol{k},\lambda}\right)^{*} \tag{2.61}$$

$$= \sum_{abcd}\varepsilon_{\mu ab}\varepsilon_{\nu cd}k^a k^c\left(\delta_{bd}-\frac{k^b k^d}{k^2}\right) \tag{2.62}$$

$$= \sum_{abc}\varepsilon_{\mu ab}\varepsilon_{\nu cb}k^a k^c \tag{2.63}$$

$$= \sum_{ac}\left(\delta_{\mu\nu}\delta_{ac}-\delta_{\mu c}\delta_{a\nu}\right)k^a k^c \tag{2.64}$$

$$= k^2\delta_{\mu\nu}-k^{\mu}k^{\nu}. \tag{2.65}$$

Thus

$$\int \mathrm{d}\Omega\, e^{\pm \mathrm{i}k_z\Delta r_{ij}}\sum_{\lambda}\left(\boldsymbol{k}\times\boldsymbol{e}_{\boldsymbol{k},\lambda}\right)_{\mu}\left(\boldsymbol{k}\times\boldsymbol{e}^{*}_{\boldsymbol{k},\lambda}\right)_{\nu} = \frac{8\pi\omega_k^2}{3}\delta_{\mu\nu}G_{\nu}\left(\omega_k\Delta r_{ij}\right), \tag{2.66}$$

where

$$G_{\nu}(u) = 3\left(\delta_{\nu z}-\frac{\delta_{\nu x}+\delta_{\nu y}}{2}\right)\frac{\operatorname{sinc}u-\cos u}{u^2}+\frac{3}{2}\left(\delta_{\nu x}+\delta_{\nu y}\right)\operatorname{sinc}u. \tag{2.67}$$

Note that in the dipole approximation

$$\lim_{u\to 0}G_{\nu}(u) = \left(\delta_{\nu z}-\frac{\delta_{\nu x}+\delta_{\nu y}}{2}\right)+\frac{3}{2}\left(\delta_{\nu x}+\delta_{\nu y}\right) = 1. \tag{2.68}$$

Now eq. (2.66) gives that the continuum limit of the spectral correlation tensor for the spin chain is

$$\begin{aligned}\Gamma_{i\mu,j\nu}(\omega) = \delta_{\mu\nu}\frac{2\mu_B^2}{3\pi}\int_0^{\infty}\mathrm{d}\omega_k\,\omega_k^3 G_{\nu}\left(\omega_k\Delta r_{ij}\right)\ :\\ (1+n_B(\omega_k))\int_0^{\infty}\mathrm{d}s\, e^{\mathrm{i}s(\omega-\omega_k)}+n_B(\omega_k)\int_0^{\infty}\mathrm{d}s\, e^{\mathrm{i}s(\omega+\omega_k)}.\end{aligned} \tag{2.69}$$

We now use that

$$n_B(-\omega) = -(1+n_B(\omega)) \tag{2.70}$$

and

$$\int_0^{\infty}\mathrm{d}s\, e^{-\mathrm{i}\omega s} = \pi\delta(\omega)-\mathrm{i}\mathcal{P}\frac{1}{\omega}, \tag{2.71}$$

where $\mathcal{P}$ denotes the Cauchy principal value, to find

$$\Gamma_{i\mu,j\nu}(\omega) = \frac{1}{2}\gamma_{i\mu,j\nu}(\omega)+\mathrm{i}S_{i\mu,j\nu}(\omega), \tag{2.72}$$

where

$$\gamma_{i\mu,j\nu}(\omega) = \delta_{\mu\nu}\frac{4\mu_B^2\omega^3}{3}G_\nu\big(|\omega|\Delta r_{ij}\big)(1+n_B(\omega)) \tag{2.73}$$

$$S_{i\mu,j\nu}(\omega) = \delta_{\mu\nu}\frac{2\mu_B^2}{3\pi}\mathcal{P}\int_0^\infty \mathrm{d}\omega_k\,\omega_k^3 G_\nu\big(\omega_k\Delta r_{ij}\big)\left(\frac{1+n_B(\omega_k)}{\omega-\omega_k}+\frac{n_B(\omega_k)}{\omega+\omega_k}\right). \tag{2.74}$$

We will now nondimensionalize γ and S. Starting with γ, we first apply the dipole approximation to find $\gamma_{i\mu,j\nu}(\omega) = \delta_{ij}\delta_{\mu\nu}\gamma(\omega)$, where[11]

$$\gamma(\omega) = \frac{4}{3}\mu_B^2\omega^3(1+n_B(\omega)). \tag{2.75}$$

Letting $\tilde{\gamma} = \gamma\tau_S$ and $\tilde{\omega} = \omega\tau_S$ gives

$$\tilde{\gamma}(\tilde{\omega}) = \left(\frac{\tau_0}{\tau_S}\right)^2\tilde{\omega}^3\left(1+\frac{1}{e^{\tau_B\tilde{\omega}/\tau_S}-1}\right) \tag{2.76}$$

in terms of the thermal correlation time $\tau_B = \beta$ and the **vacuum magnetic timescale**

$$\tau_0 = \sqrt{\frac{4}{3}\mu_B^2} = 6.35\times 10^{-23}\ \mathrm{s}. \tag{2.77}$$

In the high-temperature limit where $\tau_B\tilde{\omega}/\tau_S \ll 1$, $\tilde{\gamma}$ becomes

$$\tilde{\gamma}(\tilde{\omega}) \approx \frac{\tau_0^2}{\tau_B\tau_S}\tilde{\omega}^2. \tag{2.78}$$

The other limit where $\tau_B\tilde{\omega}/\tau_S \gg 1$ motivates the definition of the typical zero-temperature decay rate

$$\tilde{\gamma}_0 = \lim_{\tau_B\to\infty}\tilde{\gamma}(1) = \left(\frac{\tau_0}{\tau_S}\right)^2. \tag{2.79}$$

What about $\tilde{S} = S\tau_S$? Applying the dipole approximation and letting $\tilde{\omega} = \omega\tau_S$ gives

$$\tilde{S}(\tilde{\omega}) = \frac{1}{2\pi}\left(\frac{\tau_0}{\tau_S}\right)^2\mathcal{P}\int_0^\infty \mathrm{d}\tilde{\omega}_k\,\tilde{\omega}_k^3\left(\frac{1+\tilde{n}_B(\tilde{\omega}_k)}{\tilde{\omega}-\tilde{\omega}_k}+\frac{\tilde{n}_B(\tilde{\omega}_k)}{\tilde{\omega}+\tilde{\omega}_k}\right), \tag{2.80}$$

where

$$\tilde{n}_B(\tilde{\omega}) = \frac{1}{e^{\tau_B\tilde{\omega}/\tau_S}-1}. \tag{2.81}$$

To avoid the divergence of eq. (2.80), we introduce an upper frequency cutoff $\tilde{\Omega}$. Physically, one expects the coupling to high-frequency modes of the bath to weaken.[12] For simplicity, we just set the upper limit of the integral to $\tilde{\Omega}$.[13] If we set the frequency cutoff $\tilde{\Omega} \gg \tilde{\omega}$ to be far above any system frequency, we have the following limits.

---

[11] At zero temperature, $\gamma(\omega)$ becomes the **Einstein A coefficient**. Compare this to the analogous result (eq. (2.12)) for electric dipole radiation.

[12] This is not the case for the electromagnetic field, but in other contexts, one may view the bath as merely an effective model, and this cutoff is used to describe the effective interaction.

- In the high-temperature limit where $\tau_B\tilde{\Omega}/\tau_S \ll 1$, $\tilde{S}$ simplifies to[14]

$$\tilde{S}(\tilde{\omega}) \approx \frac{1}{2\pi}\frac{\tau_0^2}{\tau_B\tau_S}\mathcal{P}\int_0^{\tilde{\Omega}} \mathrm{d}\tilde{\omega}_k\, \tilde{\omega}_k^2\left(\frac{1}{\tilde{\omega}-\tilde{\omega}_k}+\frac{1}{\tilde{\omega}+\tilde{\omega}_k}\right) \tag{2.83}$$

$$= \frac{\tilde{\omega}^2}{\pi}\frac{\tau_0^2}{\tau_B\tau_S}\mathcal{P}\int_0^{\tilde{\Omega}/\tilde{\omega}} \mathrm{d}u\, \frac{u^2}{1-u^2} \tag{2.84}$$

$$= \frac{\tau_0^2}{\tau_B\tau_S}\frac{\tilde{\omega}}{\pi}\left(\tilde{\omega}\,\mathrm{atanh}\left(\frac{\tilde{\omega}}{\tilde{\Omega}}\right)-\tilde{\Omega}\right) \tag{2.85}$$

$$\approx -\frac{\tau_0^2}{\tau_B\tau_S}\frac{\tilde{\Omega}}{\pi}\tilde{\omega}. \tag{2.86}$$

- In the low-temperature limit where $\tau_B\tilde{\Omega}/\tau_S \gg 1$, $\tilde{S}$ simplifies to

$$\tilde{S}(\tilde{\omega}) \approx \frac{1}{2\pi}\left(\frac{\tau_0}{\tau_S}\right)^2\mathcal{P}\int_0^{\tilde{\Omega}} \mathrm{d}\tilde{\omega}_k\, \frac{\tilde{\omega}_k^2}{\tilde{\omega}-\tilde{\omega}_k} \tag{2.87}$$

$$= \frac{\tilde{\omega}^2}{2\pi}\left(\frac{\tau_0}{\tau_S}\right)^2\mathcal{P}\int_0^{\tilde{\Omega}/\tilde{\omega}} \mathrm{d}u\, \frac{u^2}{1-u} \tag{2.88}$$

$$= -\frac{1}{2\pi}\left(\frac{\tau_0}{\tau_S}\right)^2\left(\frac{\tilde{\Omega}^2}{2}+\tilde{\Omega}\tilde{\omega}-\tilde{\omega}^2\log\left(\frac{\tilde{\omega}}{\tilde{\Omega}-\tilde{\omega}}\right)\right) \tag{2.89}$$

$$\approx -\frac{1}{2\pi}\left(\frac{\tau_0}{\tau_S}\right)^2\left(\frac{\tilde{\Omega}^2}{2}+\tilde{\Omega}\tilde{\omega}\right). \tag{2.90}$$

In both cases, $\tilde{S}$ is small if $\tau_0\Omega \ll 1$, which we will assume. Because the Lamb-shift Hamiltonian (eq. (1.101)) scales with $\tilde{S}$, it may then be neglected.

Now that we have calculated γ, we may verify that the weak-coupling limit is valid. We already know that the bath is changed little by the system due to its infinite size, that

---

[13] This hard cutoff of setting the upper limit to $\tilde{\Omega}$ is performed in [18, p. 265]. In general, one considers a function called the spectral density that is related to the coupling in the interaction Hamiltonian. When this function includes

$$\frac{\tilde{\Omega}^2}{\tilde{\Omega}^2+\omega^2}, \tag{2.82}$$

it is said to have a Lorentz-Drude cutoff, which is sometimes considered instead of the hard cutoff [18, p. 175]. The low-frequency behavior of our spectral density classifies it as an Ohmic spectral density, which is the most common type to be considered because it arises from electromagnetic interactions in three dimensions. The exact functional form of the cutoff does not matter much because we ensure that the system transitions at frequencies far below the cutoff.

[14] To evaluate these principal value integrals, it suffices to just ignore the pole at $u = 1$.

$\left\langle B_i^\mu(t)\right\rangle = 0$, and that the secular approximation holds for the numbers of spins that we will consider because τ_0 is so small. It remains to verify that the reservoir correlation functions decay over a time scale that is much less than the relaxation time τ_R.[15] The point of this thesis is to find the relaxation time τ_R, so we cannot make a direct comparison. However, on physical grounds we do expect that the relaxation time is much slower than the system time τ_S for all realistic temperatures.[16] Recall that the rate $\gamma(\omega)$ is given by the Fourier transform (eq. (1.88)) of the reservoir correlation functions $\left\langle B_i^\mu(s)^\dagger B_j^\nu(0)\right\rangle$, which are the same for all sites and polarizations. The correlation functions are then the inverse Fourier transform of $\gamma(\omega)$:

$$\left\langle B_i^\mu(s)^\dagger B_j^\nu(0)\right\rangle = \frac{1}{2\pi}\int_{-\infty}^{\infty} \mathrm{d}\omega\, e^{-\mathrm{i}\omega s}\gamma(\omega). \tag{2.91}$$

Using the dimensionless time $\tilde{s} = s/\tau_S$ and introducing the parameter $\eta = \tau_B/\tau_S$, we find that

$$\begin{aligned}
\frac{1}{\tau_S^2}\left\langle B_i^\mu(\tilde{s})^\dagger B_j^\nu(0)\right\rangle &= \frac{1}{2\pi}\int_{-\infty}^{\infty} \mathrm{d}\tilde{\omega}\, e^{-\mathrm{i}\tilde{\omega}\tilde{s}}\tilde{\gamma}(\tilde{\omega}) && (2.92)\\
&= \left(\frac{\tau_0}{\tau_S}\right)^2 \frac{1}{2\pi}\int_{-\infty}^{\infty} \mathrm{d}\tilde{\omega}\, e^{-\mathrm{i}\tilde{\omega}\tilde{s}}\tilde{\omega}^3\left(1+\frac{1}{e^{\eta\tilde{\omega}}-1}\right) && (2.93)\\
&= \left(\frac{\tau_0}{\tau_S}\right)^2 \mathrm{i}^3\frac{\mathrm{d}^3}{\mathrm{d}\tilde{s}^3}\frac{1}{2\pi}\int_{-\infty}^{\infty} \mathrm{d}\tilde{\omega}\, e^{-\mathrm{i}\tilde{\omega}\tilde{s}}\frac{e^{\eta\tilde{\omega}}}{e^{\eta\tilde{\omega}}-1} && (2.94)\\
&= \left(\frac{\tau_0}{\tau_S}\right)^2 \mathrm{i}^3\frac{\mathrm{d}^3}{\mathrm{d}\tilde{s}^3}\frac{1}{2\pi}\int_{-\infty}^{\infty} \mathrm{d}\tilde{\omega}\, e^{-\mathrm{i}\tilde{\omega}(\tilde{s}+\mathrm{i}\eta/2)}\frac{1}{2}\operatorname{csch}\left(\frac{\eta\tilde{\omega}}{2}\right) && (2.95)\\
&= \left(\frac{\tau_0}{\tau_S}\right)^2 \mathrm{i}^3\frac{\mathrm{d}^3}{\mathrm{d}\tilde{s}^3}\left(-\frac{\mathrm{i}}{2\eta}\tanh\left(\frac{\pi}{\eta}\left(\tilde{s}+\frac{\mathrm{i}\eta}{2}\right)\right)\right) && (2.96)\\
&= \left(\frac{\tau_0}{\tau_S}\right)^2 \mathrm{i}^3\frac{\mathrm{d}^3}{\mathrm{d}\tilde{s}^3}\left(-\frac{\mathrm{i}}{2\eta}\coth\left(\frac{\pi\tilde{s}}{\eta}\right)\right) && (2.97)\\
&= \left(\frac{\tau_0}{\tau_S}\right)^2 \frac{\pi^3}{\eta^4}\sinh\left(\frac{\pi\tilde{s}}{\eta}\right)^{-4}\left(1+2\cosh\left(\frac{\pi\tilde{s}}{\eta}\right)^2\right). && (2.98)
\end{aligned}$$

At low temperatures $\tilde{s} \ll \eta$ and

$$\frac{1}{\tau_S^2}\left\langle B_i^\mu(\tilde{s})^\dagger B_j^\nu(0)\right\rangle = \left(\frac{\tau_0}{\tau_S}\right)^2 \frac{3}{\pi\tilde{s}^4}, \tag{2.99}$$

---

[15] Analogous results for the electric field are given in [18, p. 574].

[16] Also, if we instead suppose that this is true, then we expect the relaxation time to be on the order of $\gamma^{-1}(1)$. For the case to be otherwise, we must have $\tau_B \approx \tau_0$, which corresponds to a temperature of 1.2×10^{11} K or higher.

while at high temperatures $\tilde{s} \gg \eta$ and

$$\frac{1}{\tau_S^2}\left\langle B_i^{\mu}(\tilde{s})^{\dagger} B_j^{\nu}(0)\right\rangle = \left(\frac{\tau_0}{\tau_S}\right)^2 \frac{8\pi^3}{\eta^4} e^{-2\pi\tilde{s}/\eta} \tag{2.100}$$

$$= \left(\frac{\tau_0^2}{\tau_B \tau_S}\right) \frac{8\pi^3}{\eta^3} e^{-2\pi\tilde{s}/\eta}. \tag{2.101}$$

Thus if $\tau_B \ll \tau_S$, the reservoir correlation time is $\tau_C = \tau_B/2\pi$, which is comparable to the thermal correlation time. In either case, the correlation functions decay quickly for $\tilde{s} > 1$. Since $\tau_S \ll \tau_R$, this establishes the validity of the weak-coupling limit.

CHAPTER 3

COMPUTING JUMP OPERATORS

Now that we have obtained $\tilde{\gamma}$ in eq. (2.76), it remains to compute the jump operators eq. (1.71) for the interpolating Hamiltonian eq. (2.34) and solve the Lindblad equation to find the relaxation rates of the system. For simplicity, we will aim to estimate a single exponential relaxation rate for the expected value $\langle \sigma_1^z \rangle$ of a single spin.[1] These tasks will be done by numerically diagonalizing the dissipator of the system as follows. Just as we usually consider the eigenstates of a Hamiltonian to solve a closed system, we may consider the eigenoperators of the Liouvillian $\mathcal{L}$ to solve an open system. We decompose the initial system density operator as

$$\rho(0) = \sum_i c_i V_i, \tag{3.1}$$

where

$$\mathcal{L}(V_i) = \lambda_i V_i. \tag{3.2}$$

The reduced density operator for the system then evolves in time as

$$\rho(\tilde{t}) = \sum_i c_i e^{\lambda_i \tilde{t}} V_i, \tag{3.3}$$

and the desired observable is

$$\langle \sigma_1^z \rangle = \operatorname{tr}\big(\rho(\tilde{t})\sigma_1^z\big) = \sum_i c_i e^{\lambda_i \tilde{t}} \operatorname{tr}\big(V_i \sigma_1^z\big). \tag{3.4}$$

---

[1] Since are using periodic boundary conditions for the transverse-field Ising model, this expected value is the same for all spins.

Note that the eigenoperators V_i are generally not valid density operators. In this case, the diagonalization is a formal technique for solving the system, rather than a way of identifying stationary quantum states. Thus an observable like $\langle\sigma_1^z\rangle$ is seen to decay according to a sum of decaying exponentials with rates λ_i. The system and interaction Hamiltonians determine the V_i, while the initial state determines the c_i. The combination of these sources can be seen as filtering the full spectrum of the Liouvillian to produce the time evolution of $\langle\sigma_1^z\rangle$. To merely determine the decay rates and not the full time evolution, it suffices to diagonalize just the dissipator (eq. (1.102)). To understand this situation, we will borrow from solid state physics and consider **spaghetti diagrams**: plots of the dissipator eigenvalues as we vary the Hamiltonian parameter g. Figure 3.1 explains the name.

Spaghetti Diagrams
CHIANTI
ω
0
$Q_{\parallel}$

Figure 3.1: A spaghetti diagram [33].

In addition to varying the parameter g, we also would like to vary the dimensionless inverse temperature η. It is a bit confusing to decipher spaghetti diagrams across g and temperature, so we will instead perform a least squares fit to find the rate s and amplitude A of the single exponential model

$$\langle\sigma_1^z\rangle(\tilde{t}) = Ae^{-s\tilde{t}} + \langle\sigma_1^z\rangle(\infty) \tag{3.5}$$

to the true multiple exponential envelope eq. (3.4) over the time interval $[0, \tilde{t}_f]$, where

$$\tilde{t}_f = \frac{1}{10\tilde{\gamma}(1)}, \tag{3.6}$$

and instead inspect the effective relaxation rate s. While this rate depends on the particular observable and initial condition, it will still give a rough picture of what happens as we vary g.

With this setup in mind, we may now go over the rate computation process. In the interest of transparency, code snippets are given in Julia, and the information on packages and hardware used is given in appendix C. The code and source text of this thesis may be obtained by unzipping this PDF file.

We will consider a single system at a time, starting with

```
n = 2;
```

Due to the exponential growth of the Hilbert space, we will only be able to fully consider up to $N = 5$ spins.

3.1 INTERPOLATING HAMILTONIANS

First, we implement the trace norm and eq. (2.34).

```
trnorm(A) = sum(svdvals(A)) # tr(√(A' * A))
trnormalize(A) = A / trnorm(A)
∠(A, B) = acos(tr(A' * B)) # For normalized A, B
function normslerp(A, B, g)
    a, b = trnorm(A), trnorm(B)
    A /= a
    B /= b
    θ = ∠(A, B)
    √(a * b) * trnormalize((sin((1-g)*θ)*A + sin(g*θ)*B) / sin(θ))
end
Hinterp(A, B) = g -> normslerp(A, B, g);
```

We may now construct H_S from the Ising interaction and transverse-field Hamiltonians.

```
Hx(n) = -sum(siteop(σx, i, n) * siteop(σx, i+1, n) for i in 1:n)
Hz(n) = -sum(siteop(σz, i, n) for i in 1:n)
Hint = Hinterp(Hx(n), Hz(n));
```

Since the relevant properties of the dissipator depend on the transition frequencies of the system, it will be relevant to have a picture of the energy levels of H_S as g changes.

```
grange(points) = range(1e-3, 1-1e-3, length=points)
lgs = grange(64)
energies = [eigvals(Hint(g)) for g in lgs];
plot(lgs, hcat(energies...)', color=:black, alpha=0.25, key=false,
 ↪  xlabel=L"Hamiltonian parameter $g$", ylabel=L"Dimensionless energy $\tilde{E}$")
```

Code for saving plots has been omitted.

3.2 Computation of jump operators

Now we must implement eq. (1.71) for the jump operators. To do so, we must first diagonalize the Hamiltonian, collect all eigenstates with the same energy, form the associated projectors, and then sum over all pairs of energies with the same difference ω. First, we define utility functions that build the needed dictionaries to associate an energy to its eigenstates.

```
function addentry!(dict, key, value; isequal=isequal)
    for k in keys(dict)
        if isequal(k, key)
            push!(dict[k], value)
            return dict
        end
    end
    dict[key] = [value]
    dict
end;

function incentry!(dict, key; isequal=isequal)
    for k in keys(dict)
        if isequal(k, key)
            dict[k] += 1
            return dict
        end
    end
    dict[key] = 1
    dict
end;

firstvalue(i, (x, y)) = x
lastvalue(i, (x, y)) = y
dictmap(f, dict) = Dict(key => f(value) for (key, value) in dict)
function dictby(A; isequal=isequal, keyof=firstvalue, valof=lastvalue)
    i0, x0 = 1, first(A)
    k0, v0 = keyof(i0, x0), valof(i0, x0)
    dict = Dict(k0 => typeof(v0)[])
    dict = Dict()
    for (i, x) in enumerate(A)
        k, v = keyof(i, x), valof(i, x)
        addentry!(dict, k, v, isequal=isequal)
    end
    dict
end;
```

With these in place, we sum to find a projector.

```
sumprojector(A) = sum(a * a' for a in A)
projectors(eigdict) = dictmap(sumprojector, eigdict);
```

To decrease the number of jump operators that we must store, we check to see if any jump operators are identical. If M jump operators are the same operator J, then they are the same as the single jump operator $\sqrt{M}J$.

```
function combinejumps(Js)
    d = Dict()
    for J in Js
        incentry!(d, J)
    end
    [√(one(eltype(J)) * N)*J for (J, N) in d]
end;
```

Now the pieces come together to compute the jump operators. The result of this computation is a dictionary that associates each ω to the list of jump operators at that frequency. It is vital to filter out jump operators that are zero so that the computations may be done in a reasonable amount of time. To this end we must consider only approximate equality of operators to deal with floating point issues.

```
isequalto(atol=1e-9) = (x, y) -> isapprox(x, y, atol=atol)
function jumps(vals, vecs, As; combine=true, isequal=isequalto())
    eigendict = dictby(zip(vals, vecs))
    ωs = dictby(((E2 - E1, (E1, E2)) for E1 in keys(eigendict), E2 in
     ↪  keys(eigendict)),
        isequal=isequal)
    Πs = projectors(eigendict)
    Jωs = dictmap(ωs) do ΔEs
        filter(x -> !isequal(x, zero(x)),
            [sum(Πs[E1]*A*Πs[E2] for (E1, E2) in ΔEs) for A in As])
    end
    combine ? dictmap(combinejumps, Jωs) : Jωs
end
```

Everything is now wrapped up in a function that accepts the Hamiltonian H_S and computes the jump operators for each of the spin operators σ_i^μ in eq. (2.41).

```
op_to_spindim(H) = Int(log2(size(H)[1]))
dipole_interactions(n) = vcat(map(A -> [siteop(A, i, n) for i in 1:n], [σx, σy,
 ↪  σz])...)
function dipolejumps(H; kwargs...)
    vals, vecs = eigen(H)
    jumps(vals, eachcol(vecs), dipole_interactions(op_to_spindim(H)); kwargs...)
end;
```

3.3 Numerical solution of the Lindblad equation

Now that we have the jump operators, we can compute an example time evolution. So that we can see the system dynamics and decay on the same plot, the decay rate has been artificially increased from the actual value in eq. (2.77). As we discussed previously, we will ignore the Lamb shift. The simulation parameters are:

```
g = 0.5
Hsys = Hint(g)
b = SpinBasis(1//2)
sys = ⊗(repeat([b], n)...)
Jωs = dipolejumps(Hsys)
η = 1e1
α = 1e-2
up = spinup(b)
ψ0 = ⊗(repeat([up], n)...)
ρ0 = projector(ψ0)
op = dense(embed(sys, 1, sigmaz(b)));
```

Now we find lists of jump operators and their associated decay rates $\tilde{\gamma}$.

```
jumpops, rates = [], Float64[]
γ(ω, η) = (1e-1 < η*ω ? ω^3 * (1 + 1 / (exp(η*ω) - 1)) : ω^2 / η)
for (ω, Js) in Jωs
    for J in Js
        push!(rates, α * γ(ω, η))
        push!(jumpops, DenseOperator(sys, J))
    end
end
```

We now compute $\langle \sigma_1^z \rangle$ over twice the time interval eq. (3.6).

```
function fout(t, ρ)
    ρ = normalize(ρ)
    real(expect(op, ρ))
end
Hspin = DenseOperator(sys, Hsys)
tf = 2e-1 / (α * γ(1.0, η))
ts = range(0.0, tf, length=501);
```

We will look at the closed time evolution, the open time evolution, and the envelope of the open time evolution given by simulating just the dissipator.

```
_, closed_σzs = timeevolution.schroedinger(ts, ψ0, Hspin; fout=fout)
_, open_σzs   = timeevolution.master(ts, ρ0, Hspin, jumpops; rates=rates, fout=fout)
_, diss_σzs   = timeevolution.master(ts, ρ0, 0*Hspin, jumpops; rates=rates,
 ↪  fout=fout);
```

```
plot(
    title=L"Solution for $N = %$n$, $g = %$g$, $\tau_B / \tau_S = %$η$, ${(\tau_0 /
    ↪  \tau_S)}^2 = %$α$",
    xlabel=L"Time ($t / \tau_S$)",
    ylabel=L"\ev{\pauli_1^z}",
    legend=:topright
)
plot!(ts, [closed_σzs open_σzs diss_σzs], label=["Closed" "Open" "Dissipator"])
```

Code for saving plots has been omitted. With the data from an explicit simulation, we may perform a least squares fit of eq. (3.5) to check the validity of the model. Note that this fit is over twice the time interval (eq. (3.6)) used later.

```
@. decay_exponential(x, p) = diss_σzs[end] + p[1]*exp(x*p[2])
p0 = [1.0, α * γ(1, η)]
fit = curve_fit(decay_exponential, ts, diss_σzs, p0);

plot(ts, diss_σzs, label=L"\dot{\dop} = \sopr{D}\dop",
    legend=:topright,
    title="Exponential fit over short and medium times",
    xlabel=L"Time ($t / \tau_S$)",
    ylabel=L"\ev{\pauli_1^z}")
plot!(ts, decay_exponential(ts, coef(fit)), label=L"Fit: $Ae^{-s t} +
 ↪  \ev{\pauli_1^z}_\text{eq}$")
```

Code for saving plots has been omitted.

3.4 OBTAINING RELAXATION FROM SPAGHETTI (DIAGRAMS)

Now we set up the full fit, where we compute eq. (3.4) from the dissipator spectrum.

```
@. decay_exponential(x, p) = p[1]*exp(x*p[2])
function effective_rate(ℒrates, ℒops, ρ0, op, η)
    cs = hcat([vec(V.data) for V in ℒops]...) \ vec(ρ0.data)
    V0s = [tr(op * V) for V in ℒops]
    t0, tf = (0.0, 1e-1) ./ γ(1.0, η)
    ts = range(t0, tf, length=501)
    ys = real(sum(@. c * V0 * exp(real(s)*ts) for (s, c, V0) in zip(ℒrates, cs,
    ↪  V0s)))
    p0 = [1.0, -1.0 / η]
    yf = real(cs[1] * V0s[1])
    fit = curve_fit(decay_exponential, ts, ys .- yf, p0)
    fit.converged || error("Could not fit an effective exponential.")
    coef(fit)[2], stderror(fit)[2]
end
```

The jump operators are computed similarly to above, and the diagonalization uses standard numerical linear algebra.

```
function 𝒟_rates(H, n = op_to_spindim(H); η, ρ0, op)
    Jωs = dipolejumps(H)
    sys = ρ0.basis_r
    jumpops, rates = [], Float64[]
    for (ω, Js) in Jωs
        for J in Js
            push!(rates, γ(ω, η))
            push!(jumpops, DenseOperator(sys, J))
        end
    end
    ℒ = steadystate.liouvillian(0*DenseOperator(sys), jumpops; rates=rates)
    ℒrates, ℒops = steadystate.liouvillianspectrum(ℒ; nev=4^n)
    effrate = effective_rate(ℒrates, ℒops, ρ0, op, η)
    sort(real(ℒrates)), effrate...
end;
```

We may now compute the spaghetti diagrams. Note that the plots show the negated eigenvalues of the dissipator, since none are positive. Thus the higher up an eigenvalue is, the faster the rate it represents. We will indicate the limiting values at $g = 0$ and $g = 1$ by markers on the sides of the spaghetti diagram, and superimpose the rate for $\langle \sigma_1^z \rangle$ for the parameters used in the prior time evolution across g (except for where we have scaled out α).

```
function plot_𝒟_rates(Hint;
        points=16, η=1.0, ρ0, op, onplot=false,
        spectrum=true, extremes=true, effective=true,
        kwargs...)
    g0s = grange(points)
    outs = map(g -> 𝒟_rates(Hint(g); η, ρ0, op), g0s)
    rates = [o[1] for o in outs]
    r0 = [o[2] for o in outs]
    σr0 = [o[3] for o in outs]

    p = onplot
    if onplot == false
        p = plot(
            xlabel=L”Hamiltonian parameter $g$”,
            ylabel=L”Dissipaton rates ($\tilde{\gamma} / \tilde{\gamma}_0$)”,
            legendtitle=L”\log\eta”,
            legend=:topright;
            kwargs...)
    end
    if spectrum
        plot!(p, g0s, -hcat(rates...)', color=:black, alpha=0.25, label=false)

        if extremes
```

```
      rates0 = 𝒟_rates(Hint(0); η, ρ0, op)[1]
      rates1 = 𝒟_rates(Hint(1); η, ρ0, op)[1]
      scatter!(p, repeat([g0s[1] - 2e-2], length(rates0)), -rates0,
        marker=(:rtriangle, 2, rubric), markerstrokecolor=rubric,
        ↪ label=false)
      scatter!(p, repeat([g0s[end] + 2e-2], length(rates1)), -rates1,
        marker=(:ltriangle, 2, rubric), markerstrokecolor=rubric,
        ↪ label=false)
    end
  end
  if effective
    plot!(p, g0s, -r0, ribbon=σr0, label=L"%$(round(log10(η), digits=1))",
      color = (onplot == false) ? rubric : :auto)
  end
  p
end;
```

```
plot_𝒟_rates(Hint; η, ρ0, op)
```

Code for saving plots has been omitted. The fit results are computed across g and shown in different regimes of the temperature η on a logarithmic scale. Resolution is kept low due to the computational expense of finding the jump operators, computing $\mathcal{D}$, and diagonalizing it (a dense matrix with dimension 4^N).

```
plot([reduce((p, η) ->
      plot_𝒟_rates(Hint; η, ρ0, op, spectrum=false, onplot=p),
      10 .^ range(lη, lη + 1, length=4);
      init = plot(size=2 .* (400, 300 * 3//2),
        xlabel=L"Hamiltonian parameter $g$",
        ylabel=L"Decay rates for $\pauli_1^z$ ($\tilde{\gamma} /
        ↪ \tilde{\gamma}_0$)",
        legend=:topright,
        legendtitle=L"\log\eta"))
    for lη in -2:3]...,
  layout=(3,2))
```

```
savefig("$(tempname(pwd(), cleanup=false))-spin-relaxation-$(n).pdf")
```

3.5 RESULTS

The results of the preceeding computations for N from 2 to 5 are given on the following pages. For easy comparison, each set of plots for a given number of spins spans an even and odd page. To interpret the plots, note that:

- The highlighted line in each spaghetti diagram is the single-spin relaxation rate for $\eta = 10$, which shows how the full collection of rates is filtered to produce a different rate for a particular expected value.
- In figs. 3.18 to 3.21 the first three plots show relaxation rates decreasing with temperature, while the next three plots flip the order.

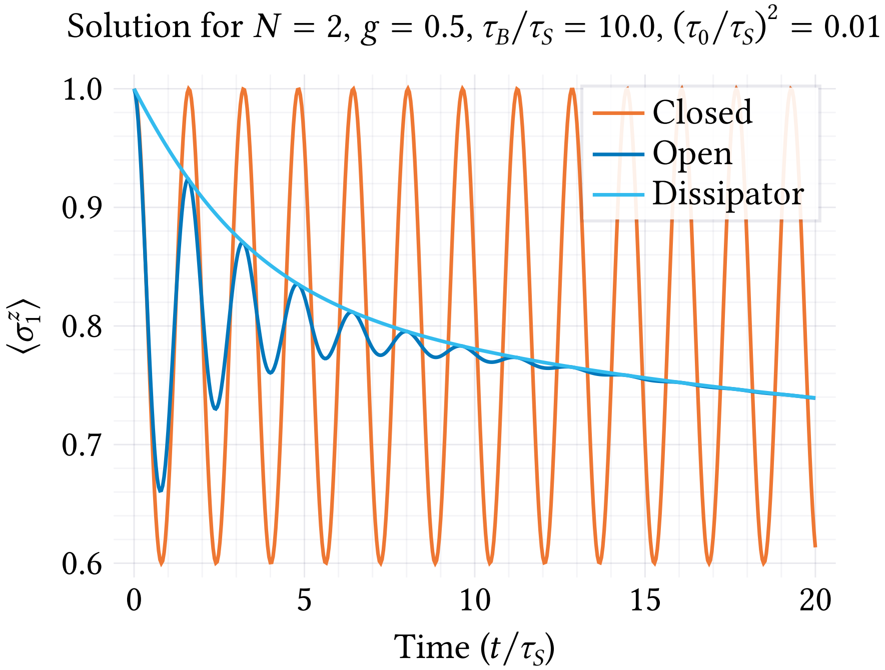

Figure 3.2: Example time evolution for $N = 2$ spins.

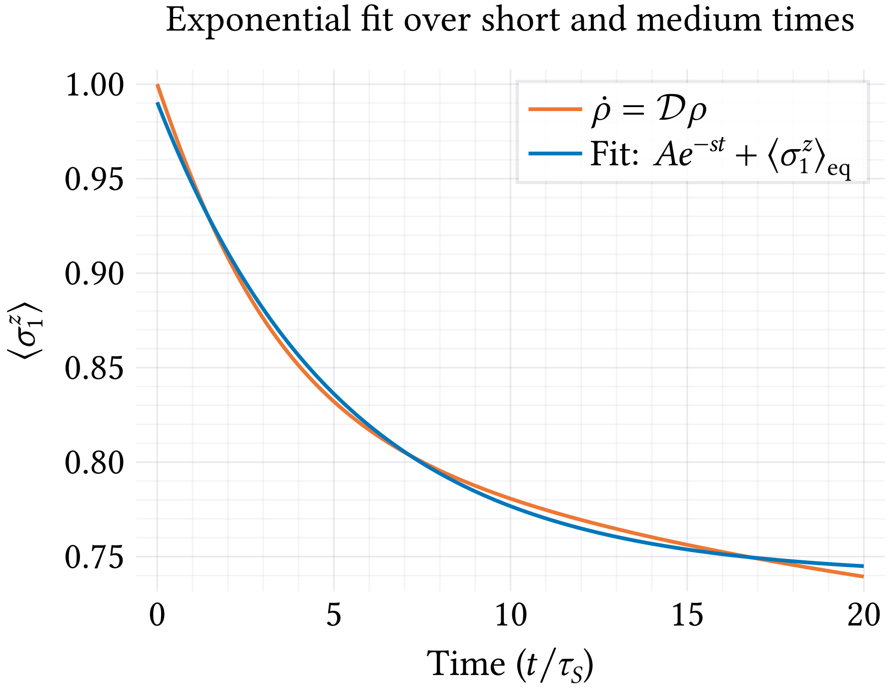

Figure 3.3: Exponential fit for $N = 2$ spins.

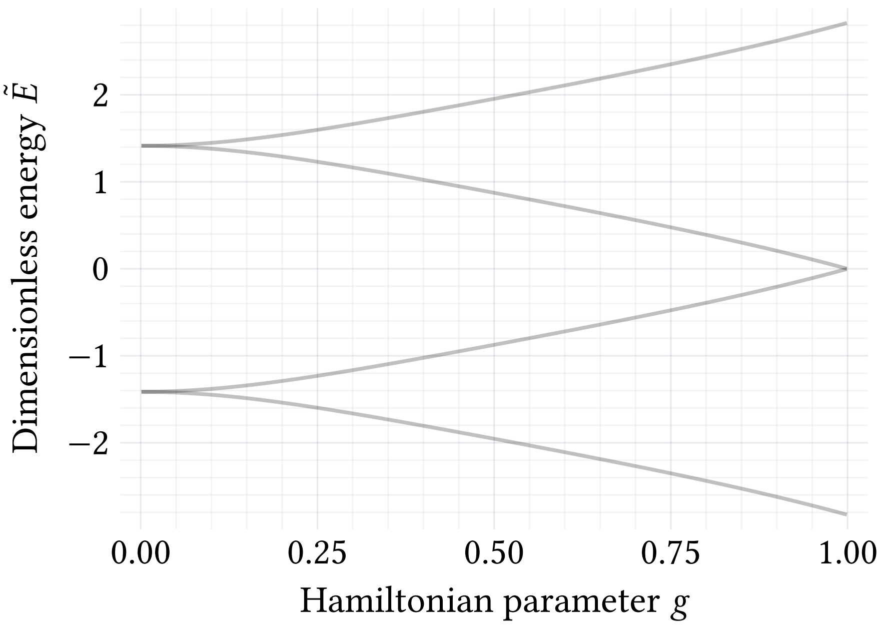

Figure 3.4: Energy levels of eq. (2.34) for $N = 2$ spins.

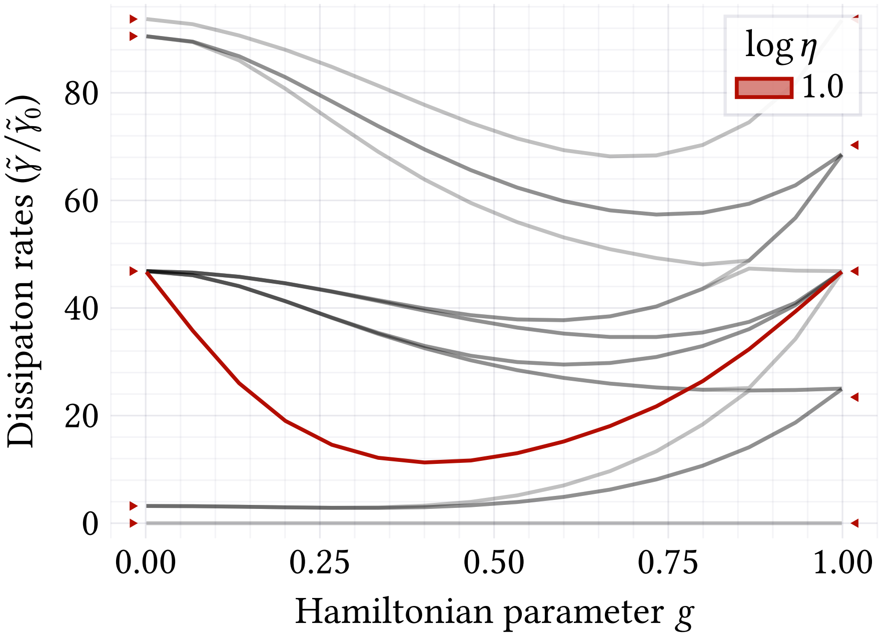

Figure 3.5: Dissipation rate spaghetti diagram for $N = 2$ spins.

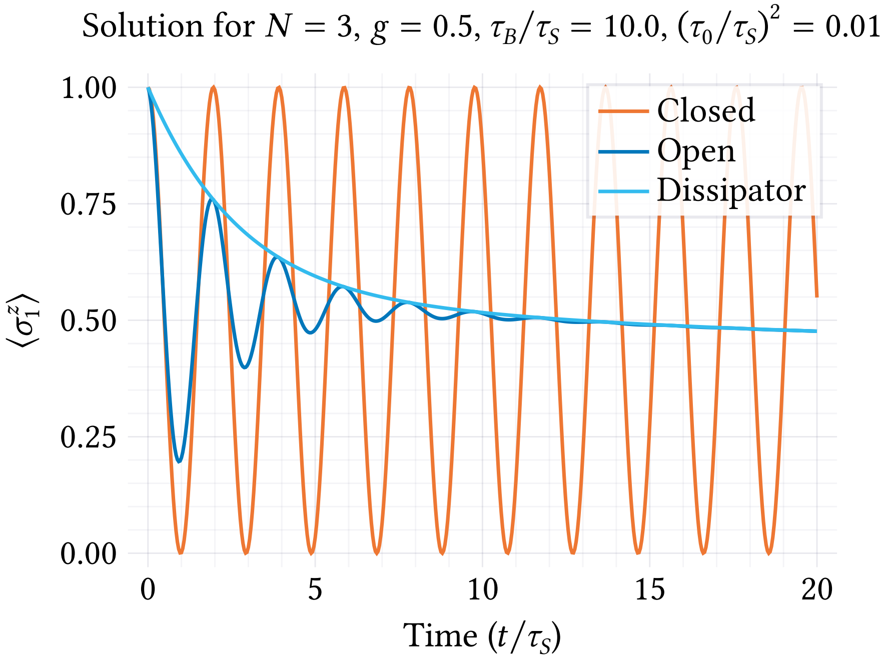

Solution for $N = 3$, $g = 0.5$, $\tau_B/\tau_S = 10.0$, $(\tau_0/\tau_S)^2 = 0.01$

Figure 3.6: Example time evolution for $N = 3$ spins.

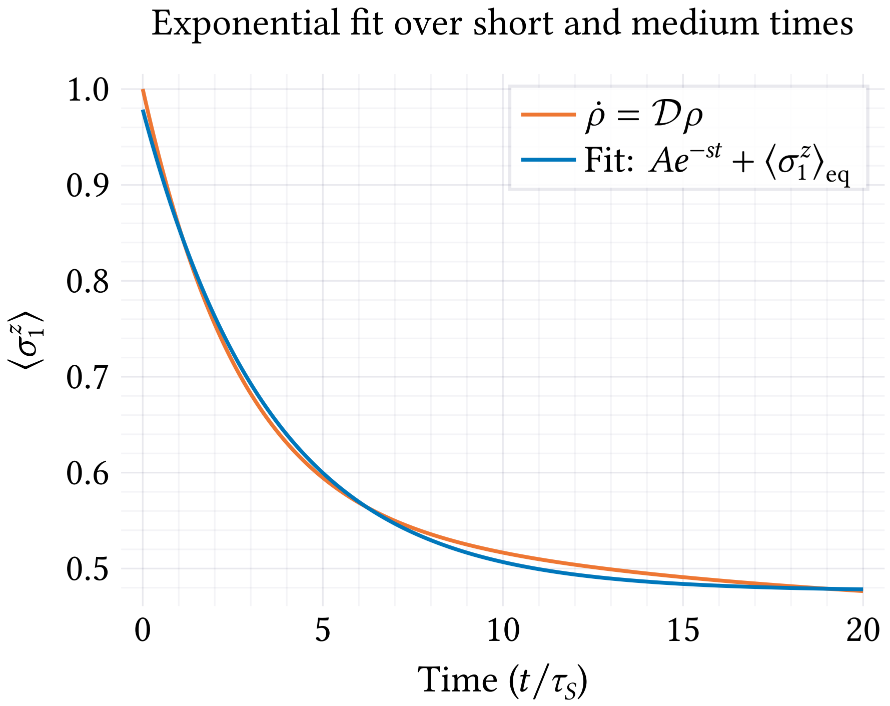

Exponential fit over short and medium times

Figure 3.7: Exponential fit for $N = 3$ spins.

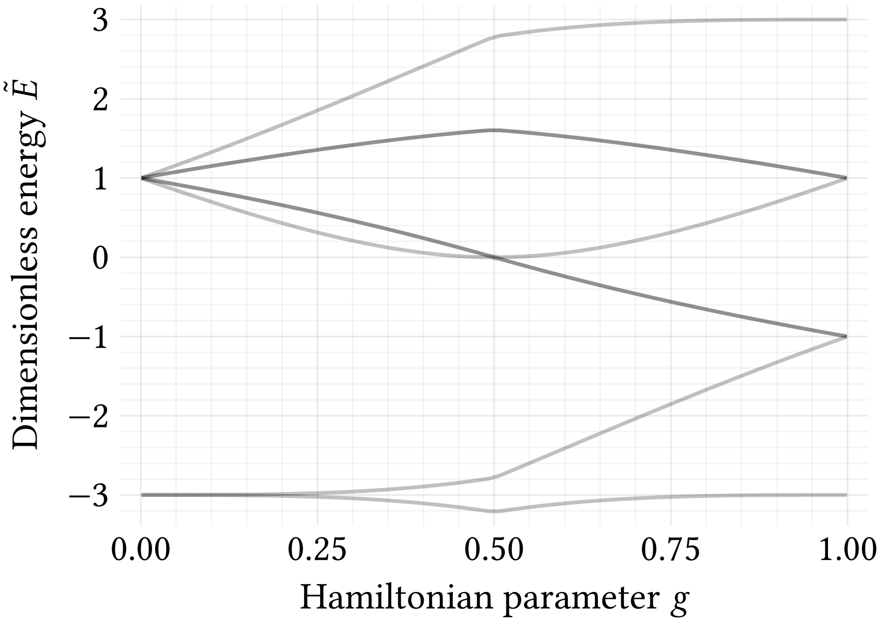

Figure 3.8: Energy levels of eq. (2.34) for $N = 3$ spins.

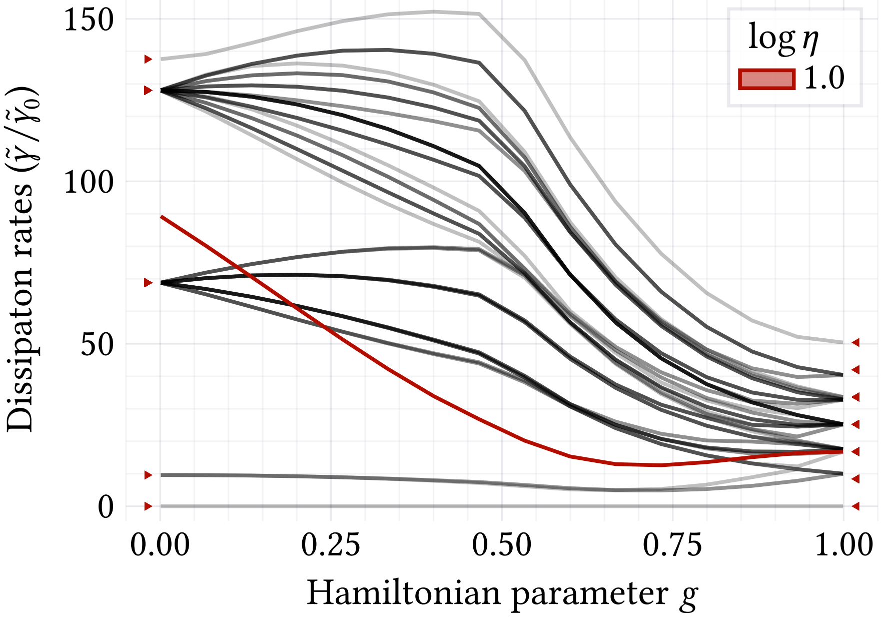

Figure 3.9: Dissipation rate spaghetti diagram for $N = 3$ spins.

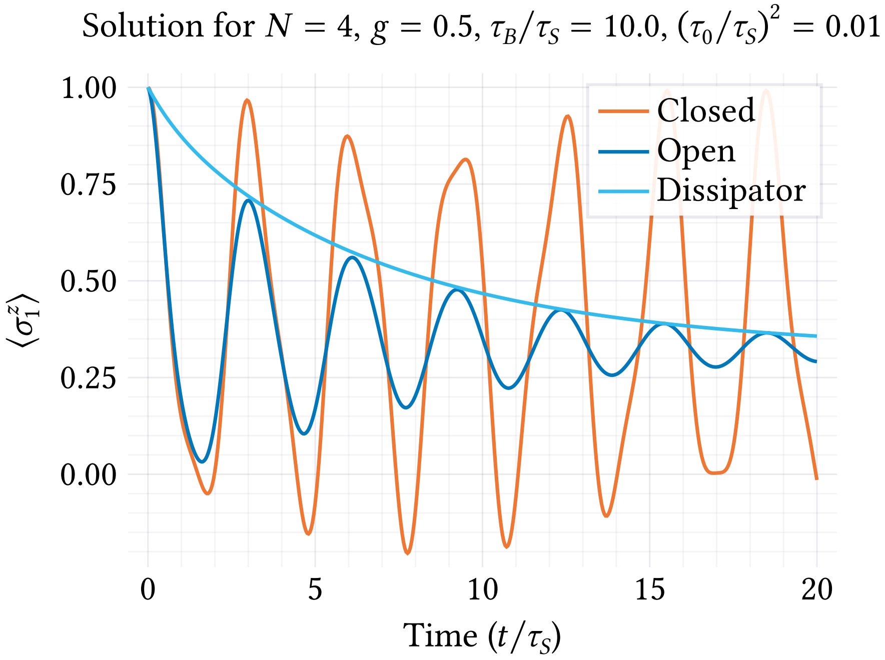

Figure 3.10: Example time evolution for $N = 4$ spins.

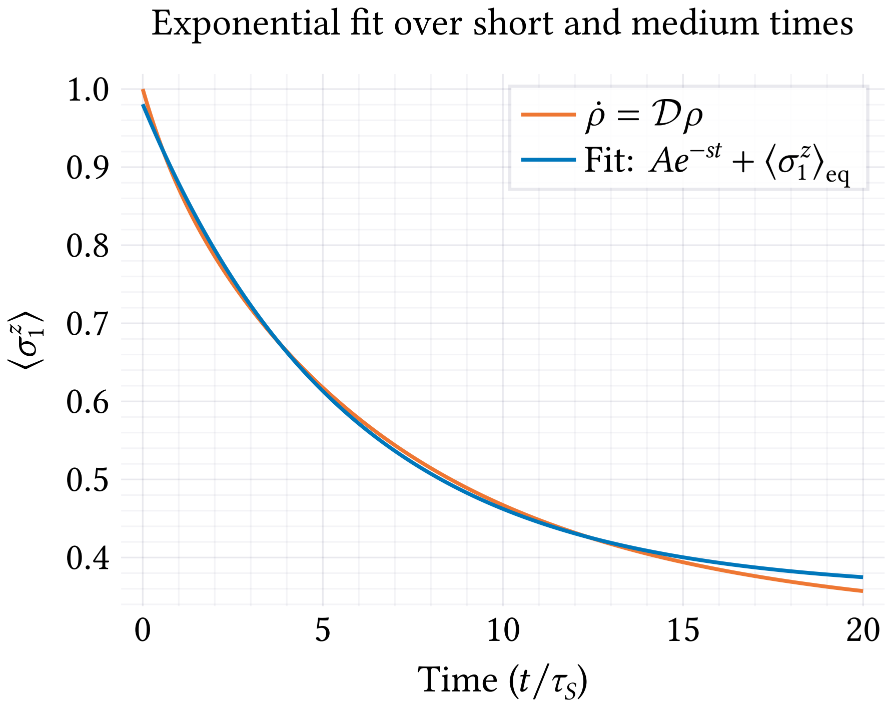

Figure 3.11: Exponential fit for $N = 4$ spins.

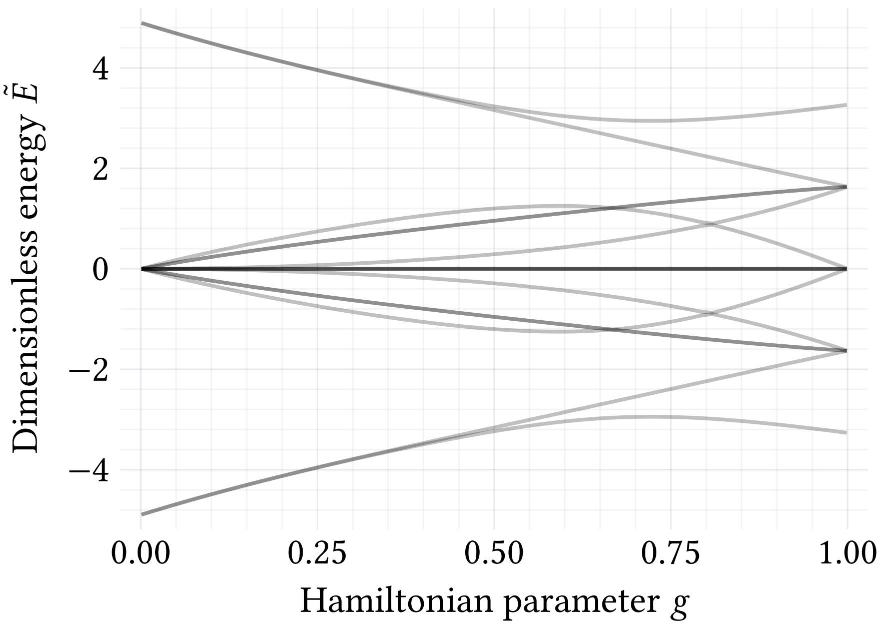

Figure 3.12: Energy levels of eq. (2.34) for $N = 4$ spins.

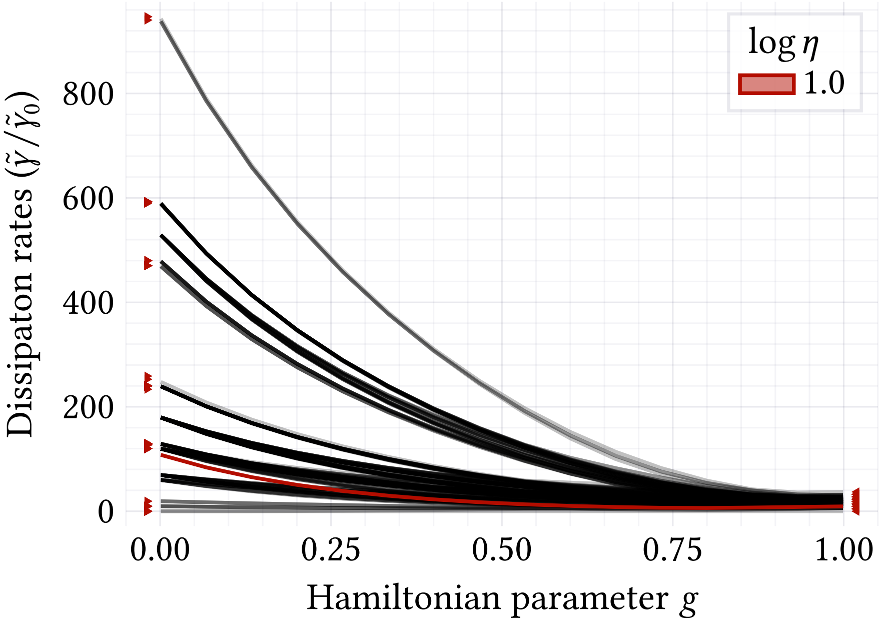

Figure 3.13: Dissipation rate spaghetti diagram for $N = 4$ spins.

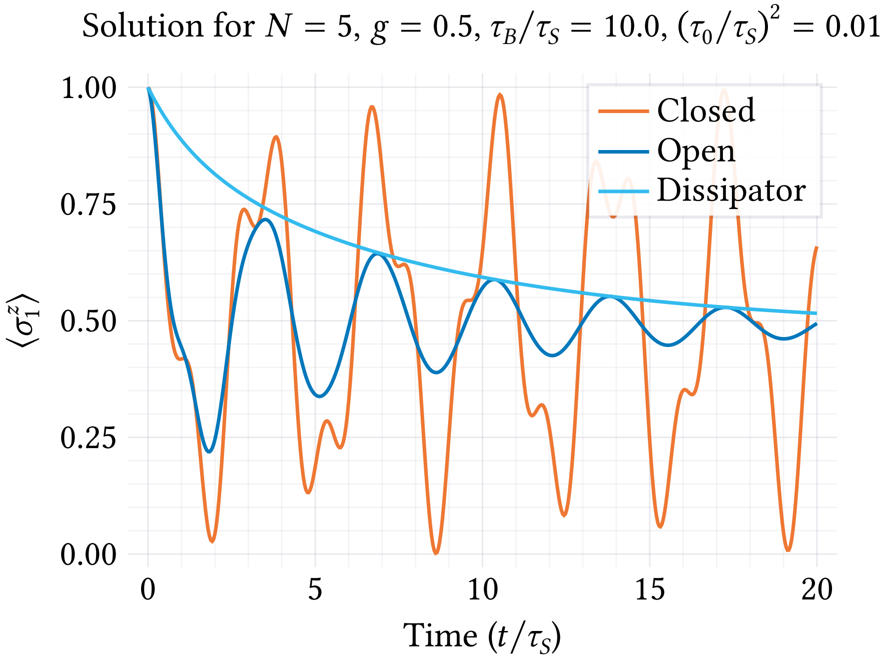

Figure 3.14: Example time evolution for $N = 5$ spins.

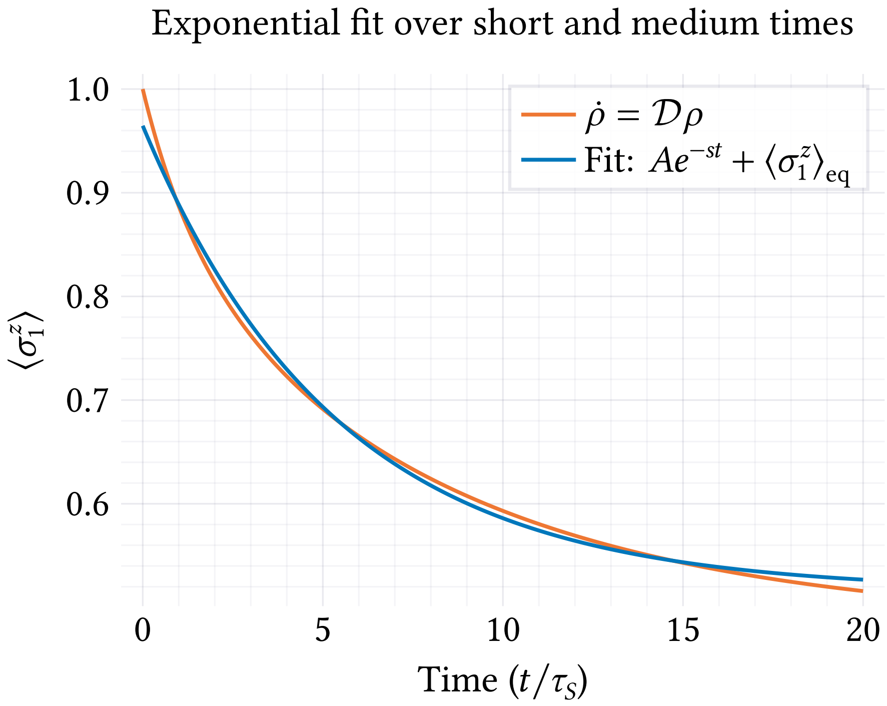

Figure 3.15: Exponential fit for $N = 5$ spins.

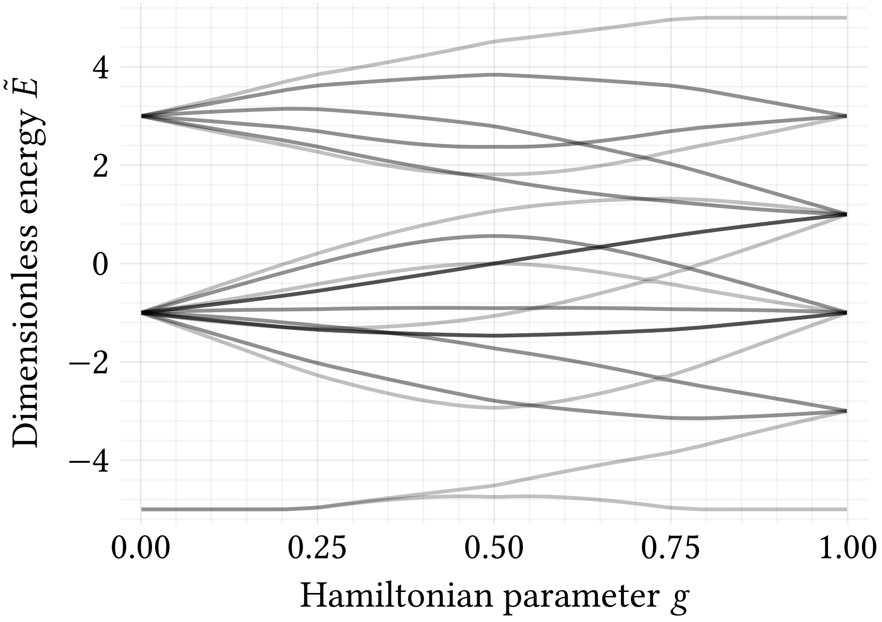

Figure 3.16: Energy levels of eq. (2.34) for $N = 5$ spins.

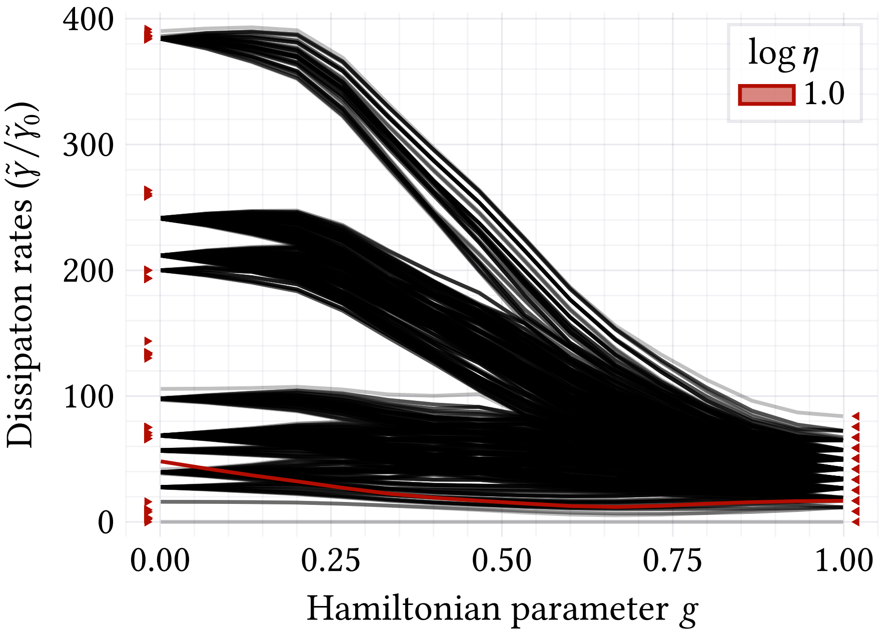

Figure 3.17: Dissipation rate spaghetti diagram for $N = 5$ spins.

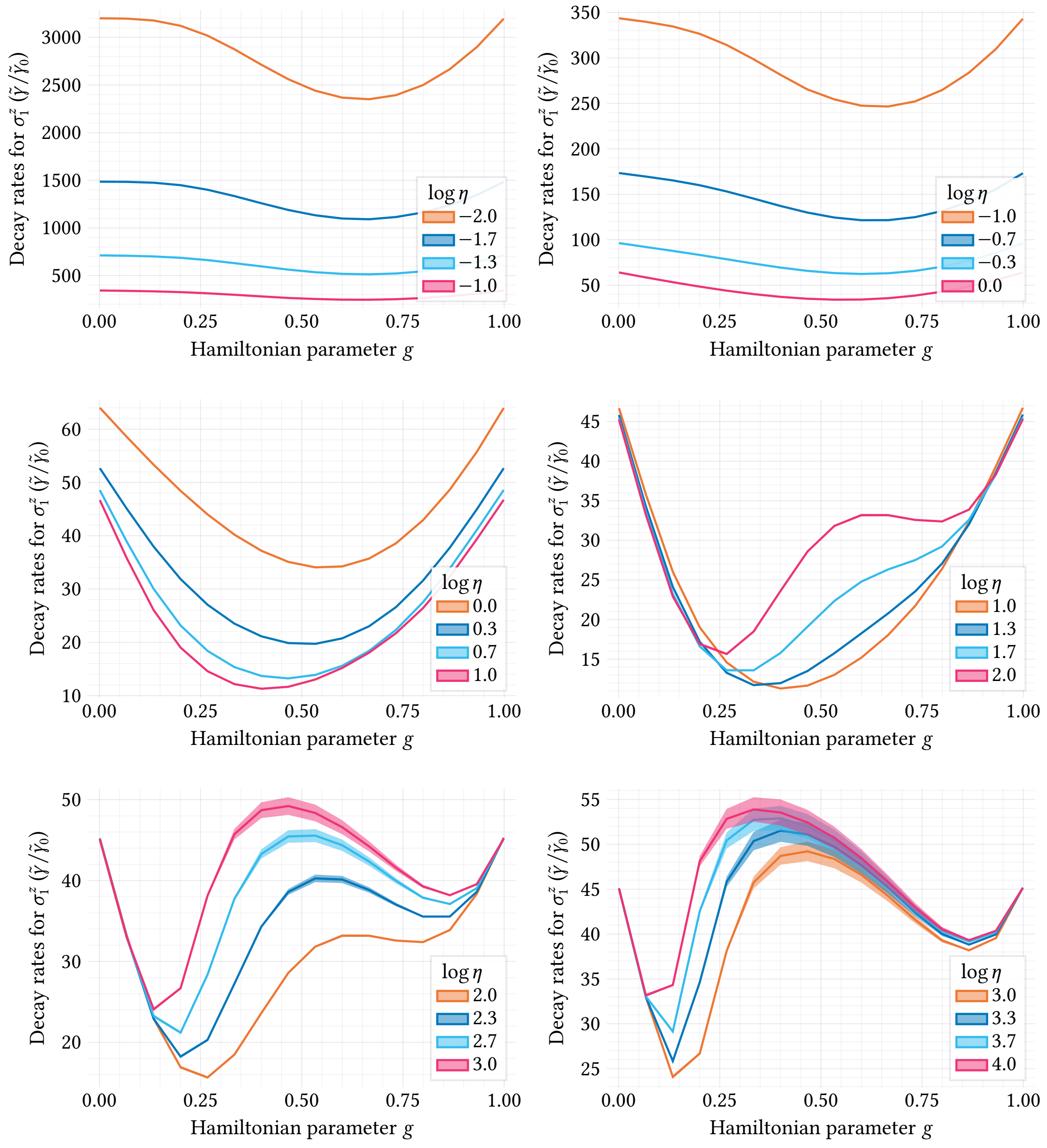

Figure 3.18: Single-spin relaxation rates in different temperature regimes for $N = 2$ spins.

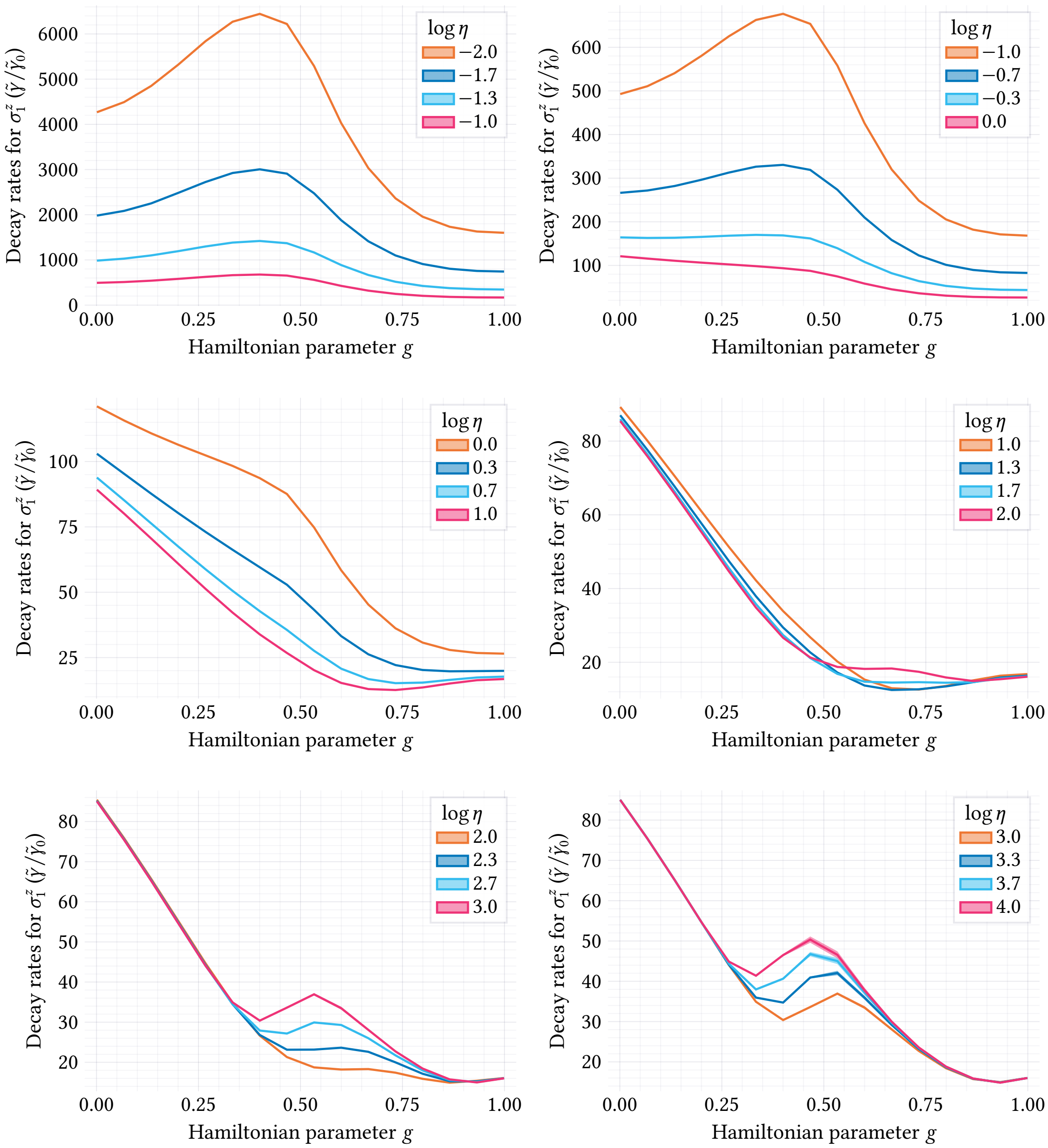

Figure 3.19: Single-spin relaxation rates in different temperature regimes for $N = 3$ spins.

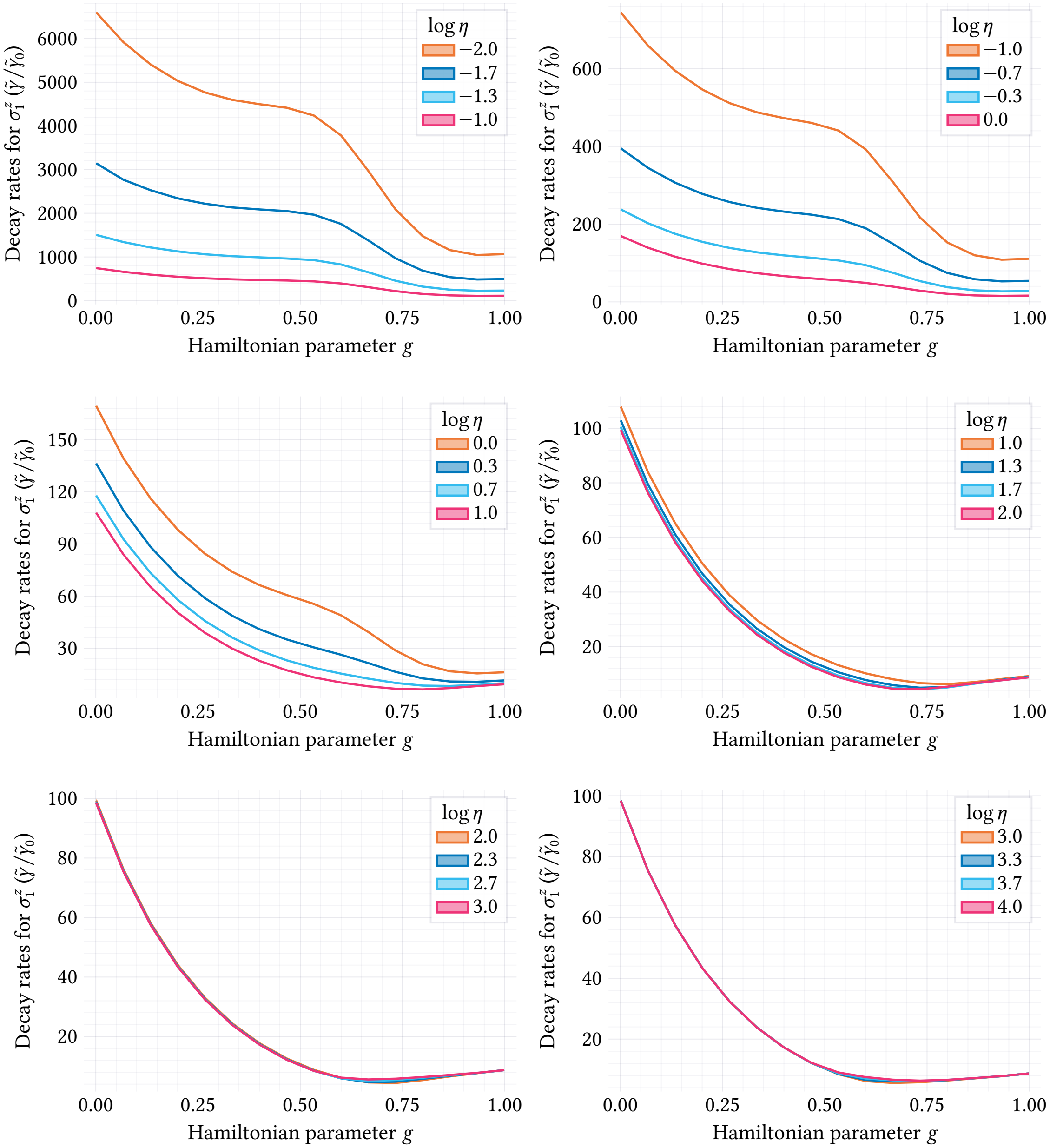

Figure 3.20: Single-spin relaxation rates in different temperature regimes for $N = 4$ spins.

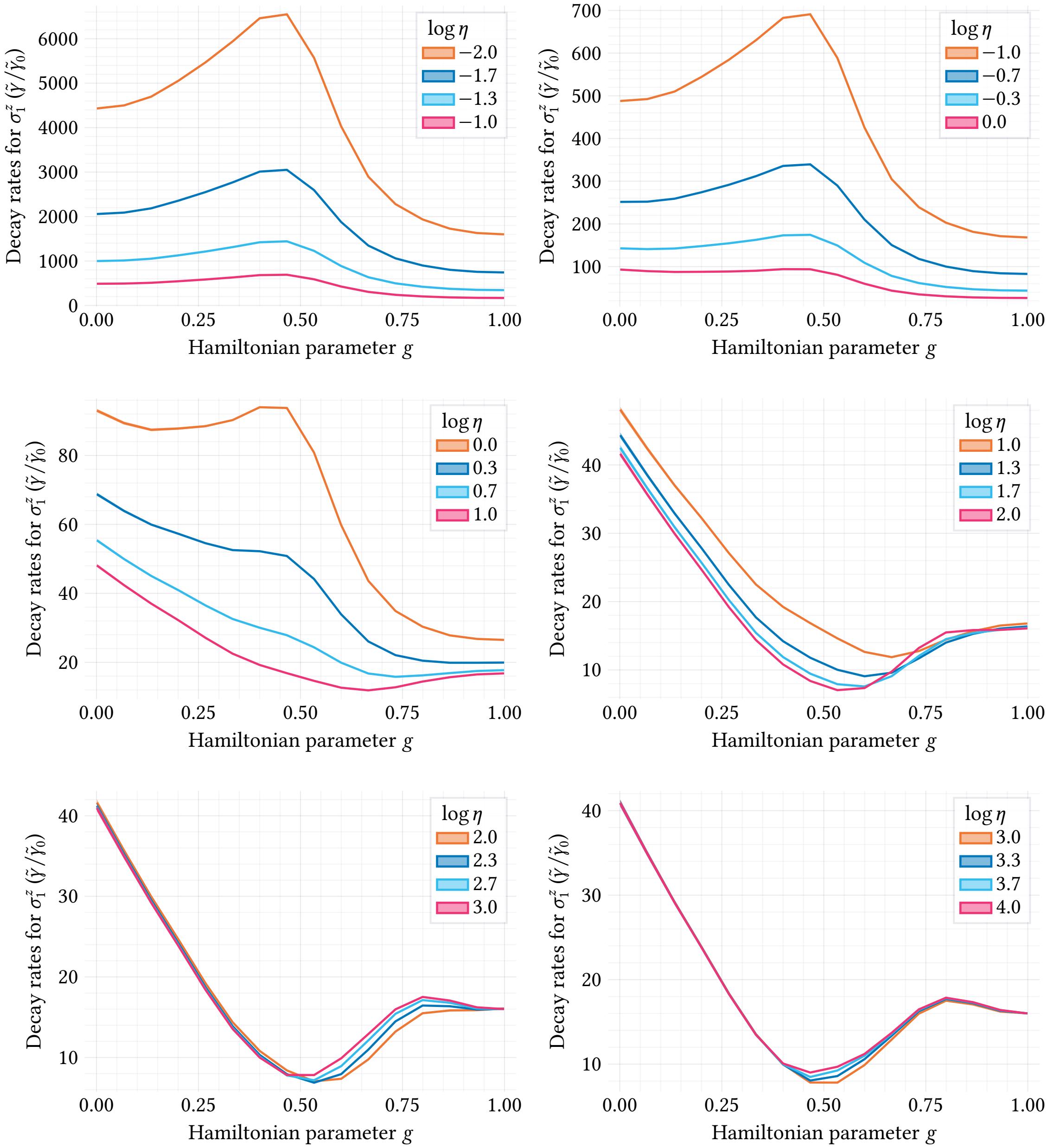

Figure 3.21: Single-spin relaxation rates in different temperature regimes for $N = 5$ spins.

CONCLUSION

We will first discuss the time evolution, energy levels, and spaghetti diagrams.

The time evolution across all systems in figs. 3.2, 3.6, 3.10 and 3.14 looks just as one expects. Motion is generally oscillatory like for the two-level atom, but as N increases higher frequencies are available for the system evolution and manifest like the wiggles in fig. 3.14.

The exponential fits at $\eta = 10$ in figs. 3.3, 3.7, 3.11 and 3.15 are reasonable, but the discrepancies from the true envelopes serve as a reminder that the spin relaxation plots to follow are to be taken with a grain of salt.

The energy levels across figs. 3.4, 3.8, 3.12 and 3.16 depend on whether N is even or odd, as expected from the solution of the full transverse-field Ising model, but generally show that the energy levels for $\hat{H}_x$ as $g \to 0$ are far more degenerate than those for $\hat{H}_z$ as $g \to 1$. This offers an explanation of the trends for the relaxation rates. Take fig. 3.16 for example. For small g, roughly half of the frequencies are zero and half of the frequencies are two (neglecting the lowest eigenvalue below -4). For large g, the energies are divided up more. For large η, eq. (2.76) is like $\tilde{\omega}^3$, and we see that the small g case has the larger sum of cubes. This difference in the energy levels for different g may explain the general shape of the limiting rates discussed below as $\eta \to \infty$. The effect only arises as N grows because there are an insufficient number of eigenvalues to split at small N. At $N = 2$, the maximal similarity between the different sides of the energy level diagram may explain the comparable decay rates found as well.

The spaghetti diagrams (figs. 3.5, 3.9, 3.13 and 3.17) are difficult to decipher. Again, since the eigenoperators V_i of $\mathcal{L}$ are not even states, it is difficult to ascribe meaning to a particular eigenvalue (noodle). Looking to fig. 3.9, the overlaid spin relaxation rate for $\eta = 10$ starts to blend in with the spaghetti near $g = 1$, but behaves differently elsewhere. Here and in later spaghetti diagrams, the overlaid rate appears to rise up as $g \to 0$ as it follows all of the other noodles, yet tends to remain within about a factor of ten away from the value at $g = 1$. The large magnitude of the spaghetti for $N = 4$ appears to be consistent with the even N behavior of the transverse-field Ising model. The full diagram for $N = 6$ could not be computed, but its largest value at $g = 0.01$ was found to be 586.9, which is similar to the general magnitude for $N = 4$.

Overall, the single-spin relaxation plots (figs. 3.18 to 3.21) demonstrate that relaxation rates do depend on the system being considered at all temperatures. It should be reiterated that these plots show the dimensionless rates, so while the difference between $g = 0$ and $g = 1$ at high temperature in fig. 3.20 is about a factor of six, this is a multiplier for an overall rate $\tilde{\gamma}_0$ that may be quite large for any practical purposes. Given that caveat, we identify two general types of behavior depending on temperature. Across all numbers of spins, the high-temperature relaxation rates approach a fixed shape that varies for each N:

- For $N = 2$ there is a minimum relaxation rate around $g = 0.65$.
- For $N = 3$ there is a maximum relaxation rate around $g = 0.40$.
- For $N = 4$ there is a remnant of a peak but the rate generally decreases with increasing g.
- For $N = 5$ there is a maximum relaxation rate around $g = 0.45$.

The story at low temperature is a bit different.

- For $N = 2$ the rates appear to quickly reach a parabola-like shape for $\eta \approx 10$. Afterwards, the fitting becomes unstable as demonstrated by the reversal of the temperature dependence for the rates and the large error ribbons in the last plot.
- For $N = 3$ rates decrease somewhat linearly until $g = 0.5$ and then level out for $\eta \approx 10$. The later plots at lower temperature demonstrate the convergence of the rates for small g but show instability in the fit for g near 0.5.
- For $N = 4$ the convergence to the previous line-flat shape is quicker and the transition from low to high g across $g = 0.5$ is smoothed. The fit is stable and the shape remains for very low temperatures in the last plot.
- For $N = 5$ the flat part of the curve has lifted to reveal a parabola shape with a minimum at about $g = 0.45$.

Again, how much does varying the parameter g change the relaxation rate of $\langle \sigma_1^z \rangle$? In short, the answer is by at most a factor of ten.

Given the deviation of the single-spin relaxation rate from the rest of the spaghetti, it is unclear how well these results generalize to other systems or observables. The large N limit remains to be explored, but is computationally intractable with these methods. It would be interesting to consider a wide range of other observables and initial states to better understand the filtering of the spaghetti diagrams to produce a single effective decay rate for the observable. Future work could also look at different systems. Given our normalization procedure, this could lead to a more systematic exploration that looks at arbitrary Hamiltonians. Perhaps the theory of random matrices could provide statistical predictions for normalized decay rates, since statistics for the eigenvalue spacings ω are well-understood.

APPENDIX A

THE GENERATOR OF A QUANTUM DYNAMICAL SEMIGROUP

The contents of this appendix follow [18].

Let $\mathcal{V}(t)$ for $t \geqslant 0$ be a family of completely positive and trace-preserving CPTP maps on $\mathcal{L}(\mathcal{H})$ with the **semigroup property** that

$$\mathcal{V}(t)\mathcal{V}(s) = \mathcal{V}(t+s). \tag{A.1}$$

In the physical context, $\mathcal{V}(t)$ is a dynamical map for the reduced dynamics of a system, and the semigroup property is that the dynamics are Markovian or memoryless, just like when one coarse-grains to the system time in the weak-coupling limit.

By analogy to Stone's theorem, we expect that there is a generator $\mathcal{L}$ of the semigroup such that

$$\mathcal{V}(t) = e^{\mathcal{L}t}. \tag{A.2}$$

We are interested in obtaining a **master equation** of the form

$$\dot{\rho} = \mathcal{L}\rho. \tag{A.3}$$

We may find $\mathcal{L}$ as follows. Since $\mathcal{V}(t)$ is CPTP, it may be decomposed with the help of the Kraus representation theorem as

$$\mathcal{V}(t)\rho = \sum_i M_i(t)\rho M_i^\dagger(t), \tag{A.4}$$

where $\sum_i M_i^\dagger(t) M_i = 1$. We can express the M_i in terms of an orthonormal complete basis $\{F_n\}$ for $\mathcal{L}(\mathcal{H})$ as $M_i = \sum_n F_n \langle F_n | M_i \rangle$. Then eq. (A.4) becomes

$$\mathcal{V}(t)\rho = \sum_{mn} c_{mn}(t) F_m \rho F_n^\dagger , \tag{A.5}$$

where

$$c_{mn}(t) \equiv \sum_i \langle F_m | M_i(t) \rangle \langle M_i(t) | F_n \rangle . \tag{A.6}$$

For convenience, we may choose $F_{d^2} = 1/\sqrt{d}$, where $d = \dim(\mathcal{H})$. With an eye towards simplifying eq. (A.11), we eliminate the explicit time dependence of eq. (A.6) by defining

$$a_{mn} \equiv \lim_{t\to 0^+} \frac{c_{mn}(t) - d\delta_{d^2 d^2}}{t} \tag{A.7}$$

and introduce the sum of Kraus operators

$$\begin{aligned} F &= \frac{1}{\sqrt{d}} \sum_{n=1}^{d^2-1} a_{nd^2} F_n && \text{(A.8)} \\ &= \frac{F + F^\dagger}{2} + \mathrm{i}\frac{F - F^\dagger}{2\mathrm{i}} \equiv G - \mathrm{i}H, && \text{(A.9)} \end{aligned}$$

where we have decomposed the sum F into Hermitian and anti-Hermitian parts. Now we may write the master equation $\dot{\rho} = \mathcal{L}\rho$ as

$$\begin{aligned} \dot{\rho} &= \lim_{\Delta t \to 0^+} \frac{\mathcal{V}(\Delta t)\rho - \rho}{\Delta t} && \text{(A.10)} \\ &= \lim_{\Delta t \to 0^+} \left(\frac{c_{d^2 d^2} - d}{d\Delta t}\rho + \sum_{m,n=1}^{d^2-1} \frac{c_{mn}(\Delta t)}{\Delta t} F_m \rho F_n^\dagger \right. \\ &\qquad \left. + \frac{1}{\sqrt{d}} \sum_{n=1}^{d^2-1} \left(\frac{c_{nd^2}(\Delta t)}{\Delta t} F_n \rho + \frac{c_{d^2 n}(\Delta t)}{\Delta t} \rho F_n^\dagger \right) \right) && \text{(A.11)} \\ &= \frac{a_{d^2 d^2}}{d}\rho + F\rho + \rho F^\dagger + \sum_{m,n=1}^{d^2-1} a_{mn} F_m \rho F_n^\dagger && \text{(A.12)} \\ &= \frac{a_{d^2 d^2}}{d}\rho + \{G, \rho\} - \mathrm{i}[H, \rho] + \sum_{m,n=1}^{d^2-1} a_{mn} F_m \rho F_n^\dagger && \text{(A.13)} \\ &= \{G', \rho\} - \mathrm{i}[H, \rho] + \sum_{m,n=1}^{d^2-1} a_{mn} F_m \rho F_n^\dagger , && \text{(A.14)} \end{aligned}$$

where $G' = G + a_{d^2 d^2} \mathbb{1} \big/ d$. Since $\mathcal{V}(t)$ is trace-preserving, $\operatorname{tr} \dot{\rho} = 0$. Applying this condition to eq. (A.14) and cycling the trace gives

$$0 = \operatorname{tr}\left(2G'\rho + \sum_{m,n=1}^{d^2-1} a_{mn} F_n^\dagger F_m \rho \right), \tag{A.15}$$

so $G' = -\sum_{m,n=1}^{d^2-1} a_{mn} F_n^\dagger F_m / 2$. This allows us to write eq. (A.14) as

$$\dot{\rho} = -\mathrm{i}[H, \rho] + \sum_{m,n=1}^{d^2-1} a_{mn} \left(F_m \rho F_n^\dagger - \frac{1}{2} \left\{ F_n^\dagger F_m, \rho \right\} \right), \tag{A.16}$$

which is the first form of the **Lindblad equation**. This may be simplified further if we diagonalize the coefficient matrix a by applying a unitary transformation u to give $a = u\gamma u^\dagger$, where the $\{\gamma_k\}_{k=1}^{d^2-1}$ are the non-negative eigenvalues of a. This is possible since the coefficient matrix c is seen from eq. (A.6) to be Hermitian, and eq. (A.7) then gives that a is Hermitian. We may then express $F_{n \neq d^2} = \sum_{k=1}^{d^2-1} L_n u_{nk}$ in terms of the **Lindblad** or **jump operators** L_n to find

$$\dot{\rho} = -\mathrm{i}[H, \rho] + \sum_{k=1}^{d^2-1} \gamma_k \left(L_k \rho L_k^\dagger - \frac{1}{2} \left\{ L_k^\dagger L_k, \rho \right\} \right), \tag{A.17}$$

which is the diagonal form of the Lindblad equation.

It has been proven that that this is the most general generator for a quantum dynamical semigroup when the system is finite-dimensional [34] and when the system is infinite-dimensional but $\mathcal{L}$ is bounded [35]. This is not much help, since the Hamiltonians for even simple infinite-dimensional systems like the harmonic oscillator are unbounded. Regardless, most examples where $\mathcal{L}$ is unbounded may still be cast into Lindblad form with little or no modification.

APPENDIX B

THE TRANSVERSE-FIELD ISING MODEL

We would like to solve the Hamiltonian eq. (2.22), which we nondimensionalize as

$$\frac{4}{J}H = -\sum_{i\in\mathbb{Z}_N} \left(\sigma_i^x\sigma_{i+1}^x + g\sigma_i^z\right) \tag{B.1}$$

for the periodic transverse-field Ising chain with N spins. We will drop the $4/J$ in what follows. We notice that the operators

$$\sigma_i^\pm = \frac{\sigma_i^x \pm \mathrm{i}\sigma_i^y}{2} \tag{B.2}$$

satisfy

$$\sigma_i^z = 2\sigma_i^+\sigma_i^- - 1 \tag{B.3}$$

and have commutators

$$\begin{aligned}
\left[\sigma_i^+, \sigma_j^-\right] &= \frac{1}{4}\left[\sigma_i^x + \mathrm{i}\sigma_i^y, \sigma_j^x - \mathrm{i}\sigma_j^y\right] && \text{(B.4)}\\
&= \frac{1}{4}\left(\left[\sigma_i^x, \sigma_j^x\right] + \left[\sigma_i^y, \sigma_j^y\right] + \mathrm{i}\left[\sigma_i^y, \sigma_j^x\right] - \mathrm{i}\left[\sigma_i^x, \sigma_j^y\right]\right) && \text{(B.5)}\\
&= \delta_{ij}\sigma_i^z. && \text{(B.6)}
\end{aligned}$$

Thus their anticommutators are

$$\begin{aligned}
\left\{\sigma_i^+, \sigma_j^-\right\} &= 2\sigma_i^+\sigma_j^- - \left[\sigma_i^+, \sigma_j^-\right] && \text{(B.7)}\\
&= 2\sigma_i^+\sigma_j^- - \delta_{ij}\sigma_i^z && \text{(B.8)}\\
&= \delta_{ij}1 + 2\sigma_i^+\sigma_j^-(1-\delta_{ij}). && \text{(B.9)}
\end{aligned}$$

It could be helpful to think of the $\sigma_i^\pm$ as fermion creation and annihilation operators, but they do not anticommute at different sites.

How might we construct operators that satisfy the fermionic canonical anticommutation relations (CARs) from the Pauli operators? Suppose we have such operators c_i. Given a tuple $\boldsymbol{n} = (n_i)_{i\in\mathbb{Z}_N}$, we have the corresponding states

$$|\boldsymbol{n}\rangle = \prod_{i\in\mathbb{Z}_N} \left(c_i^\dagger\right)^{n_i} |\boldsymbol{0}\rangle \,, \tag{B.10}$$

where $|\boldsymbol{0}\rangle$ denotes the vacuum state. It then follows that

$$c_i \, |\boldsymbol{n}\rangle = -n_i(-1)^{n_{<i}} \, |\boldsymbol{n}_{i\leftarrow 0}\rangle \tag{B.11}$$

$$c_i^\dagger \, |\boldsymbol{n}\rangle = -(1-n_i)(-1)^{n_{<i}} \, |\boldsymbol{n}_{i\leftarrow 1}\rangle \,, \tag{B.12}$$

where $\boldsymbol{n}_{i\leftarrow m} = \boldsymbol{n}$ with $n_i = m$ and $n_{<i} = \sum_{j<i} n_j$.

Thus the number operator is

$$c_i^\dagger c_i \, |\boldsymbol{n}\rangle = (1-0)(-1)^{n_{<i}} n_i (-1)^{n_{<i}} \, |\boldsymbol{n}_{i\leftarrow 1}\rangle \tag{B.13}$$

$$= n_i \, |\boldsymbol{n}\rangle \,. \tag{B.14}$$

This leads us to consider

$$c_i = -\left(\prod_{j<i} -\sigma_j^z\right)\sigma_i^- \tag{B.15}$$

acting on the states

$$|\boldsymbol{n}\rangle = \prod_{i\in\mathbb{Z}_N} \left(\sigma_i^+\right)^{n_i} |\boldsymbol{0}\rangle \,, \tag{B.16}$$

where $|\boldsymbol{0}\rangle = |{\uparrow}\rangle^{\otimes N}$ is the state with all z-spins up, or all zero qubits. This gives the same result as eq. (B.11), so the c_i satisfy the CARs. This process of mapping spin-1/2 sites to non-local fermions is known as the **Jordan-Wigner transformation**. We may then compute that the inverse transformations are

$$\sigma_i^+ \sigma_i^- = c_i^\dagger c_i \tag{B.17}$$

$$\sigma_i^z = 2c_i^\dagger c_i - 1 \tag{B.18}$$

$$\sigma_i^x = -\left(\prod_{j<i}\left(1 - 2c_j^\dagger c_j\right)\right)\left(c_i^\dagger + c_i\right) \tag{B.19}$$

$$\sigma_i^y = \mathrm{i}\left(\prod_{j<i}\left(1 - 2c_j^\dagger c_j\right)\right)\left(c_i^\dagger - c_i\right). \tag{B.20}$$

While σ_i^x remains complicated, the product $\sigma_i^x \sigma_{i+1}^x$ does not. For $i < N-1$,

$$\begin{aligned} \sigma_i^x \sigma_{i+1}^x &= \left(\prod_{j<i} \left(2c_j^\dagger c_j - 1\right) \right) \left(c_i^\dagger + c_i\right) \left(\prod_{j<i+1} \left(2c_j^\dagger c_j - 1\right) \right) \left(c_{i+1}^\dagger + c_{i+1}\right) && \text{(B.21)} \\ &= \left(c_i^\dagger + c_i\right)\left(1 - 2c_i^\dagger c_i\right)\left(c_{i+1}^\dagger + c_{i+1}\right) && \text{(B.22)} \\ &= \left(c_i^\dagger - c_i\right)\left(c_{i+1}^\dagger + c_{i+1}\right), && \text{(B.23)} \end{aligned}$$

and for $i = N-1$,

$$\sigma_{N-1}^x \sigma_0^x = \left(\prod_{j<N-1} \left(2c_j^\dagger c_j - 1\right) \right) \left(c_{N-1}^\dagger + c_{N-1}\right)\left(c_0^\dagger + c_0\right). \tag{B.24}$$

We may now perform the Jordan-Wigner transformation of eq. (B.1) to obtain

$$\begin{aligned} H = &\sum_i \left(c_i - c_i^\dagger\right)\left(c_{i+1}^\dagger + c_{i+1}\right) - g \sum_i 2c_i^\dagger c_i + gN1 \\ &- \left(1 - \prod_{j<N-1} \left(2c_j^\dagger c_j - 1\right)\right)\left(c_{N-1} - c_{N-1}^\dagger\right)\left(c_0^\dagger + c_0\right). \end{aligned} \tag{B.25}$$

We now Fourier transform with

$$c_i = \frac{1}{\sqrt{N}} \sum_k e^{\mathrm{i}ki} C_k \tag{B.26a}$$

$$C_k = \frac{1}{\sqrt{N}} \sum_i e^{-\mathrm{i}ki} c_i \tag{B.26b}$$

and

$$c_i^\dagger = \frac{1}{\sqrt{N}} \sum_k e^{-\mathrm{i}ki} C_k^\dagger \tag{B.26c}$$

$$C_k^\dagger = \frac{1}{\sqrt{N}} \sum_i e^{\mathrm{i}ki} c_i^\dagger. \tag{B.26d}$$

We now propagate the periodic boundary conditions to the Fourier-transformed operators.

$$c_0 = \frac{1}{\sqrt{N}} \sum_k C_k \tag{B.27}$$

$$c_N = \frac{1}{\sqrt{N}} \sum_k e^{\mathrm{i}kN} C_k. \tag{B.28}$$

We then must require that

$$kN \equiv 0 \pmod{2\pi} \tag{B.29}$$

$$k = \frac{2\pi n}{N} - \frac{N - [N \text{ odd}]}{N}\pi, \quad n \in \mathbb{Z}_N. \tag{B.30}$$

For N odd, what is C_π?

$$C_\pi = \frac{1}{\sqrt{N}} \sum_i e^{-\mathrm{i}\pi i} c_i. \tag{B.31}$$

Since $e^{-\mathrm{i}\pi i} = e^{\mathrm{i}\pi i}$, $C_\pi = C_{-\pi}$.

We now verify that this operator Fourier transformation is a unitary operation. That is, it preserves the fermionic CARs.

Proof. Consider N fermionic operators c_i and a $N \times N$ unitary matrix $\boldsymbol{U}$. We may change bases with

$$C_k^\dagger = \sum_i U_{ik} c_i^\dagger. \tag{B.32}$$

Then

$$\begin{aligned}
\left\{C_k, C_{k'}^\dagger\right\} &= \sum_{ij} U_{ik}^* U_{jk'} \left\{c_i, c_j^\dagger\right\} && \text{(B.33)}\\
&= \sum_i U_{ik}^* U_{ik'} && \text{(B.34)}\\
&= \left(\boldsymbol{U}^\dagger \boldsymbol{U}\right)_{kk'} && \text{(B.35)}\\
&= \delta_{kk'}, && \text{(B.36)}
\end{aligned}$$

and similar for the other fermionic (anti)-commutation relations.

For the Fourier transform,

$$F_{ik} = \frac{1}{\sqrt{N}} e^{\mathrm{i}ki}. \tag{B.37}$$

We may then confirm that

$$\begin{aligned}
\left(\boldsymbol{F}^\dagger \boldsymbol{F}\right)_{kk'} &= \sum_i \frac{1}{N} e^{\mathrm{i}(k'-k)i} && \text{(B.38)}\\
&= \delta_{kk'}. && \text{(B.39)}
\end{aligned}$$

Thus the Fourier transform is unitary. □

We are now equipped to Fourier transform eq. (B.25) as follows. Since

$$\frac{1}{N}\sum_{i\in\mathbb{Z}_N} e^{\mathrm{i}(k'-k)i} = \delta_{kk'}, \tag{B.40}$$

and also

$$C_{-k} = C_k^* \tag{B.41}$$

$$= \frac{1}{\sqrt{N}}\sum_i e^{-\mathrm{i}(-k)i} c_i \tag{B.42}$$

$$= \frac{1}{N}\sum_{ik'} e^{\mathrm{i}(k'+k)i} C_{k'}, \tag{B.43}$$

we have that

$$\sum_i c_i^\dagger c_i = \frac{1}{N}\sum_{ikk'} e^{\mathrm{i}(k'-k)i} C_k^\dagger C_{k'} \tag{B.44}$$

$$= \sum_k C_k^\dagger C_k, \tag{B.45}$$

$$\sum_i \left(c_i^\dagger c_{i+1} + c_{i+1}^\dagger c_i\right) = \frac{1}{N}\sum_{ikk'} e^{\mathrm{i}(k'-k)i}\left(e^{\mathrm{i}k'} + e^{-\mathrm{i}k}\right) C_k^\dagger C_{k'} \tag{B.46}$$

$$= \sum_k 2\cos k\, C_k^\dagger C_k, \tag{B.47}$$

$$\sum_i \left(c_{i+1} c_i + c_i^\dagger c_{i+1}^\dagger\right) = \frac{1}{N}\sum_{ikk'} \left(e^{\mathrm{i}(k'+k)i} e^{\mathrm{i}k} C_k C_{k'} + e^{-\mathrm{i}(k'+k)i} e^{-\mathrm{i}k'} C_k^\dagger C_{k'}^\dagger\right) \tag{B.48}$$

$$= \sum_k \left(e^{-\mathrm{i}k} C_{-k} C_k + e^{\mathrm{i}k} C_k^\dagger C_{-k}^\dagger\right). \tag{B.49}$$

Thus eq. (B.25) is now

$$H = -\sum_k 2\cos k\, C_k^\dagger C_k + \sum_k \left(e^{-\mathrm{i}k} C_{-k} C_k + e^{\mathrm{i}k} C_k^\dagger C_{-k}^\dagger\right) - \sum_k 2g C_k^\dagger C_k + gN1 \tag{B.50}$$

$$= -\sum_k (g + \cos k)\left(C_k^\dagger C_k + C_{-k}^\dagger C_{-k}\right) + \sum_k \mathrm{i}\sin k\left(C_{-k} C_k - C_k^\dagger C_{-k}^\dagger\right) + gN1 \tag{B.51}$$

$$= -\sum_k (g + \cos k)\left(C_k^\dagger C_k - C_{-k} C_{-k}^\dagger\right) + \sum_k \mathrm{i}\sin k\left(C_{-k} C_k - C_k^\dagger C_{-k}^\dagger\right) \tag{B.52}$$

$$= \sum_k \boldsymbol{v}_k^\dagger \boldsymbol{H}_k \boldsymbol{v}_k, \tag{B.53}$$

where

$$\boldsymbol{H}_k = \begin{bmatrix} -(g+\cos k) & -\mathrm{i}\sin k \\ \mathrm{i}\sin k & g+\cos k \end{bmatrix}, \tag{B.54}$$

$$\boldsymbol{v}_k = \begin{bmatrix} C_k \\ C_{-k}^\dagger \end{bmatrix}, \tag{B.55}$$

and we have used that

$$\sum_k \cos k = 0. \tag{B.56}$$

Since the $\boldsymbol{H}_k$ are Hermitian, they may be diagonalized by a unitary transformation of the $\boldsymbol{v}_k$.[1] The $\boldsymbol{H}_k$ are traceless, so they have the eigenvalues

$$E_k^\pm = \pm\sqrt{-\det \boldsymbol{H}_k} \tag{B.62}$$

$$= \pm\sqrt{g^2 + 2g\cos k + \cos^2 k + \sin^2 k} \tag{B.63}$$

$$= \pm\sqrt{g^2 + 2g\cos k + 1}. \tag{B.64}$$

The eigenvectors are then

$$\boldsymbol{q}_k^\pm = \begin{bmatrix} -\mathrm{i}\sin k \\ E_k^\pm + g + \cos k \end{bmatrix}, \tag{B.65}$$

except if $k = 0$ or $-\pi$, in which case

$$\boldsymbol{q}_k^- = \begin{bmatrix} 1 \\ 0 \end{bmatrix} \quad \text{and} \quad \boldsymbol{q}_k^+ = \begin{bmatrix} 0 \\ 1 \end{bmatrix}. \tag{B.66}$$

---

[1] The unitary transformation of the $C_{\pm k}$ to obtain $\eta_k^\pm$ is an instance of a fermionic **Bogoliubov transformation**:

$$C_k = u f_k + v g_k^\dagger \tag{B.57a}$$

and

$$C_{-k} = -v f_k^\dagger + u g_k. \tag{B.57b}$$

For these transformations to preserve the CARs,

$$\left\{C_k^\dagger, C_k\right\} = |u|^2\left\{f_k^\dagger, f_k\right\} + |v|^2\left\{g_k, g_k^\dagger\right\} + u^* v\left\{f_k^\dagger, g_k^\dagger\right\} + v^* u\{g_k, f_k\} \tag{B.58}$$

$$= \left(|u|^2 + |v|^2\right)1, \tag{B.59}$$

so we must have

$$|u|^2 + |v|^2 = 1. \tag{B.60}$$

We may choose

$$u = e^{\mathrm{i}\phi_1}\cos\theta \tag{B.61a}$$

$$v = e^{\mathrm{i}\phi_2}\sin\theta \tag{B.61b}$$

for real angles ϕ_1, ϕ_2, and θ.

The $k = -\pi$ case does not appear if N is odd. If also $g = 1$, then $\boldsymbol{H}_{-\pi} = \boldsymbol{0}$. To construct the unitary transformation, we must normalize the $\boldsymbol{q}_k^\pm$. We find that

$$\begin{aligned}
\left\|\boldsymbol{q}_k^\pm\right\|^2 &= \left(E_k^\pm + g + \cos k\right)^2 + \sin^2 k && \text{(B.67)}\\
&= \left(E_k^\pm\right)^2 + g^2 + \cos^2 k + 2g\cos k + 2E_k^\pm(g + \cos k) + 1 - \cos^2 k && \text{(B.68)}\\
&= 2E_k^\pm\left(E_k^\pm + g + \cos k\right). && \text{(B.69)}
\end{aligned}$$

Now

$$\begin{aligned}
\frac{\left(\boldsymbol{q}_k^\pm\right)_1}{\left\|\boldsymbol{q}_k^\pm\right\|} &= \frac{-\mathrm{i}\sin k}{\sqrt{2E_k^\pm\left(E_k^\pm + g + \cos k\right)}} && \text{(B.70)}\\
&= \frac{-\mathrm{i}\sin k}{\sqrt{2\left|E_k^\pm\right|\left(\left|E_k^\pm\right| \pm (g + \cos k)\right)}} && \text{(B.71)}
\end{aligned}$$

and

$$\begin{aligned}
\frac{\left(\boldsymbol{q}_k^\pm\right)_2}{\left\|\boldsymbol{q}_k^\pm\right\|} &= \pm\sqrt{\frac{E_k^\pm + (g + \cos k)}{2E_k^\pm}} && \text{(B.72)}\\
&= \pm\sqrt{\frac{\left|E_k^\pm\right| \pm (g + \cos k)}{2\left|E_k^\pm\right|}} && \text{(B.73)}
\end{aligned}$$

$$\boldsymbol{U}_k^\dagger = \begin{bmatrix} \left(\hat{\boldsymbol{q}}_k^-\right)^\dagger \\ \left(\hat{\boldsymbol{q}}_k^+\right)^\dagger \end{bmatrix}. \tag{B.74}$$

Then with $E_k = \left|E_k^\pm\right|$,

$$\eta_k^\pm = \frac{\mathrm{i}\sin k}{\sqrt{2E_k(E_k \pm (g + \cos k))}} C_k \pm \sqrt{\frac{E_k \pm (g + \cos k)}{2E_k}} C_{-k}^\dagger \tag{B.75}$$

so that

$$\begin{aligned}
\left\{\left(\eta_k^\pm\right)^\dagger, \eta_k^\pm\right\} &= \frac{\sin^2 k}{2E_k(E_k \pm (g + \cos k))} 1 + \frac{E_k \pm (g + \cos k)}{2E_k} 1 && \text{(B.76)}\\
&= 1 && \text{(B.77)}\\
\left\{\left(\eta_k^\pm\right)^\dagger, \eta_k^\mp\right\} &= \frac{\sin^2 k}{2E_k\sqrt{E_k \pm (g + \cos k)}\sqrt{E_k \mp (g + \cos k)}} 1 \\
&\quad - \frac{\sqrt{E_k \pm (g + \cos k)}\sqrt{E_k \mp (g + \cos k)}}{2E_k} 1 && \text{(B.78)}\\
&= 0. && \text{(B.79)}
\end{aligned}$$

Note that eq. (B.75) is consistent with the edge cases in the limits $k \to -\pi$ and $k \to 0$. If also $g = 1$, then we impose that $\eta_{-\pi} = C_{\pi}^{\dagger}$, which is the same as if $g \neq 1$.

Equation (B.53) becomes

$$H = \sum_k E_k^+ \left(\eta_k^+\right)^\dagger \eta_k^+ + \sum_k E_k^- \left(\eta_k^-\right)^\dagger \eta_k^- . \tag{B.80}$$

Since

$$\left(\eta_{-k}^-\right)^\dagger = \eta_k^+ =: \eta_k \tag{B.81}$$

and $E_{-k}^{\pm} = E_k^{\pm}$, we may reduce eq. (B.80) to

$$H = \sum_k E_k \eta_k^\dagger \eta_k - \sum_k E_k \left(1 - \eta_k^\dagger \eta_k\right) \tag{B.82}$$

$$= \sum_k 2E_k \eta_k^\dagger \eta_k - 1 \sum_k E_k . \tag{B.83}$$

APPENDIX C

COMPUTER DETAILS

In the interest of transparency and reproducibility, hardware and version information are included below. The setup code that runs before any of the code snippets in the text is given in appendix C.2.

C.1 JULIA VERSION INFORMATION

```
versioninfo()
```

```
Julia Version 1.6.0
Commit f9720dc2eb (2021-03-24 12:55 UTC)
Platform Info:
  OS: Linux (x86_64-pc-linux-gnu)
  CPU: Intel(R) Core(TM) i7-4710MQ CPU @ 2.50GHz
  WORD_SIZE: 64
  LIBM: libopenlibm
  LLVM: libLLVM-11.0.1 (ORCJIT, haswell)
Environment:
  JULIA_PROJECT = .
  JULIA_NUM_THREADS = 8
```

```
using Pkg
Pkg.activate(".")
```

```
  Activating environment at `~/drive/thesis/notebooks/Project.toml`
```

```
Pkg.status()
```

```
      Status `~/drive/thesis/notebooks/Project.toml`
  [537997a7] AbstractPlotting v0.15.27
  [7d9fca2a] Arpack v0.4.0
  [6e4b80f9] BenchmarkTools v0.7.0
  [ad839575] Blink v0.12.5
  [13f3f980] CairoMakie v0.3.19
  [5ae59095] Colors v0.12.7
  [150eb455] CoordinateTransformations v0.6.1
  [e9467ef8] GLMakie v0.1.30
  [7073ff75] IJulia v1.23.2
  [d1acc4aa] IntervalArithmetic v0.17.8
  [c8e1da08] IterTools v1.3.0
  [5ab0869b] KernelDensity v0.6.2
  [b964fa9f] LaTeXStrings v1.2.1
  [2fda8390] LsqFit v0.12.0
  [ee78f7c6] Makie v0.12.0
  [eff96d63] Measurements v2.5.0
  [3b7a836e] PGFPlots v3.3.6
  [ccf2f8ad] PlotThemes v2.0.1
  [58dd65bb] Plotly v0.3.0
  [91a5bcdd] Plots v1.11.2
  [92933f4c] ProgressMeter v1.5.0
  [438e738f] PyCall v1.92.3
  [6e0679c1] QuantumOptics v0.8.2
  [4f57444f] QuantumOpticsBase v0.2.7
  [189a3867] Reexport v0.2.0
  [f3b207a7] StatsPlots v0.14.19
  [24249f21] SymPy v1.0.42
  [ac1d9e8a] ThreadsX v0.1.7
  [1986cc42] Unitful v1.7.0
  [276b4fcb] WGLMakie v0.3.4
  [0f1e0344] WebIO v0.8.15
  [37e2e46d] LinearAlgebra
```

```
using LinearAlgebra
BLAS.vendor()
```

```
:openblas64
```

C.2 NOTEBOOK PREAMBLE

```
using Plots, LaTeXStrings
using Unitful, Measurements
using LinearAlgebra, Arpack, QuantumOptics
using LsqFit, Roots
using ThreadsX

import PGFPlotsX
# If reevaluating, so no duplicates
!isempty(PGFPlotsX.CUSTOM_PREAMBLE) && pop!(PGFPlotsX.CUSTOM_PREAMBLE)
push!(PGFPlotsX.CUSTOM_PREAMBLE, ”
    \\usepackage{amsmath}
    \\usepackage{physics}
    \\usepackage{siunitx}
    \\usepackage[full]{textcomp} % to get the right copyright, etc.
    \\usepackage[semibold]{libertinus-otf}
    \\usepackage[T1]{fontenc} % LY1 also works
    \\setmainfont[Numbers={OldStyle,Proportional}]{Libertinus Serif}
    \\usepackage[supstfm=libertinesups,supscaled=1.2,raised=-.13em]{superiors}
    \\setmonofont[Scale=MatchLowercase]{JuliaMono} % We need lots of unicode, like ⊗
    \\usepackage[cal=cm,bb=boondox,frak=boondox]{mathalfa}
    \\input{$(pwd())/latexdefs.tex}
    ”);
pgfplotsx()

using PlotThemes
_fs = 12
theme(:vibrant,
    size=(400, 300),
    dpi=300,
    titlefontsize = _fs,
    tickfontsize = _fs,
    legendfontsize = _fs,
    guidefontsize = _fs,
    legendtitlefontsize = _fs
)
```

```
rubric = RGB(0.7, 0.05, 0.0); # The red color used in the thesis document.

# Pauli matrices
const σ0 = [1 0; 0 1]
const σx = [0 1; 1 0]
const σy = [0 -im; im 0]
const σz = [1 0; 0 -1]
const σp = [0 1; 0 0]
const σm = [0 0; 1 0]

⊗ₖ(a, b) = kron(b, a);
function siteop(A, i, n)
    i = i > 0 ? 1 + ((i - 1) % n) : throw(ArgumentError("Site index must be
     ↪  positive."))
    ops = repeat([one(A)], n)
    ops[i] = A
    reduce(⊗ₖ, ops)
end
```

BIBLIOGRAPHY

[1] W. Gerlach and O. Stern, "Über die Richtungsquantelung im Magnetfeld", Ann. Phys. **379**, 673–699 (1924) (page 9).

[2] H. Schmidt-Böcking, L. Schmidt, H. J. Lüdde, W. Trageser, A. Templeton, and T. Sauer, "The Stern-Gerlach experiment revisited", EPJ H **41**, 327–364 (2016) (page 10).

[3] P. Busch, M. Grabowski, and P. J. Lahti, *Operational Quantum Physics* (Springer Science & Business Media, Nov. 27, 1997), 237 pp. (page 12).

[4] P. Busch, "Quantum States and Generalized Observables: A Simple Proof of Gleason's Theorem", Phys. Rev. Lett. **91**, 120403 (2003) (pages 12, 15).

[5] A. M. Gleason, "Measures on the Closed Subspaces of a Hilbert Space", in *The Logico-Algebraic Approach to Quantum Mechanics: Volume I: Historical Evolution*, edited by C. A. Hooker, The University of Western Ontario Series in Philosophy of Science (Springer Netherlands, Dordrecht, 1975), pp. 123–133 (page 12).

[6] R. F. Streater and A. S. Wightman, *PCT, Spin and Statistics, and All That* (Princeton University Press, 1989) (page 14).

[7] V. Moretti, "Mathematical Foundations of Quantum Mechanics: An Advanced Short Course", version 4, Int. J. Geom. Methods Mod. Phys. **13**, 1630011 (2016) (pages 15, 16).

[8] K. He, Q. Yuan, and J. Hou, "Entropy-preserving maps on quantum states", Linear Algebra and its Applications **467**, 243–253 (2015) (page 15).

[9] L. Molnár and P. Szokol, "Maps on states preserving the relative entropy II", Linear Algebra and its Applications **432**, 3343–3350 (2010) (page 15).

[10] I. Bengtsson and K. Życzkowski, *Geometry of Quantum States: An Introduction to Quantum Entanglement* (Cambridge University Press, Aug. 18, 2017), 637 pp. (page 16).

[11] J. v. Neumann, "Uber Einen Satz Von Herrn M. H. Stone", Ann. Math. **33**, 567–573 (1932) (page 16).

[12] M. H. Stone, "On One-Parameter Unitary Groups in Hilbert Space", Ann. Math. **33**, 643–648 (1932) (page 16).

[13] J. R. Shewell, "On the Formation of Quantum-Mechanical Operators", American Journal of Physics **27**, 16–21 (1959) (page 18).

[14] B. C. Hall, *Quantum Theory for Mathematicians* (Springer New York, June 19, 2013), 554 pp. (pages 18, 19).

[15] H. Weyl, "Quantenmechanik und Gruppentheorie", Z. Physik **46**, 1–46 (1927) (page 18).

[16] R. Alicki, "Comment on "Reduced Dynamics Need Not Be Completely Positive"", Phys. Rev. Lett. **75**, 3020–3020 (1995) (page 19).

[17] P. Pechukas, "Reduced Dynamics Need Not Be Completely Positive", Phys. Rev. Lett. **73**, 1060–1062 (1994) (pages 20, 21).

[18] H. P. Breuer and F. Petruccione, *The theory of open quantum systems* (Oxford University Press, 2002), pp. 74–141 (pages 21, 28, 39, 40, 71).

[19] M. E. Cuffaro and W. C. Myrvold, "On the Debate Concerning the Proper Characterization of Quantum Dynamical Evolution", Philosophy of Science **80**, 1125–1136 (2013) (page 21).

[20] A. Shaji and E. C. G. Sudarshan, "Who's afraid of not completely positive maps?", Physics Letters A **341**, 48–54 (2005) (page 21).

[21] R. Kubo, "Statistical-mechanical theory of irreversible processes. I. General theory and simple applications to magnetic and conduction problems", J. Phys. Soc. Jpn. **12**, 570–586 (1957) (page 26).

[22] P. C. Martin and J. Schwinger, "Theory of many-particle systems. I", Phys. Rev. **115**, 1342–1373 (1959) (page 26).

[23] F. Bechstedt, "Thermodynamic Green Functions", in *Many-Body Approach to Electronic Excitations: Concepts and Applications*, edited by F. Bechstedt, Springer Series in Solid-State Sciences (Springer, Berlin, Heidelberg, 2015), pp. 209–230 (page 26).

[24] D. J. Griffiths and D. F. Schroeter, *Introduction to Quantum Mechanics*, 3rd edition (Cambridge University Press, Cambridge ; New York, NY, Aug. 1, 2018), 508 pp. (page 29).

[25] P. Pfeuty, "The one-dimensional Ising model with a transverse field", Annals of Physics **57**, 79–90 (1970) (pages 30–32).

[26] D. J. Griffiths, *Introduction to Electrodynamics* (Cambridge University Press, June 29, 2017), 624 pp. (page 30).

[27] C. Kittel, *Introduction to Solid State Physics*, 8th edition (Wiley, Hoboken, NJ, Nov. 11, 2004), 704 pp. (page 30).

[28] R. Blatt and C. F. Roos, "Quantum simulations with trapped ions", Nat. Phys. **8**, 277–284 (2012) (page 30).

[29] K. Kim, S. Korenblit, R. Islam, E. E. Edwards, M.-S. Chang, C. Noh, H. Carmichael, G.-D. Lin, L.-M. Duan, C. C. J. Wang, J. K. Freericks, and C. Monroe, "Quantum simulation of the transverse Ising model with trapped ions", New J. Phys. **13**, 105003 (2011) (page 30).

[30] *STM Permissions Guidelines*, STM, https://www.stm-assoc.org/intellectual-property/permissions/permissions-guidelines/ (visited on 04/20/2021) (page 32).

[31] M. Kardar, *Statistical Physics of Particles* (Cambridge University Press, June 7, 2007), 331 pp. (page 33).

[32] R. Shankar, *Principles of Quantum Mechanics* (Springer Science & Business Media, Dec. 6, 2012), 676 pp. (page 34).

[33] M. Bernasconi, S. Miret-Artés, and P. Toennies, "Giorgio Benedek: an extraordinary universal scientist", Journal of physics. Condensed matter : an Institute of Physics journal **24**, 100401 (2012) (page 44).

[34] V. Gorini, A. Kossakowski, and E. C. G. Sudarshan, "Completely positive dynamical semigroups of N-level systems", J. Math. Phys. **17**, 821–825 (1976) (page 73).

[35] G. Lindblad, "On the generators of quantum dynamical semigroups", Commun. Math. Phys. **119**, 48 (1976) (page 73).

[36] C. Ates, B. Olmos, J. P. Garrahan, and I. Lesanovsky, "Dynamical phases and intermittency of the dissipative quantum Ising model", Phys. Rev. A **85**, 043620 (2012).

[37] C. M. Bender, "Introduction to PT-Symmetric Quantum Theory", Contemporary Physics **46**, 277–292 (2005).

[38] C. M. Bender and S. Boettcher, "Real Spectra in Non-Hermitian Hamiltonians Having $\mathsc{P}\mathsc{T}$ Symmetry", Phys. Rev. Lett. **80**, 5243–5246 (1998).

[39] M. Bhattacharya, M. J. A. Stoutimore, K. D. Osborn, and A. Mizel, "Understanding the damping of a quantum harmonic oscillator coupled to a two-level system using analogies to classical friction", American Journal of Physics **80**, 810–815 (2012).

[40] P. Calabrese, F. H. L. Essler, and M. Fagotti, "Quantum Quench in the Transverse-Field Ising Chain", Phys. Rev. Lett. **106**, 227203 (2011).

[41] A. O. Caldeira and A. J. Leggett, "Influence of damping on quantum interference: An exactly soluble model", Phys. Rev. A **31**, 1059–1066 (1985).

[42] J. Chalker, "Quantum Theory of Condensed Matter", 42.

[43] G. Chiribella, G. M. D'Ariano, and P. Perinotti, "Informational derivation of quantum theory", Phys. Rev. A **84**, 012311 (2011).

[44] J. Ma, H. Zhang, B. Lavorel, F. Billard, E. Hertz, J. Wu, C. Boulet, J.-M. Hartmann, and O. Faucher, "Observing collisions beyond the secular approximation limit", Nat. Commun. **10**, 5780 (2019).

[45] J. Ma, H. Zhang, B. Lavorel, F. Billard, J. Wu, C. Boulet, J.-M. Hartmann, and O. Faucher, "Ultrafast collisional dissipation of symmetric-top molecules probed by rotational alignment echoes", Phys. Rev. A **101**, 043417 (2020).

[46] M. Schlosshauer, "Quantum decoherence", Phys. Rep. **831**, 1–57 (2019).

[47] P. A. M. Dirac, *The Principles of Quantum Mechanics* (Clarendon Press, 1981), 340 pp.

[48] P. A. M. Dirac and N. H. D. Bohr, "The quantum theory of the emission and absorption of radiation", Proceedings of the Royal Society of London. Series A, Containing Papers of a Mathematical and Physical Character **114**, 243–265 (1927).

[49] V. J. Emery and A. Luther, "Low- temperature properties of the Kondo Hamiltonian", Phys. Rev. B **9**, 215–226 (1974).

[50] E. Ercolessi, "A short course on quantum mechanics and methods of quantization", Int. J. Geom. Methods Mod. Phys. **12**, 1560008 (2015).

[51] J. Erhart, S. Sponar, G. Sulyok, G. Badurek, M. Ozawa, and Y. Hasegawa, "Experimental demonstration of a universally valid error–disturbance uncertainty relation in spin measurements", Nat. Phys. **8**, 185–189 (2012).

[52] C. A. Fuchs, *Quantum Foundations in the Light of Quantum Information*, (June 29, 2001) http://arxiv.org/abs/quant-ph/0106166 (visited on 10/04/2020).

[53] C. A. Fuchs, *Quantum Mechanics as Quantum Information (and only a little more)*, (May 8, 2002) http://arxiv.org/abs/quant-ph/0205039 (visited on 10/04/2020).

[54] A. Furuta, *One Thing Is Certain: Heisenberg's Uncertainty Principle Is Not Dead*, Scientific American, https://www.scientificamerican.com/article/heisenbergs-uncertainty-principle-is-not-dead/ (visited on 10/06/2020).

[55] H. J. Groenewold, "On the principles of elementary quantum mechanics", Physica **12**, 405–460 (1946).

[56] R. Haag, N. M. Hugenholtz, and M. Winnink, “On the equilibrium states in quantum statistical mechanics”, Commun.Math. Phys. **5**, 215–236 (1967).

[57] L. Hardy, *Quantum Theory From Five Reasonable Axioms*, (Sept. 25, 2001) http://arxiv.org/abs/quant-ph/0101012 (visited on 10/03/2020).

[58] O. Hart, G. Goldstein, C. Chamon, and C. Castelnovo, “Steady-state superconductivity in electronic materials with repulsive interactions”, Phys. Rev. B **100**, 060508 (2019).

[59] M. Heyl, A. Polkovnikov, and S. Kehrein, “Dynamical Quantum Phase Transitions in the Transverse-Field Ising Model”, Phys. Rev. Lett. **110**, 135704 (2013).

[60] D. Manzano, “A short introduction to the Lindblad master equation”, AIP Adv. **10**, 025106 (2020).

[61] D. F. V. James, P. G. Kwiat, W. J. Munro, and A. G. White, “Measurement of qubits”, Phys. Rev. A **64**, 052312 (2001).

[62] E. Jaynes and F. Cummings, “Comparison of quantum and semiclassical radiation theories with application to the beam maser”, Proc. IEEE **51**, 89–109 (1963).

[63] J. Jin, A. Biella, O. Viyuela, L. Mazza, J. Keeling, R. Fazio, and D. Rossini, “Cluster Mean-Field Approach to the Steady-State Phase Diagram of Dissipative Spin Systems”, Phys. Rev. X **6**, 031011 (2016).

[64] J. Jin, A. Biella, O. Viyuela, C. Ciuti, R. Fazio, and D. Rossini, “Phase diagram of the dissipative quantum Ising model on a square lattice”, Phys. Rev. B **98**, 241108 (2018).

[65] E. Kapit, “The upside of noise: engineered dissipation as a resource in superconducting circuits”, Quantum Sci. Technol. **2**, 033002 (2017).

[66] H. Kim, M. C. Bañuls, J. I. Cirac, M. B. Hastings, and D. A. Huse, “Slowest local operators in quantum spin chains”, version 2, Phys. Rev. E **92**, 012128 (2015).

[67] E. Lieb, T. Schultz, and D. Mattis, “Two soluble models of an antiferromagnetic chain”, Annals of Physics **16**, 407–466 (1961).

[68] G. W. Mackey, “Quantum Mechanics and Hilbert Space”, Am. Math. Mon. **64**, 45–57 (1957).

[69] G. McCauley, B. Cruikshank, D. I. Bondar, and K. Jacobs, “Accurate Lindblad-form master equation for weakly damped quantum systems across all regimes”, Npj Quantum Inf. **6**, 1–14 (2020).

[70] V. Moretti, *Spectral Theory and Quantum Mechanics: Mathematical Foundations of Quantum Theories, Symmetries and Introduction to the Algebraic Formulation*, 2nd ed., La Matematica per Il 3+2 (Springer International Publishing, 2017).

[71] M. A. Nielsen, "The Fermionic canonical commutation relations and the Jordan-Wigner transform", 8.

[72] M. Ozawa, "Universally valid reformulation of the Heisenberg uncertainty principle on noise and disturbance in measurement", Phys. Rev. A **67**, 042105 (2003).

[73] P. Pearle, "Simple derivation of the Lindblad equation", Eur. J. Phys. **33**, 805–822 (2012).

[74] P. Pechukas, "Pechukas Replies:" Phys. Rev. Lett. **75**, 3021–3021 (1995).

[75] A. Peres, "Separability Criterion for Density Matrices", Phys. Rev. Lett. **77**, 1413–1415 (1996).

[76] *Phys. Rev. A 67, 042105 (2003) - Universally valid reformulation of the Heisenberg uncertainty principle on noise and disturbance in measurement*, https://journals.aps.org/pra/abstract/10.1103/PhysRevA.67.042105 (visited on 10/06/2020).

[77] F. A. Pollock, C. Rodríguez-Rosario, T. Frauenheim, M. Paternostro, and K. Modi, "Operational Markov Condition for Quantum Processes", Phys. Rev. Lett. **120**, 040405 (2018).

[78] J. Prior, A. W. Chin, S. F. Huelga, and M. B. Plenio, "Efficient Simulation of Strong System-Environment Interactions", Phys. Rev. Lett. **105**, 050404 (2010).

[79] T. Prosen and B. Zunkovic, "Exact solution of Markovian master equations for quadratic fermi systems: thermal baths, open XY spin chains, and non-equilibrium phase transition", New J. Phys. **12**, 025016 (2010).

[80] T. Prosen and M. Žnidarič, "Matrix product simulations of non-equilibrium steady states of quantum spin chains", J. Stat. Mech. **2009**, P02035 (2009).

[81] D. W. Preston, "Doppler-free saturated absorption: Laser spectroscopy", Am. J. Phys. **64**, 1432–1436 (1996).

[82] C. E. Shannon, "A mathematical theory of communication", Bell Syst. Tech. J. **27**, 379–423 (1948).

[83] R. W. Spekkens, "Evidence for the epistemic view of quantum states: A toy theory", Phys. Rev. A **75**, 032110 (2007).

[84] C. J. Turner, K. Meichanetzidis, Z. Papić, and J. K. Pachos, "Optimal free descriptions of many-body theories", Nat. Commun. **8**, 14926 (2017).

[85] H. Weimer, “Variational Principle for Steady States of Dissipative Quantum Many-Body Systems”, Phys. Rev. Lett. **114**, 040402 (2015).

[86] S. Weinberg, “Quantum mechanics without state vectors”, Phys. Rev. A **90**, 042102 (2014).

[87] P. Werner, K. Völker, M. Troyer, and S. Chakravarty, “Phase Diagram and Critical Exponents of a Dissipative Ising Spin Chain in a Transverse Magnetic Field”, Phys. Rev. Lett. **94**, 047201 (2005).

[88] H. D. Zeh, “On the interpretation of measurement in quantum theory”, Found. Phys. **1**, 69–76 (1970).

INDEX

antiunitary, 16
assignment map, 19

Bloch vector, 27
Bogoliubov transformation, 80
Born approximation, 24
Born rule, 12

canonical commutation relations, 17
closed, 15
completely positive, 21

density operator, 12
dissipator, 25
dynamical map, 20

effect, 11
Einstein A coefficient, 29, 38
ensemble, 11
entangled, 14

Heisenberg equation of motion, 17
Heisenberg picture, 17

interaction picture, 22

Jordan-Wigner transformation, 76
jump operator, 73
jump operators, 25

KMS boundary condition, 26

Lamb shift Hamiltonian, 25
Lindblad equation, 25, 73
Lindblad operators, 73
Liouville equation, 16
Liouvillian, 25

magnetic field operator, 34
Markov approximation, 24
master equation, 71

natural units, 7, 16

observable, 12
open dynamics, 19
open system, 19
operation, 12

partial trace, 15
Pauli operators, 27
Poisson bracket, 17
positive operator valued measure, 12
probability measure, 11
product effect, 14
product state, 14
projection valued measure, 12

quantum mechanics, 10

Redfield equation, 24
reservoir correlation functions, 23

rotating wave, 25

Schrödinger picture, 17
secular approximation, 25
semigroup property, 71
spaghetti diagrams, 44
strongly continuous, 16
subsystem, 14
superoperator, 25

tensor, 14
tensor product, 14
thermal state, 25
transverse-field Ising model, 30

unitary, 16

vacuum magnetic timescale, 38
von Neumann equation, 16

weak-coupling approximation, 24
weak-coupling limit, 20
Weyl quantization, 18